



TEZ ŞABLONU ONAY FORMU  
THESIS TEMPLATE CONFIRMATION FORM

1. Şablonda verilen yerleşim ve boşluklar değiştirilmemelidir.
2. Jüri tarihi Başlık Sayfası, İmza Sayfası, Abstract ve Öz'de ilgili yerlere yazılmalıdır.
3. İmza sayfasında jüri üyelerinin unvanları doğru olarak yazılmalıdır.
4. Tezin son sayfasının sayfa numarası Abstract ve Öz'de ilgili yerlere yazılmalıdır.
5. Bütün chapterlar, referanslar, ekler ve CV sağ sayfada başlamalıdır. Bunun için **kesmeler** kullanılmıştır. **Kesmelerin kayması** fazladan boş sayfaların oluşmasına sebep olabilir. Bu gibi durumlarda paragraf (¶) işaretine tıklayarak kesmeleri görünür hale getirin ve yerlerini **kontrol edin**.
6. Figürler ve tablolar kenar boşluklarına taşmamalıdır.
7. Şablonda yorum olarak eklenen uyarılar dikkatle okunmalı ve uygulanmalıdır.
8. Tez yazdırılmadan önce PDF olarak kaydedilmelidir. Şablonda yorum olarak eklenen uyarılar PDF dokümanında yer almamalıdır.
9. **Bu form aracılığıyla oluşturulan PDF dosyası arkalı-önlü baskı alınarak tek bir spiralli cilt haline getirilmelidir.**
10. Spiralli hale getirilen tez taslağınızdaki ilgili alanları imzalandıktan sonra, [Tez Jüri Atama Formu](#) ile birlikte bölüm sekreterliğine teslim edilmelidir.
11. Tez taslağınız bölüm sekreterliğiniz aracılığıyla format ve görünüm açısından kontrol edilmek üzere FBE'ye ulaştırılacaktır.
12. FBE tarafından kontrol işlemleri tamamlanan tez taslakları, öğrencilere teslim edilmek üzere bölüm sekreterliklerine iletilecektir.
13. Tez taslaklarının kontrol işlemleri tamamlandığında, bu durum öğrencilere METU uzantılı öğrenci e-posta adresleri aracılığıyla duyurulacaktır.
14. Tez taslakları bölüm sekreterlikleri tarafından öğrencilere iletileceği için öğrencilerimizin tez taslaklarını enstitümüzden elden alma konusunda ısrarcı olmamaları beklenmektedir.
15. Tez yazım süreci ile ilgili herhangi bir sıkıntı yaşarsanız, [Sıkça Sorulan Sorular \(SSS\)](#) sayfamızı ziyaret ederek yaşadığınız sıkıntıyla ilgili bir çözüm bulabilirsiniz.

1. Do not change the spacing and placement in the template.
2. Write defense date to the related places given on Title page, Approval page, Abstract and Öz.
3. Write the titles of the examining committee members correctly on Approval Page.
4. Write the page number of the last page in the related places given on Abstract and Öz pages.
5. All chapters, references, appendices and CV must be started on the right page. **Section Breaks** were used for this. **Change in the placement** of section breaks can result in extra blank pages. In such cases, make the section breaks visible by clicking paragraph (¶) mark and **check their position**.
6. All figures and tables must be given inside the page. Nothing must appear in the margins.
7. All the warnings given on the comments section through the thesis template must be read and applied.
8. Save your thesis as pdf and Disable all the comments before taking the printout.
9. **Print two-sided the PDF file that you have created through this form and make a single spiral bound.**
10. Once you have signed the relevant fields in your thesis draft that you spiraled, submit it to the department secretary together with your [Thesis Jury Assignment Form](#).
11. Your thesis draft will be delivered to the GSNAS via your department secretary for controlling in terms of format and appearance.
12. The thesis drafts that are controlled by GSNAS, will be sent to the department secretary to be delivered to the students.
13. This will be announced to the students via their METU students e-mail addresses when the control of the thesis drafts has been completed.
14. As the thesis drafts will be delivered to the students by the department secretaries, we are expecting from our students no to insist about getting their theses drafts from the Institute.
15. If you have any problems with the thesis writing process, you may visit our [Frequently Asked Questions \(FAQ\)](#) page and find a solution to your problem.

Yukarıda bulunan tüm maddeleri okudum, anladım ve kabul ediyorum. / I have read, understand and accept all of the items above.

Name : Çağıl Merve  
Surname : TANIK  
E-Mail : cmervecan@gmail.com  
Date : 25.02.2020  
Signature : \_\_\_\_\_



ON THE ANALYSIS AND DESIGN OF A NOVEL FULLY COMPLIANT  
SLIDER-CRANK MECHANISM

A THESIS SUBMITTED TO  
THE GRADUATE SCHOOL OF NATURAL AND APPLIED SCIENCES  
OF  
MIDDLE EAST TECHNICAL UNIVERSITY

BY

ÇAĞIL MERVE TANIK

IN PARTIAL FULFILLMENT OF THE REQUIREMENTS  
FOR  
THE DEGREE OF DOCTOR OF PHILOSOPHY  
IN  
MECHANICAL ENGINEERING

JANUARY 2020



Approval of the thesis:

**ON THE ANALYSIS AND DESIGN OF A NOVEL FULLY COMPLIANT  
SLIDER-CRANK MECHANISM**

submitted by **ÇAĞIL MERVE TANIK** in partial fulfillment of the requirements for  
the degree of **Doctor of Philosophy in Mechanical Engineering, Middle East  
Technical University** by,

Prof. Dr. Halil Kalıpçılar  
Dean, Graduate School of **Natural and Applied Sciences**

Prof. Dr. Sahir Arıkan  
Head of the Department, **Mechanical Engineering**

Assoc. Prof. Dr. Yiğit Yazıcıoğlu  
Supervisor, **Mechanical Engineering, METU**

Assoc. Prof. Dr. Volkan Parlaktaş  
Co-Supervisor, **Mechanical Eng., Hacettepe University**

**Examining Committee Members:**

Prof. Dr. Suat Kadioğlu  
Mechanical Engineering, METU

Assoc. Prof. Dr. Yiğit Yazıcıoğlu  
Mechanical Engineering, METU

Prof. Dr. Erdem Acar  
Mechanical Engineering, TOBB ETU

Assoc. Prof. Dr. Tuncay Karaçay  
Mechanical Engineering, Gazi University.

Assoc. Prof. Dr. Mehmet Bülent Özer  
Mechanical Engineering, METU

Date: 31.01.2020

**I hereby declare that all information in this document has been obtained and presented in accordance with academic rules and ethical conduct. I also declare that, as required by these rules and conduct, I have fully cited and referenced all material and results that are not original to this work.**

Name, Last name : ađıl Merve Tanık

Signature :

## ABSTRACT

### ON THE ANALYSIS AND DESIGN OF A NOVEL FULLY COMPLIANT SLIDER-CRANK MECHANISM

Tanık, Çağıl Merve  
Doctor of Philosophy, Mechanical Engineering  
Supervisor: Assoc. Prof. Dr. Yiğit Yazıcıoğlu  
Co-Supervisor: Assoc. Prof. Dr. Volkan Parlaktaş

January 2020, 106 pages

In the literature, authors have made contributions in the area of partially compliant slider-crank mechanisms those possess rigid joints that may cause backlash inherently. On contrary, fully compliant mechanisms offer no backlash which is a valuable property for the cases where high preciseness is required. In this paper, we proposed an original “fully” compliant slider-crank mechanism design. To the best of our knowledge, this is the first study in the literature on a compliant slider-crank mechanism without a rigid prismatic joint. An analysis and design procedure for this mechanism is proposed. Kinematic performance of the mechanism is investigated analytically. Dimensions of the mechanism are optimized to obtain maximum translational output, while keeping deflections of the flexible hinges equal to each other and as small as possible. A design table displaying relationships between output stroke, axis drift of the output segment in unitless form, and critical stresses at the compliant segments are presented. As an example, a compliant mechanism is designed by using rigid body replacement technique. Then, by using nonlinear finite element analysis technique, analytical results are verified. Finally, a real model is built to compare output stroke and axis drift with the derived analytical approaches.

The results of experiments verified that the proposed theoretical approaches are consistent.

Keywords: Fully Compliant Mechanisms, Slider-Crank Mechanisms, No Backlash, Straight Line Motion Generation

## ÖZ

### TAMAMEN ESNEK ORJİNAL BİR KOL-KIZAK MEKANİZMASI ANALİZİ VE TASARIMI ÜZERİNE

Tanık, Çağıl Merve  
Doktora, Makina Mühendisliği  
Tez Yöneticisi: Doç. Dr. Yiğit Yazıcıoğlu  
Ortak Tez Yöneticisi: Doç. Dr. Volkan Parlaktaş

Ocak 2020, # sayfa

Çeşitli yazarlar kısmen esnek kol kızak mekanizmaları alanında literatüre katkıda bulunmuşlardır. Bu tip mekanizmalarda rijit mafsallardan kaynaklanan boşluk sorunu bulunmaktadır. Bunun yanında tamamen esnek mekanizmalar yapılarında rijit mafsal olmadığı için boşluksuz çalışabilmektedirler. Bu çalışmada original, tamamen esnek kol kızak mekanizması ilk olarak ortaya atılmıştır ve literatürdeki ilk prizmatik mafsalı olmayan kol kızak mekanizmasıdır. Analiz ve dizayn prosedürü önerilmiştir. Kinematik performansı analitik olarak incelenmiştir. En yüksek çıkış deplasmanına sahip mekanizmanın ölçüleri optimize edilirken esnek mafsallardaki bükülmelerin birbirine eşit değerde ve olabildiğince küçük olması sağlanmıştır. Çıkış hareketi, eksen kayması ve kritik stres ilişkilerinin bulunduğu bir dizayn tablosu gösterilmiştir. Örnek olarak bir esnek mekanizma rijit gövde değişim tekniği ile dizayn edilmiştir. Sonrasında lineer olmayan sonlu eleman analizi ile analitik sonuçlar doğrulanmıştır. En son olarak gerçek model üretilmiş ve sonuçlar özel yapım test düzeneği ile ölçülmüştür. Sonuçlar karşılaştırılarak teorik ve deneysel değerlerin birbiriyle uyumlu olduğu gösterilmiştir.

Anahtar Kelimeler: Tamamen Esnek Mekanizmalar, Kol-Kızak Mekanizmaları,  
Boşluksuz Tasarım, Düz Çizgi Hareket Üretimi

To my husband, Prof. Dr. Engin Tanik, for his advice, love, and faith. And to my son, Mert, to letting me experience the kind of love that people freely die for.

## **ACKNOWLEDGMENTS**

I would like to express my deepest gratitude to my supervisors Assoc. Prof. Dr. Yiğit Yazıcıoğlu and Assoc. Prof. Dr. Volkan Parlaktaş for their guidance, advice, criticism, encouragements and insight throughout the research.

I would also like to thank my husband Prof. Dr. Engin Tanık for his support and patience during the thesis study.

## TABLE OF CONTENTS

ABSTRACT .....	v
ÖZ .....	vii
ACKNOWLEDGMENTS .....	x
TABLE OF CONTENTS .....	xi
LIST OF TABLES .....	xiv
LIST OF FIGURES .....	xv
LIST OF ABBREVIATIONS .....	xviii
LIST OF SYMBOLS .....	xix
1. INTRODUCTION .....	1
1.1. Compliant Slider-Crank Mechanism Studies in the Literature.....	1
1.2. Compliant Translational Joint Studies in the Literature.....	6
1.3. Objective and Scope of the Thesis .....	11
1.4. Outline of the Thesis .....	11
2. COMPLIANT MECHANISMS .....	13
2.1. Introduction to Compliant Mechanisms .....	13
2.2. Flexibility and Deflection.....	15
2.2.1. Stiffness and Strength.....	15
2.2.2. Flexibility.....	16
2.2.3. Material Selection in Compliant Mechanisms.....	17
2.2.4. Pseudo-Rigid-Body Model .....	18

2.2.5. Small-Length Flexural Pivots .....	19
2.2.6. Moment at the Free End .....	24
2.2.7. Fixed Guided Beam .....	25
2.2.8. Pseudo-Rigid Body Replacement.....	27
3. THE PROPOSED FULLY COMPLIANT SLIDER-CRANK MECHANISM.....	29
4. KINEMATIC ANALYSIS OF THE CASCADE PARALLELOGRAM FOUR- BAR MECHANISM.....	33
4.1. Kinematic Analysis .....	33
4.2. A Novel Kinematic Analysis Approach for the PRBM .....	35
4.3. Transmission Angle .....	40
5. DESIGN APPROACH FOR THE RIGID BODY EQUIVALENT OF THE COMPLIANT SLIDER-CRANK MECHANISM .....	41
5.1. Objectives of the Design Approach .....	41
5.2. Function Generation with Complex Number Modelling .....	41
5.3. Function Generation for Three Precision Points.....	43
6. DESIGN OF THE FULLY COMPLIANT SLIDER-CRANK MECHANISM.....	47
6.1. Dimension Synthesis of the Fully Compliant Cascade Parallelogram Four- Bar Mechanism.....	47
6.2. Stroke of the System .....	52
6.3. Axis Drift of the System.....	52
6.4. Stress Analysis for Small Length Flexural Hinges .....	52
6.5. Stress Analysis for Fixed Guided Flexible Segment.....	53

6.6. Determination of the Torque Value for the Cascade Four-Bar Mechanism with Fixed Guided Flexible Segment .....	56
7. FINITE ELEMENT ANALYSIS .....	61
7.1. Proposed Design .....	61
7.2. Effective Length Analysis .....	61
7.3. Finite Element Analysis with Effective Length.....	63
7.3.1. Boundary Conditions and Meshing.....	64
7.3.2. Stroke Analysis for Fully Compliant Slider-Crank Mechanism.....	66
7.3.3. Stress Analysis for Fully Compliant Slider-Crank Mechanism.....	71
7.3.4. Study of Mesh Refinement for Fully Compliant Slider-Crank Mechanism .....	73
8. EXPERIMENTAL ANALYSIS OF THE FULLY COMPLIANT SLIDER-CRANK MECHANISM .....	75
8.1. Manufacturing of the Prototype .....	75
8.2. Experimental Validation.....	77
9. CONCLUSIONS .....	81
9.1. Summary.....	81
9.2. Key Findings and Outcomes.....	82
9.3. Future Work.....	83
REFERENCES.....	85
A. Properties of Polypropylene .....	89
B. MathCad and MatLab Codes for the Calculations .....	90
CURRICULUM VITAE.....	105

## LIST OF TABLES

### TABLES

Table 1.1. Benchmarked flexible translational joints ‘-: poor, 0: normal; +: good’ [19].....	7
Table 1.2. Comparison of Stiffness ratios for the configurations in Figure 1.7 [20] .....	10
According to Table 2.1 modulus of elasticity of alloy materials are nearly constant. Furthermore, yield strength may vary dramatically depending on their alloy and manufacturing processes. Increasing the yield strength of a material also makes the material more brittle.....	17
Table 2.1. Ratio of Yield Strength to Young’s Modulus for Several Materials[2] .	18
Table 6.1. Design table for fully compliant slider-crank mechanisms .....	57
Table 7.1. Theoretical and FEA stroke data of the fully compliant slider-crank mechanism.....	70
Table 7.2. Number of elements through the thickness vs. maximum von-Mises stress for fixed-guided flexural hinge.....	74
Table 8.1. Theoretical and experimental stroke data of the fully compliant slider-crank mechanism .....	77
Table 8.2. Theoretical and experimental axis drift data of the fully compliant slider-crank mechanism .....	78

## LIST OF FIGURES

### FIGURES

Figure 1.1. Partially compliant RSSP mechanism and its PRBM [14] .....	3
Figure 1.2. Single piece compliant slider-crank and its PRBM [10].....	4
Figure 1.3. Manufactured partially compliant slider-crank mechanism [16].....	4
Figure 1.4. Representation of experimental test rig [17] .....	5
Figure 1.5. Model mechanisms: (a) classical articulated slider–crank mechanism, (b) partly compliant slider–crank mechanism, and (c) small-length flexural pivot [18].....	6
Figure 1.6 CT joint conceptual designs [19].....	8
Figure 1.7 Three-dimensional constructions for the figures in (a) Type 1 (b) Type 2 .....	9
Figure 1.8 (a) A solid model for the spatial compliant translational joint, (b) and (c) geometric parameters of the spatial compliant translation joint [20] .....	10
Figure 2.1. Cantilever beam with end forces .....	15
Figure 2.2. Cantilever beam (a) and its Pseudo-Rigid-Body Model (b).....	20
Figure 2.3. Cantilever beam (a) and its Pseudo-Rigid-Body Model (b).....	23
Figure 2.4. Flexible Beam with a Moment at the Free End .....	24
Figure 2.5. (a) Flexible beam with a constant end angle, (b) free-body diagram of the half beam, and (c) pseudo-rigid-body model [2] .....	25
Figure 2.6. A Complaint Four-Bar and Slider-Crank Mechanism and Pseudo Rigid Body Models .....	28
Figure 3.1. a) Partially compliant slider-crank with prismatic joint b) proposed fully compliant slider-crank .....	30
Figure 3.2. a) PRBM b) isometric view of the mechanism whose slider is composed of fixed guided compliant segments .....	31
Figure 4.1. Structure parameters and variables for the kinematic analysis.....	34
Figure 4.2. PRBM with an imaginary parallelogram four-bar mechanism .....	36

Figure 4.3. Structure parameters and variables for the cascade four-bar mechanism .....	37
Figure 5.1. Vector loop for a four-bar mechanism with coupler point P [26] .....	42
Figure 5.2. Four-bar mechanism in forward and fully withdrawn positions .....	44
Figure 5.3. Four-bar mechanism in three positions .....	44
Figure 5.4. Four-bar mechanism in three positions (forward-undeflected-fully withdrawn) with design parameters .....	45
Figure 6.1. Pseudo-rigid-body model of fixed guided beam [2] .....	48
Figure 6.2. Fully compliant slider-crank mechanism overlapped with its PRBM ..	49
Figure 6.3. Isometric view of the mechanism without fillets.....	50
Figure 6.4. Dimensions of the mechanism without fillets .....	51
Figure 6.5. Isometric view of the mechanism with fillets.....	51
Figure 6.6. Free body diagram of one-half of the beam .....	54
Figure 6.7. Flow chart of the design procedure.....	59
Figure 7.1. Small length flexural hinge dimensions with and without fillets .....	63
Figure 7.2. Flow chart of the analysis.....	64
Figure 7.3. Meshing of the model.....	65
Figure 7.4. Representation of the boundary conditions .....	65
Figure 7.5. Stroke analyses for fully compliant slider-crank mechanism (5° right)	66
Figure 7.6. Stroke analyses for fully compliant slider-crank mechanism (5° left)..	67
Figure 7.7. Stroke analyses for fully compliant slider-crank mechanism (10° right) .....	67
Figure 7.8. Stroke analyses for fully compliant slider-crank mechanism (10° left)	68
Figure 7.9. Stroke analyses for fully compliant slider-crank mechanism (15° right) .....	68
Figure 7.10. Stroke analyses for fully compliant slider-crank mechanism (15° left) .....	69
Figure 7.11. Stroke analyses for fully compliant slider-crank mechanism (20° right) .....	69

Figure 7.12. Stroke analyses for fully compliant slider-crank mechanism (20° left)	70
Figure 7.13. Maximum stress values at compliant segments for fully compliant slider-crank mechanism (20° left)	71
Figure 7.14. Maximum stress values at compliant segments for fully compliant slider-crank mechanism (20° right)	72
Figure 7.15. Number of elements through the thickness vs. maximum von-Mises stress for fixed-guided flexural hinge	74
Figure 8.1. CAD design of the prototype	75
Figure 8.2. Manufacturing process of the prototype	76
Figure 8.3. Experimental setup	76
Figure 8.4. Theoretical and experimental stroke and axis drift data of the fully compliant slider-crank mechanism	79

## LIST OF ABBREVIATIONS

### ABBREVIATIONS

3D	Three Dimensional
CAE	Computer Aided Engineering
CT	Compliant Translational
DOF	Degree of Freedom
FEA	Finite Element Analysis
MEMS	Micro Electromechanical Systems
MPRB	Modified Pseudo-Rigid Body
PRBM	Pseudo-Rigid Body Model
RSSP	Revolute Spherical Spherical Prismatic
SLF	Small Length Flexural

## LIST OF SYMBOLS

### SYMBOLS

$a$	Horizontal component of free end, length of rigid link, angular acceleration, curve fitting parameter, constant
$b$	Vertical component of free end, distance, width, curve fitting parameter, constant
$c$	Distance
$c_\theta$	Parametric angle coefficient
$C_t$	Constant
$d$	Width of connection slot, diameter
$E$	Modulus of elasticity
$F$	Force
$I$	Second moment of area
$K$	Spring constant
$K_\theta$	Stiffness coefficient
$L$	Length
$l$	Length
$M$	Moment
$n$	Horizontal coefficient of applied force, factor of safety
$nP$	Horizontal component of force
$P$	Vertical component of force

$S_y$	Yield strength
$T$	Torque
$t_h$	Thickness of flexural hinge
$w$	Width of flexural hinge
$\hat{x}$	Initial position vector
$\theta$	Pseudo rigid body angle, angular deflection
$\gamma$	Characteristic radius factor, angle of rotation for shafts
$\gamma K_\theta$	Pseudo rigid body constant
$\delta$	Deflection
$\theta$	Angle
$\sigma$	Normal stress
$\phi$	Direction angle of force

# CHAPTER 1

## INTRODUCTION

### 1.1. Compliant Slider-Crank Mechanism Studies in the Literature

Compliant mechanisms have flexible segments instead of rigid joints that also transfer some or all of their motion through deformation of these segments. They have two main categories as partially or fully compliant [1]. Partially compliant mechanisms have at least one traditional (rigid) joint that may cause inherent backlash. By definition, a fully compliant mechanism does not possess a conventional rigid joint. Thus, in fully compliant mechanisms whole motion is obtained from deflection of compliant segments [2]. This property is advantageous for the cases where precision is crucial. Compliant mechanisms have further advantages such as reduced number of parts, low cost, less wear, and no need for lubrication. Additionally, stored elastic energy due to deformation of compliant members returns mechanism to its original position. Pseudo-rigid body model (PRBM) is used to simplify the analysis of systems that undergo large, nonlinear deflections [3]. Yu et al. [4] proposed a new 3 degree-of-freedom (DOF) model based on the PRBM for large deflection beams. In Lui and Yan's study [5] modified pseudo-rigid body (MPRB) modelling approach with fixed guided beam flexurals was examined.

Four link mechanisms (four-bar and slider-crank) have significant importance in the industry. Slider-crank mechanisms have numerous applications especially when kinematic inversions are considered. To the best of our knowledge, studies on compliant slider-crank mechanisms are very limited in the literature. In this part we will focus on the studies about compliant slider-crank mechanisms.

Hao et al. [6] proposed a multi-mode compliant gripper with a compliant slider-crank mechanism pair. In Alqasimi et al.'s study [7], a new model for a bistable compliant mechanism with crank-slider mechanism was presented. In Pardeshi et al.'s study [8], for motion amplification purpose, monolithic compliant slider-crank mechanism was proposed. Dao and Huang proposed an optimal design of a flexible slider-crank mechanism with flexure hinges that have circular cross-section [9].

Furthermore, there are some compliant mechanism studies based on linear-motion in the literature. Pavlovic' and Pavlovic' [10] introduced compliant parallel-guiding mechanism's design procedure. A new compliant mechanism which can realize the link's axial translation was presented. An inherent parasitic motion of the compliant parallel four-bar mechanism was compensated by exploiting center shift of a generalized cross-spring pivot in Zhao et al.'s study [11]. Zhao et al. [12] designed a stiffness-adjustable compliant linear-motion mechanism.

There are some studies [13], [14] on spatial compliant mechanisms that possesses out of plane motions. The compliant version of very common spatial slider-crank mechanism, shown in Figure 1.1, RSSP has been proposed by Parlaktaş and Tanık [14]. In this study, all possible configurations of novel partially compliant spatial RSSP mechanisms were classified and discussed. A method was derived for determination of the deflection of the flexural. By this way, deflection values or all crank positions were obtained. A design procedure for this mechanisms was introduced. To show the feasibility of the proposed mathematical model, a prototype was built. Finally, analytical and experimental results were compared to show the consistency.

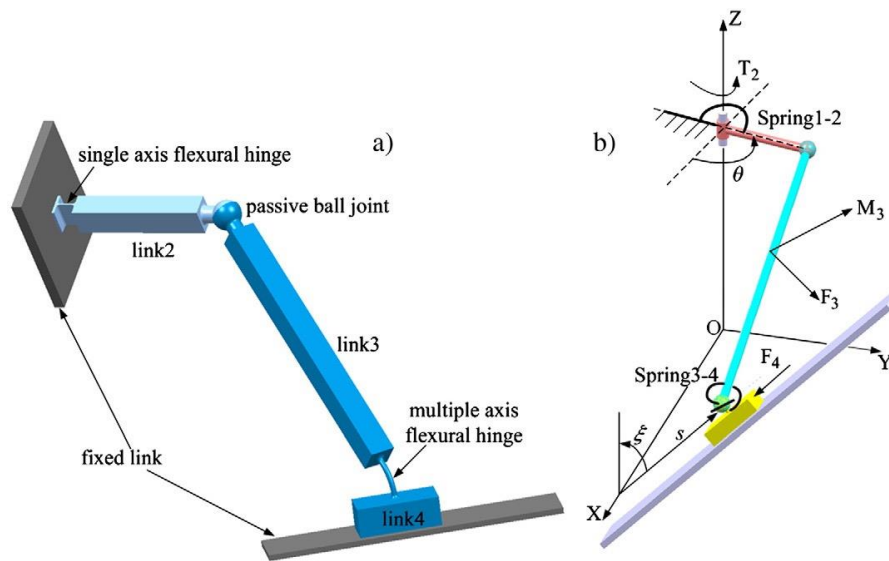


Figure 1.1. Partially compliant RSSP mechanism and its PRBM [14]

In another study of the same authors, “single piece” compliant spatial slider-crank mechanism shown in Figure 1.2 was proposed [15]. In the previous study [14], the spatial slider-crank mechanism that is “partially compliant” was introduced. There was no torsional loading because of a rigid ball joint. However, there was no ball joint for the case that is single piece. Accordingly, multiple axis flexural hinges had torsional loading. The design procedure of this compliant mechanism is different from the partially compliant one. In this study, bending and twist of the multiple axis flexural hinges were determined separately. To manufacture a mechanism fundamental angles were obtained. A prototype was built to verify and the results with the experiments. A fatigue test was performed. There was no failure indication after one and half million cycles.

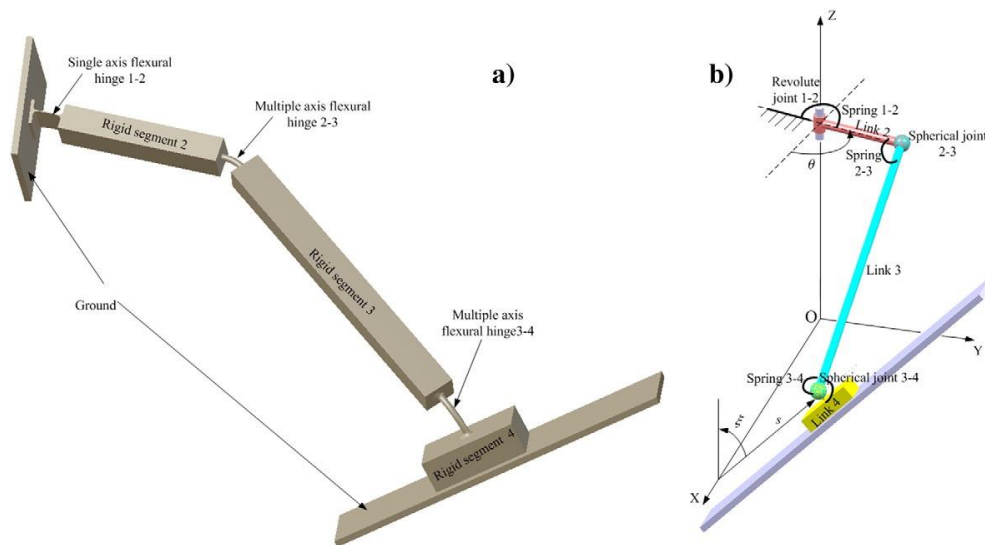


Figure 1.2. Single piece compliant slider-crank and its PRBM [10]

The transmission angle of a compliant slider-crank mechanism shown in Figure 1.3 was introduced by Tanik [16]. The transmission angle is an important parameter to indicate the quality of motion transmission. However, there was no study in the literature about transmission characteristics of compliant mechanisms. In this study two theorems were proposed to show transmission angle similarity conditions of the compliant slider-crank and its rigid body counterpart. A prototype was manufactured to verify one of these theorems experimentally. Finally, the discussion of eccentric slider effect on motion transmission quality was done.



Figure 1.3. Manufactured partially compliant slider-crank mechanism [16]

Another study about compliant slider-crank mechanism is Erkaya et al.'s study [17]. In this paper numerical and experimental approaches were investigated. The effects of joint clearance were analyzed both on articulated and partially compliant mechanisms. The main contribution of small flexural pivot having joint clearance was investigated. For that purpose, bearings' and links' vibrations were considered. To measure the vibrations five accelerometers were located as shown in Figure 1.4. The results had been showed that performance of the mechanism is not good because of the joint clearance. To minimize the effects of the joint clearance, the suspension effects of flexural pivot were used.

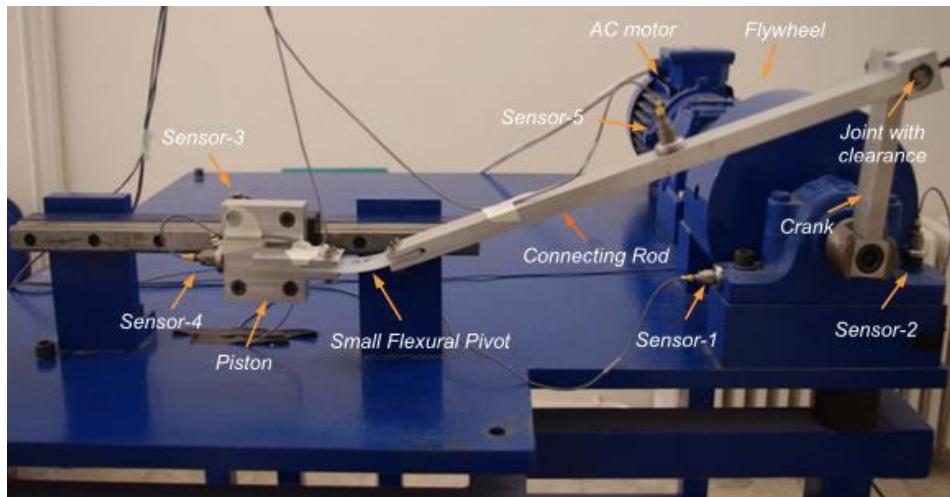


Figure 1.4. Representation of experimental test rig [17]

Erkaya et al.'s second study investigated the dynamics of a partially compliant mechanism with joint clearance [18]. A spatial slider-crank mechanism shown in Figure 1.5 was used as an example. The kinematic and dynamic performances of compliant mechanisms and traditional ones were compared. To have mobility between piston and connecting rod links a multi-axis SLF pivot was used. To simplify the analysis, PRBM was used to obtain the mathematical model of compliant mechanism. The results showed that chaotic behavior on the outputs of the mechanism was because of the clearance in joints.

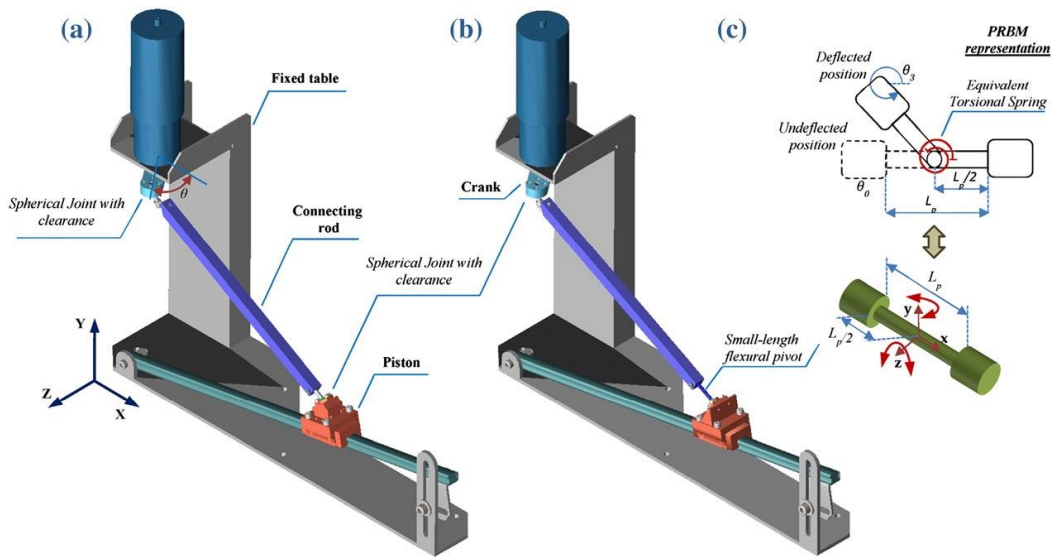


Figure 1.5. Model mechanisms: (a) classical articulated slider–crank mechanism, (b) partly compliant slider–crank mechanism, and (c) small-length flexural pivot

[18]

## 1.2. Compliant Translational Joint Studies in the Literature

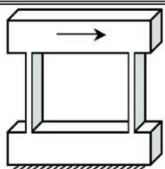
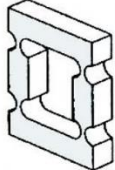
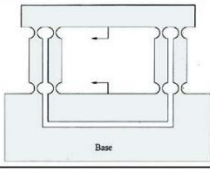
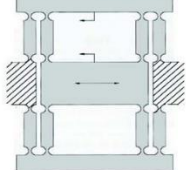
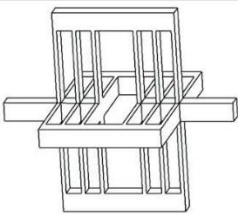
Rigid joints, like sliders, hinges, ball joints, and Hooke’s joints have different degrees of freedom. However, in rigid joints assemblies backlash problem arises because of the clearance between mating parts [19]. In traditional joints increased clearance and wear are main problems hence, there is relative motion that causes friction. Rigid joints suffer from poor accuracy and repeatability because of backlash and wear issues. Therefore, researchers try to develop new compliant joints to provide large-displacement.

Trease et al. proposed a translational and a rotational compliant joint [19]. They developed analytic stiffness equations for each joint. To verify superior stiffness properties, they used parametric computer models. A design chart was presented based on the parametric models that allows rapid sizing of the joints for particular performance. Range of motion of a joint had been calculated with FEA, where stress concentration effects included.

A parallel four-bar forms most of the translational joints. Flexibility of these joints is derived from leaf springs Table 1.1 (a) or notch joints Table 1.1 (b). The compound four-bar joints in Table 1.1 (c) and (d) delivered a larger range of straight-line motion. The range of all four joints was limited whereas they had acceptable off-axis stiffness. The proposed compliant translational joint was shown in Table 1.1 (e).

Table 1.1. Benchmarked flexible translational joints ‘-: poor, 0: normal; +: good’

[19]

		Range of Motion	Axis Drift	Stress Concentration	Off-Axis Stiffness	Compactness
(a)		0	-	0	0	+
(b)		-	-	-	0	+
(c)		-	0	-	0	+
(d)		-	+	-	0	+
(e)		+	+	+	+	+

The compliant translational (CT) joint, shown in Figure 1.6, had been proposed as a new improvement of the joint that is called as leaf spring joint. Leaf spring joints suffer from off-axis stiffness, deviation from straight-line motion, and limited range of motion.

The (CT) joint had been presented in Trease et al.'s paper was modeled and analyzed with analytical and CAE methods as appropriate. The design charts were presented. It was based on parametric analyses, and sizing of the joints for various applications.

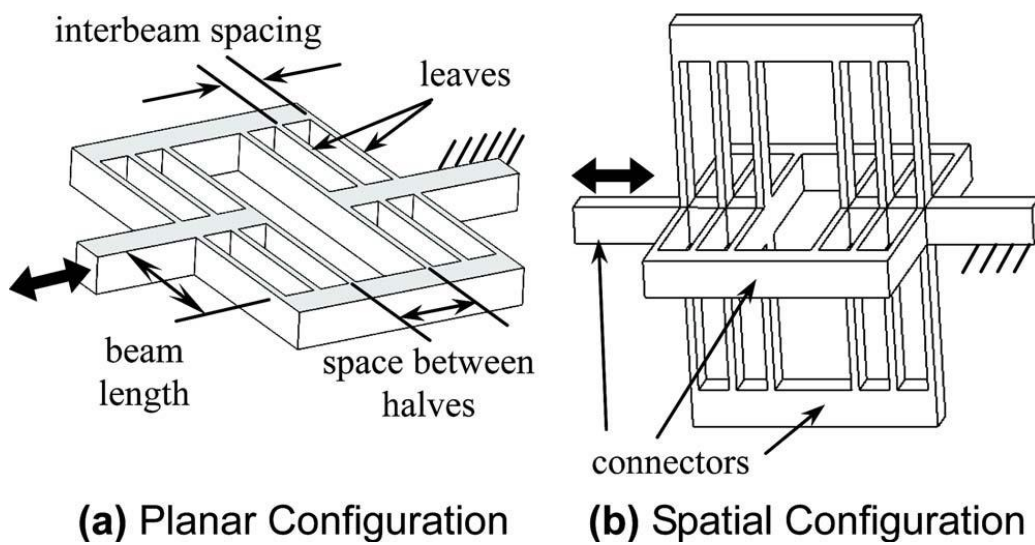


Figure 1.6 CT joint conceptual designs [19]

Another design of a compliant translational joint was presented in Yang et al.'s study [20]. Their design had small axis drift and large stiffness ratio. The characteristics of leaf-spring type compliant translational joints were investigated. Different types of constructions shown in Figure 1.7 were analyzed. A novel 3D compliant translational joint was proposed to conduct the analysis. A design optimization was employed via FEA. Then, a real model of the optimized design was fabricated by rapid prototyping, and experiments were conducted. Experimental and numerical results were compared to verify the design requirements.

It has been proposed that the geometry and material parameters (beam spans, number of beams, length, thickness, and width). Therefore, analysis of the influence of the

design parameters on the stiffness of the structure was an important procedure for sizing new mechanisms.

To evaluate the performance of the four types of constructions, 3D construction was built for each configuration in Figure 1.7.

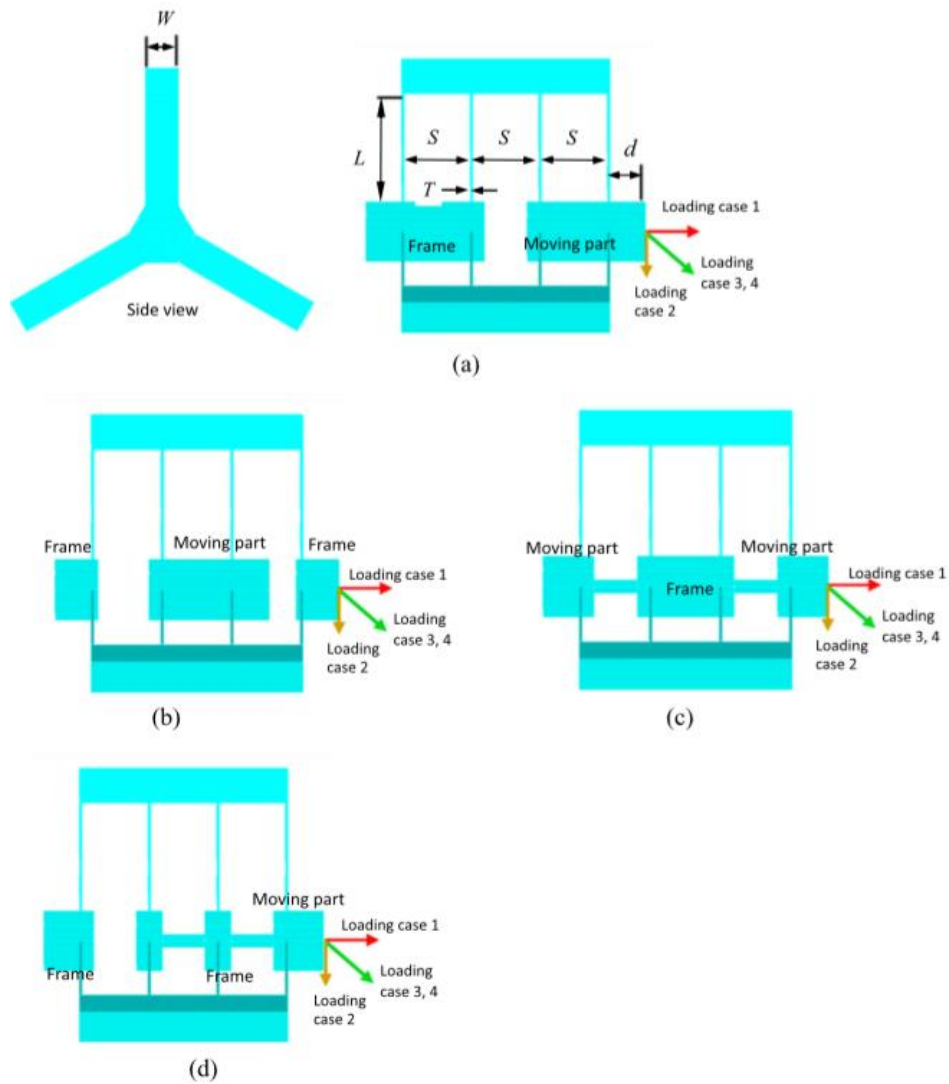


Figure 1.7 Three-dimensional constructions for the figures in (a) Type 1 (b) Type 2 (c) Type 3 (d) Type 4 [20]

To choose the best performing one FEA were conducted. Table 1.2 shows the simulation result. From the results, Type 4 shown in Figure had been chosen for

further design analysis. Figure 1.8 shows the joint's solid model.

Table 1.2. Comparison of Stiffness ratios for the configurations in Figure 1.7 [20]

	Configuration	Type 1	Type 2	Type 3	Type 4
Loading case 1	Axial disp. (mm)	4.832	4.831	4.833	4.91
Loading case 2	Off-axis disp. (mm)	-0.1102	-0.0149	-0.1562	-0.1156
	Stiffness ratio	43.8	324.2	30.94	42.47
Loading case 3	Axial disp. (mm)	4.921	4.857	4.862	4.934
	Off-axial disp. (mm)	-0.2228	-0.0557	-0.1956	-0.1487
	Stiffness ratio	22.08	87.1	24.86	33.18
Loading case 4	Axial disp. (mm)	9.879	9.476	9.558	9.646
	Off-axial disp. (mm)	-0.9372	-0.2028	-0.5393	-0.4026
	Stiffness ratio	10.54	46.72	17.72	23.96

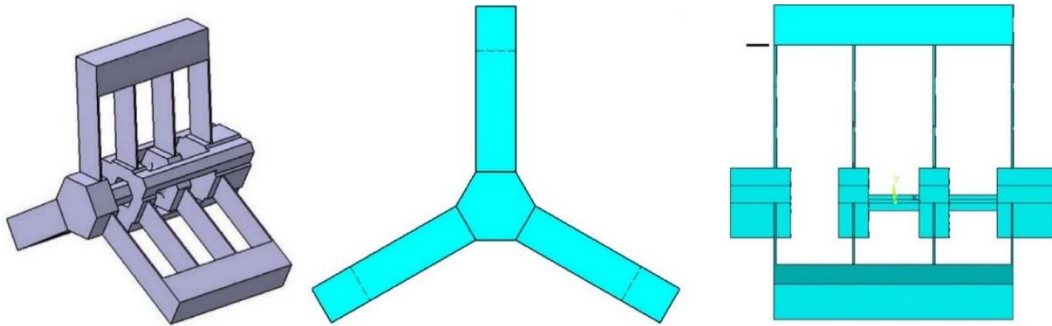


Figure 1.8 (a) A solid model for the spatial compliant translational joint, (b) and (c) geometric parameters of the spatial compliant translation joint [20]

Finally, experimental setup was built to obtain the performance of the design. It was verified that the difference between simulated data and experimental stiffness ratios was in an acceptable range.

### **1.3. Objective and Scope of the Thesis**

Partially compliant mechanisms possess prismatic joints (slider) in their structure. Prismatic joints inherently have disadvantages due to backlash and friction problems. On the contrary, fully compliant mechanisms offer no backlash which is a valuable property for the cases where high precision is required. In this study our main aim is to propose a fully compliant slider-crank mechanism that performs large stroke.

To the best of our knowledge, this is the first complete study on a fully compliant slider crank mechanism with a presented generalized design procedure. An approach for optimum link proportions of the rigid body equivalent is proposed. The optimization objective is to maximize the translational motion of the slider equivalent while minimizing the relative link rotations. Minimization of link rotations is essential to keep maximum stresses in an acceptable range for the compliant counterpart. Input-output motion relationship of the mechanism is determined. Resultant stresses at flexural hinges are determined analytically. A design table is prepared for generalization of the dimensions that will be beneficial for other researchers. As a case study, an optimum mechanism is analyzed via finite element analysis (FEA) method and analytical results are verified. A real model is manufactured and experiments are conducted. As well, it is ensured that the results of experiments are consistent with the theoretical approaches.

### **1.4. Outline of the Thesis**

Outline of the thesis as follows.

Chapter 2, Compliant Mechanisms: A review of compliant mechanisms is done. PRBM is briefly explained. Deflection and stress equations are derived.

Chapter 3, The Proposed Fully Compliant Slider-Crank Mechanism: PRBM of fully compliant parallel- guiding mechanism is displayed.

Chapter 4, Kinematic Analysis of the Cascade Parallelogram Four-Bar Mechanism: Kinematic analysis of the PRBM is performed. A novel kinematic analysis approach for the PRBM is proposed.

Chapter 5, Design Approach of the Rigid Body Equivalent of the Compliant Slider-Crank Mechanism: The design approach targets three main objectives. In this part these objectives are discussed. And then the design of the rigid body equivalence is performed considering these three objectives.

Chapter 6, Design of the Fully Compliant Slider-Crank Mechanism: By using the rigid body replacement method, the fully compliant slider-crank mechanism is dimensioned. The summary of the design procedure of the fully compliant slider-crank mechanism is presented in Table 6.1.

Chapter 7, Finite Element Analysis: After the analytical design stage, solid model of the mechanism is constructed. Then FEA method is employed by using ANSYS® to compare theoretical and numerical results.

Chapter 8, Experimental Analysis of the Fully Compliant Slider-Crank Mechanism: A real model of the mechanism is built for collecting experimental data. We compared the theoretical and experimental values.

Chapter 9, Conclusions: The summary of the study is presented. Key findings and outcomes of the study are given, and further recommendations are made.

## CHAPTER 2

### COMPLIANT MECHANISMS

#### 2.1. Introduction to Compliant Mechanisms

A mechanism is a mechanical device used to transfer or transform motion, force, or energy. Rigid-link mechanisms gain their mobility from the movable joints [21].

Compliant mechanisms have flexible segments instead of rigid joints. As in rigid mechanisms, compliant mechanisms also transfer or transform force or motion. However, contrary to rigid ones, compliant mechanisms consist flexible segments instead of rigid joints. Compliant mechanisms are divided into two categories as fully or partially compliant. Whole motion of fully compliant mechanisms is obtained from the deflection of compliant members. Whereas, partially compliant mechanisms contain one or more rigid joints along with compliant members [2].

The advantages of compliant mechanisms can be divided into two subgroups: cost reduction and increased performance. Compliant mechanisms have fewer parts. Some special mechanisms may be produced even as a single piece from injection-moldable material. The dramatic reduction in part count may reduce assembly time and increase production rate. As a result, it is possible to decrease manufacturing costs with compliant mechanisms. Less assembly time also requires fewer assemble stages and assembling devices. Furthermore, fewer parts may also reduce the mass of the mechanism so the required material for manufacturing.

Compliant mechanisms use flexural segments instead of rigid joints. Rigid joints wear and require maintenance such as lubrication. Especially in harsh environment maintenance may not be possible. Flexural joints do not require any maintenance.

The wear in a rigid joint also adversely effects precision of the mechanisms. Flexural joints reduce or eliminate backlash. Furthermore, vibration and noise can be reduced by flexural joints. As a result, compliant mechanisms may be used instead of rigid mechanisms for operations where precision is important.

An important advantage of compliant mechanisms is the ease with which they are miniaturized. Simple microstructures, actuators, and sensors are seeing wide usage, and many other micro electromechanical systems (MEMS) show great promise.

Another special property of compliant mechanism is the energy storage characteristic. Because the compliant mechanisms move by flexural joints, strain energy is collected on flexural members. The stored strain energy can then be released and used for different manners. For example, any mechanism may return to its rest position using its stored energy without using an external source. Another example is bow-and-arrow. Energy is stored along the limbs and released instantly in order to throw an arrow. Furthermore, stored strain energy may be used to decrease input torque.

Although compliant mechanisms have numerous advantages, there are still some challenges. One of the most important challenge is the difficulty of designing and analyzing compliant mechanisms [2]. Flexural members make it harder to design and analyze compliant mechanisms compared to rigid ones. Flexural members increase complexity of mechanisms. Knowledge of different areas such as solid mechanics, mechanism analysis and synthesis, material sciences etc. is a necessity. Furthermore, many of the flexural members undergo large deflections. For this reason, linearized beam deflection equations are insufficient for compliant mechanism analysis and synthesis. In the past it was common to design compliant mechanisms by trial and error. Although, there are new theories recently, it is still a big challenge to design a compliant mechanism.

Energy storage on flexural segments is also a disadvantage of the compliant mechanisms. When transferring energy from input link to output link, all of the energy is not transferred and some of the energy is stored on flexural members.

Another disadvantage of the compliant mechanisms is fatigue sensitivity. Since flexural segments are exposed to cyclic loads most of the time, a proper fatigue analysis is required. Fatigue life of the mechanism should be estimated for performing prescribed functions. Furthermore, strength of the flexing member may also be a limiting property for the expected motion.

Finally, it should be noted that, a compliant link cannot provide a full or continuous rotation like links that have rigid revolute pinned joints.

## 2.2. Flexibility and Deflection

### 2.2.1. Stiffness and Strength

Deformation of a material under a certain load is related its stiffness. Stiffness affects the amount of deformation of a material under a certain load. On the other hand, strength defines the maximum stress that material can withstand without failure [2].

Stiffness is function of both material's mechanical properties and geometry of the structure.

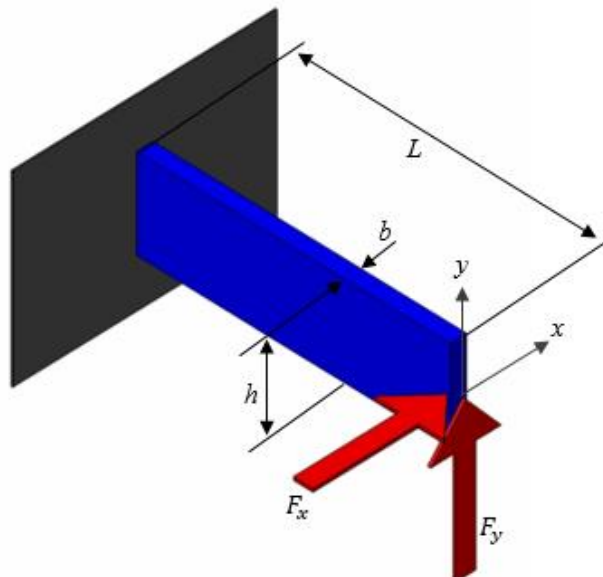


Figure 2.1. Cantilever beam with end forces

The stiffness of a structure for bending is expressed by  $EI$  while for axial loading it is expressed by  $EA$ , where  $E$  is the modulus of elasticity,  $I$  is the cross-sectional moment of inertia and  $A$  is the cross sectional.

According to Figure 2.1, the material of the cantilever beam is isotropic. If a force applied in x-direction ( $F_x$ ) the deformation along x-axis is defined as:

$$\delta_x = \frac{2\sigma_y L^2}{3Eb} \quad (2-1)$$

Where  $\sigma_y$  is the yield strength of the material.

Similarly deformation along y-axis caused by  $F_y$  is defined as:

$$\delta_y = \frac{2\sigma_x L^2}{3Eh} \quad (2-2)$$

Combining Equation (2-1) and (2-2) one can obtain:

$$\delta_x = \frac{h}{b} \delta_y \quad (2-3)$$

Equation (2-3) shows that structures which have the same strength in all directions, may have different stiffness in different directions. Stiffness and strength are not necessarily relevant. In some cases, it may be possible to prevent failure by decreasing the stiffness.

### **2.2.2. Flexibility**

Flexibility defines bending capability of the materials opposed to the stiffness. Flexibility of a member may be changed by changing the material type or geometry of the member.

Deflection ( $\delta$ ) in linear range can be expressed as:

$$\delta = 4F \frac{1}{E} \frac{L^3}{bh^3} \quad (2-4)$$

Equation (2-4) shows that deflection of a beam is function of force ( $F$ ), materials mechanical property ( $1/E$ ) and, geometry ( $L^3/bh^3$ ).

Flexibility and ductility may be confusing. Although these terms look similar, both defines different properties. For example, glass is not a ductile material but it may become flexible by decreasing the thickness.

### 2.2.3. Material Selection in Compliant Mechanisms

The main criterion for material selection is the modulus of elasticity of the material and the geometry. Maximum deflection of the member can be achieved by the maximizing the ratio between strength and modulus of elasticity of the material [2].

The maximum deformation of a beam is defined as ( $\delta_{max} = \frac{2 S_y L^2}{3 E h}$ ).

According to Table 2.1 modulus of elasticity of alloy materials are nearly constant. Furthermore, yield strength may vary dramatically depending on their alloy and manufacturing processes. Increasing the yield strength of a material also makes the material more brittle.

Among the tabulated data Polypropylene has the highest  $\sigma/E$  ratio. This ratio indicates that Polypropylene is one of the most suitable material for compliant mechanisms. Despite its low yield strength polypropylene is very suitable material for many applications by its low cost and high fatigue strength.

Table 2.2. Ratio of Yield Strength to Young's Modulus for Several Materials[2]

<b>Ratio of yield strength to Young's modulus for several materials</b>			
<b>Material</b>	<b><math>E</math> (GPa)</b>	<b><math>S_y</math> (MPa)</b>	<b><math>(S_y/E) \times 1000</math></b>
Steel (1010 hot rolled)	207	179	0.87
Steel (4140 Q&TQ@400)	207	1641	7.9
Aluminum (1100 annealed)	71.7	34	0.48
Aluminum (7075 annealed)	71.7	503	7.0
Titanium (Ti-35A annealed)	114	207	1.8
Titanium (Ti-13 heat treated)	114	1170	10
Beryllium copper (CA170)	128	1170	9.2
Polycrystalline silicon	169	930	5.5
Polyethylene (HDPE)	1.4	28	20
Nylon (type 66)	2.8	55	20
Polypropylene	1.4	34	25
Kevlar (82 vol%) in epoxy	86	1517	18
E-glass (73.3 vol %) in epoxy	56	1640	29

#### **2.2.4. Pseudo-Rigid-Body Model**

PRBM is an easy way to analyze and design compliant mechanisms. According to this approach the compliant mechanism is replaced with a rigid mechanism which can simulate the compliancy of the mechanism by torsional springs at the joints. The

compliant mechanism now can be analyzed similar to rigid ones after the replacement [2].

A methodology for compliant mechanism design that uses a PRBM of the compliant mechanism with compliance modeled by torsional and linear springs is introduced [22]. Idealized models require FEA or elliptic integral solutions however PRBM is much easier to analyze. The most important attribute of the PRBM is ability in simplifying the design process.

Closed-formed elliptic-integral solutions are used to develop deflection approximations for an initially straight, flexible segment with linear material properties [23], [24].

#### **2.2.5. Small-Length Flexural Pivots**

If a small segment of a beam is noticeably thinner compared to rest of the beam the deflection takes place at this zone when an end moment or a force is applied to the beam in Figure 2.2 and this thinner segment called as small-length flexural pivot. Usually length of small segment is 10 or more times shorter that the rest of the beam length [2].

$$L \gg l \quad (2-5)$$

$$(EI)_L \gg (EI)_l \quad (2-6)$$

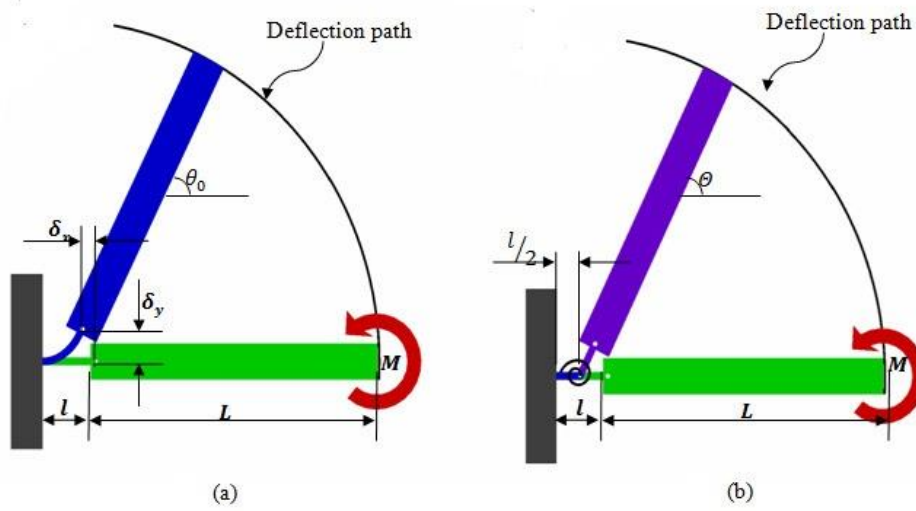


Figure 2.2. Cantilever beam (a) and its Pseudo-Rigid-Body Model (b)

For the flexible segment with end moment loading the deflection equations are derived as follows [2]:

$$\theta_0 = \frac{Ml}{EI} \quad (2-7)$$

$$\frac{\delta_y}{l} = \frac{1 - \cos\theta_0}{\theta_0} \quad (2-8)$$

$$\frac{\delta_x}{l} = 1 - \frac{\sin\theta_0}{\theta_0} \quad (2-9)$$

To model SLF pivots these equations could be used with PRBM. Figure 2.2 shows a member and its PRBM. The model consists of two rigid equal links that are connected with a characteristic pivot. The stiffness of beam is modeled by a torsional spring and the displacement is represented with a characteristic pivot. An accurate solution is obtained with this model gives the deflection path of the beam end under a given end load.

The angle of pseudo rigid link is the pseudo rigid body angle,  $\theta$  that is equal to the beam end angle for small-length flexural pivots.

$$\theta = \theta_0(\text{small-length flexural pivots}) \quad (2-10)$$

The  $x$  and  $y$  coordinates of the beam's end ( $a$  and  $b$ , respectively) are approximated as [2]:

$$a = \frac{l}{2} + \left(L + \frac{l}{2}\right) \cos \theta \quad (2-11)$$

$$b = \left(L + \frac{l}{2}\right) \sin \theta \quad (2-12)$$

Or, expressed in non-dimensional form [2],

$$\frac{a}{l} = \frac{1}{2} + \left(\frac{L}{l} + \frac{1}{2}\right) \cos \theta \quad (2-13)$$

and,

$$\frac{b}{l} = \left(\frac{L}{l} + \frac{1}{2}\right) \sin \theta \quad (2-14)$$

To model the beam's resistance to deflection a torsional spring with spring constant  $K$  is used. The required torque to deflect the torsional spring at an angle  $\theta$  is [2]:

$$T = K\theta \quad (2-15)$$

$K$  (spring constant) could be found from the elementary beam theory. For a beam with an end moment, the end angle is [2]:

$$\theta_0 = \frac{Ml}{(EI)_l} \quad (2-16)$$

Rearranging to solve for  $M$  results in [2]:

$$M = \frac{(EI)_l}{l} \theta_0 \quad (2-17)$$

Since  $M = T$  and  $\theta = \theta_0$ , the spring constant can be found as [2]:

$$K = \frac{(EI)_l}{l} \quad (2-18)$$

This model is more accurate for bending dominant cases than transverse and axial loading dominant cases. This simple model has an advantage for pure bending. Since no assumptions about small deflection are made in their derivation, equations are accurate even for large deflections.

As seen in the Figure 2.3 a force deforms the beam. Assuming the magnitude and direction of the force is known, vertical and horizontal components can be determined using  $\phi$  with respect to beam. It should be noted that this force is a nonfollower force which means that the direction of force remains constant regardless of the deflection of the beam. This force ( $F$ ) can be defined with its components as [2]:

$$F = P\sqrt{n^2 + 1} \quad (2-19)$$

$$\phi = \text{atan} \frac{1}{-n} \quad (2-20)$$

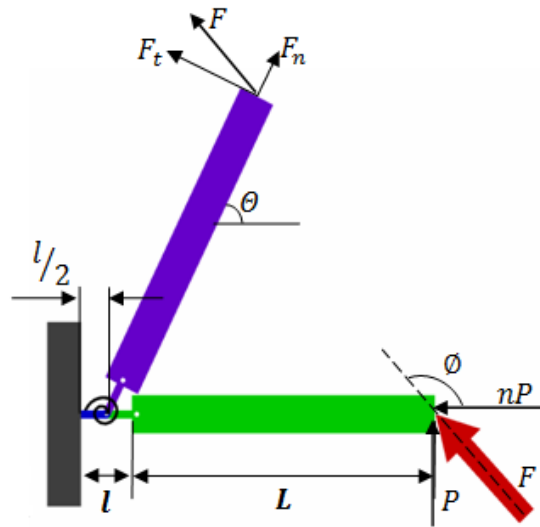


Figure 2.3. Cantilever beam (a) and its Pseudo-Rigid-Body Model (b)

At the any deformed position effective force can be separated into its vertical and horizontal components with respect to the beam position. The vertical component of the force  $F_t$  creates a moment at the torsional spring which can be defined as [2]:

$$T = F_t(L + \frac{l}{2}) \quad (2-21)$$

Since  $F_t$  is the main driving force of the deformation, it is called as *active force*. On the other hand since the horizontal component of the force ( $F_n$ ) does not contribute to the deflection, it is called as *passive force*. The active and the passive forces change during the deformation as long as the angle of affecting force ( $F$ ) remains constant. Then the active force is [2],

$$F_t = F \sin(\phi - \theta) \quad (2-22)$$

### 2.2.6. Moment at the Free End

The flexible beam with an end moment at its free end is shown in Figure 2.4.

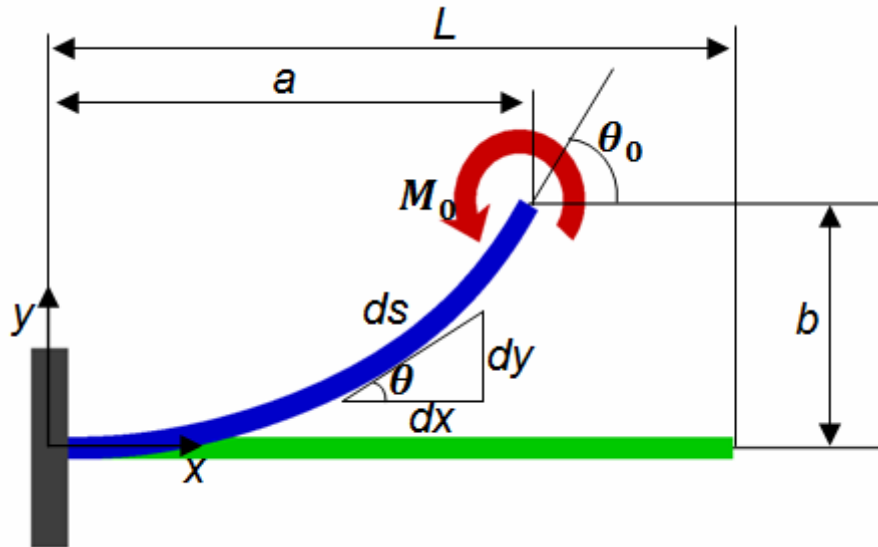


Figure 2.4. Flexible Beam with a Moment at the Free End

The coordinates of the free end, maximum normal stress value and angle of the beam end are determined as [2].

$$a = l[1 - 0.7346(1 - \cos\theta)] \quad (2-23)$$

$$b = 0.7346l\sin\theta \quad (2-24)$$

$$\theta_0 = 1.5164\theta \quad (2-25)$$

$$\sigma_{max} = \frac{M_0 c}{I} \quad (2-26)$$

### 2.2.7. Fixed Guided Beam

A beam that is fixed at one end; the other end goes through a deflection such that the angular deflection at the end remains constant, and the beam shape is antisymmetric about the center. This type of beam occurs in parallel motion mechanisms and it is called fixed guided beam.

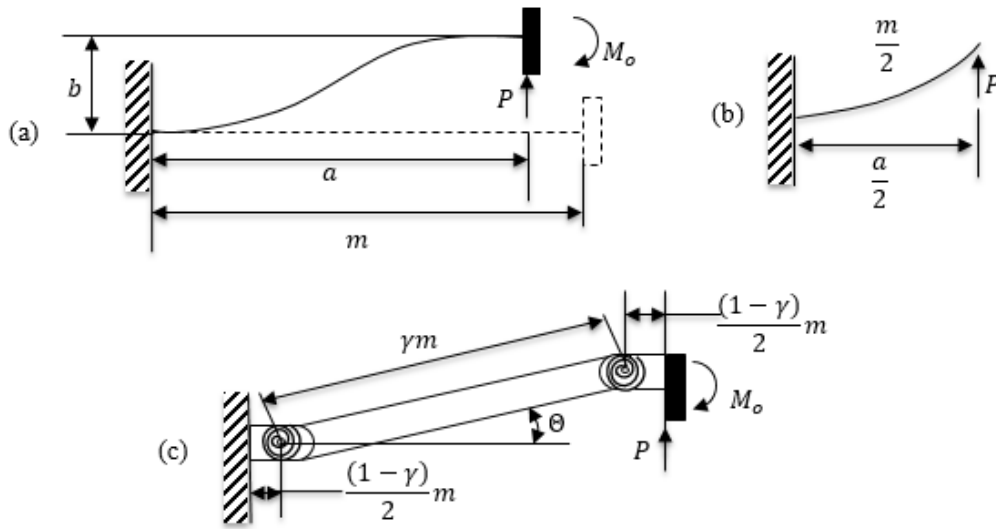


Figure 2.5. (a) Flexible beam with a constant end angle, (b) free-body diagram of the half beam, and (c) pseudo-rigid-body model [2]

The Bernoulli-Euler assumption states that the moment is directly proportional to the curvature, which implies that the moment is also zero at mid-length. If there is no moment at the midpoint, the free-body diagram for one-half of the flexible member is as shown in Figure 2.5. The half-beam only has a force at the end, so it is similar to the flexible segment with a force at the free end. The pseudo-rigid-body model of the half is then the same as discussed previously, only half the beam length is used. A pseudo-rigid-body model of the entire segment may be derived by combining the two antisymmetric one-half beams as shown in Figure 2.5. The value of the characteristic radius factor,  $\gamma$  for  $n = 0$  &  $\phi = 90^\circ$  [2]:

$$F_t = F \sin(\phi - \theta) \quad (2-27)$$

with a parameterization limit of [2]

$$\theta_{max} = 64.3^\circ \quad (2-28)$$

for the flexible beam with a constant end angle and the corresponding pseudo-rigid-body model in Figure 2.5, the parametric angle coefficient,  $c_\theta$  is trivial [2],

$$c_\theta = 0 \quad (2-29)$$

Another equation is needed to predict the reaction moment  $M_o$ , that is required to maintain a constant end angle. Summing moments at either end of the free-body diagram in Figure 2.5 yields [2],

$$Pa - M_o = \frac{Pa}{2} \quad (2-30)$$

Or

$$M_o = \frac{Pa}{2} \quad (2-31)$$

Substituting for  $a$  results in [2],

$$M_o = \frac{Pl}{2} [1 - \gamma(1 - \cos\theta)] \quad (2-32)$$

$$(\alpha^2)_t = 2K_\theta\theta \quad (2-33)$$

for each of the two spring. The torsional spring constant,  $K$ , for the springs is [2]:

$$K = 2\gamma K_\theta \frac{EI}{l} \quad (2-34)$$

Since each spring is twice as stiff as the springs of a fixed-free beam, and there are two springs, this segment is four times as stiff as a segment of the same length with fixed-free end conditions. This is consistent with small-deflection beam theory.

The maximum stress occurs at the beam ends where the maximum moment occurs and has a value of [2]:

$$\sigma_{max} = \frac{Pac}{2I} \text{ (at both ends of the beam)} \quad (2-35)$$

Where  $c$  is the distance from the neutral axis to the outer surface of the beam.

### 2.2.8. Pseudo-Rigid Body Replacement

Transforming a compliant mechanism into its PRBM is an important stage in compliant mechanisms analysis. On the other hand, sometimes it is necessary to transform a rigid mechanism to its compliant counterpart. For both situations there are some basic steps for performing these transformations [2].

When transforming a compliant mechanism with small length flexural segments to its rigid body counterpart, characteristic pivot is placed in the center of flexural segment. The torsional spring which simulates the resistive force created by deformation is placed on the characteristic pivot. The distances between joints remain constant during these transformation.

For the compliant mechanisms which includes flexing cantilever beam, the transformation procedure differs from small length flexural segment. There is a linear relationship between flexural segment and rigid link length [2].

$$a = \gamma l \quad (2-36)$$

Where  $a$  is length of the rigid link and  $l$  is the length of the compliant link [2]. The characteristic radius factor value changes according to  $n$  values.

In Figure 2.6 a four bar and slider crank mechanism's pseudo-rigid-body replacements are shown. In both mechanisms the black mechanism represents compliant mechanism and grey one is its pseudo-rigid-body model.

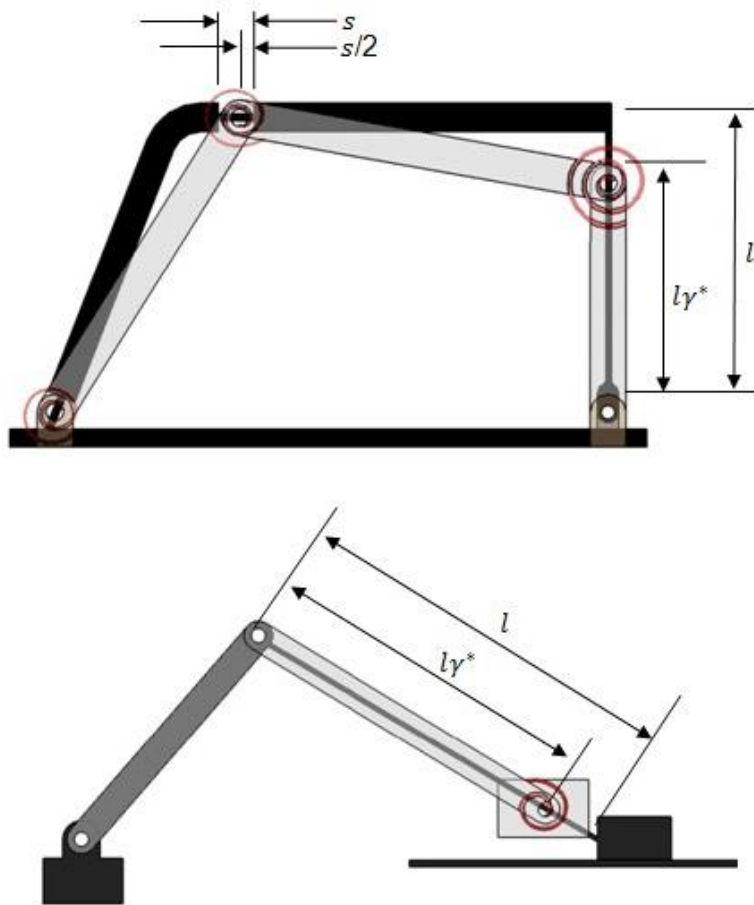


Figure 2.6. A Compliant Four-Bar and Slider-Crank Mechanism and Pseudo Rigid Body Models

## CHAPTER 3

### THE PROPOSED FULLY COMPLIANT SLIDER-CRANK MECHANISM

In the literature, there are studies on partially compliant slider-crank mechanisms that possess rigid prismatic joints (slider) in their structure. However, to the best of our knowledge, this is the first study on a fully compliant slider-crank mechanism. An approach for optimum link proportions of the rigid body equivalent is proposed. The optimization objective is to maximize the translational motion of the slider equivalent while minimizing relative link rotations. Minimization of link rotations is essential to keep maximum stresses at flexible hinges in an acceptable range. Input-output motion relationships of the mechanism are determined. Resultant stresses at flexural hinges are determined analytically. A design table is prepared for generalization of the dimensions that will be beneficial for other researchers. As a design example, an optimum mechanism is analyzed via FEA method and analytical results are verified. A real model is manufactured and experiments are conducted. Also, it is ensured that the results of experiments are consistent with the theoretical approaches.

In Figure 3.1.a, a partially compliant slider-crank mechanism that possesses a prismatic joint between the slider and ground is presented. In our design, we replaced the prismatic joint by two identical and parallel compliant segments and a rigid segment as shown in Figure 3.1.b. By this way, if properly designed, translational motion at the output which acts as a slider can be achieved. Alternatively, compliant version of Roberts or Watt [21] type four bar mechanisms can be implemented for slider replacement. Specific points on coupler link of these mechanisms trace an approximate straight line. However, their coupler link performs rotation as well as translation. In our case, the output link performs no rotation but only translation (curvilinear translation). In the literature, paired double parallelogram mechanisms are used as sliders [19], [25]. The advantage of this structure is straight line motion

with no rotation. However, there is a major disadvantage; if PRBM of this type of mechanism is constructed, it can be calculated that  $DOF < 0$ . This case yields no mobility. However, compliant version of this mechanism moves with axial deformation of compliant segments as well as bending. This property increases the stresses, therefore decreases stroke of the mechanism dramatically. Our major concern in this study is to increase the stroke as much as possible and keep the stresses in an acceptable range.

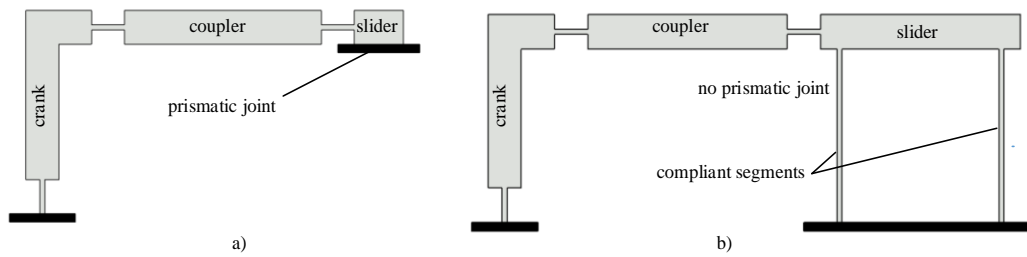


Figure 3.1. a) Partially compliant slider-crank with prismatic joint b) proposed fully compliant slider-crank

PRBM of this fully compliant slider-crank mechanism is displayed in Figure 3.2.a. The PRBM is essentially a six-link mechanism, where first of the two movable links from the left are connected to a parallelogram four-bar mechanism. The coupler link of this parallelogram four-bar acts as a slider, if the fixed guided segments 1 and 2 are long enough and rigid segment 4 stays parallel to its initial position in Figure 3.2.b. These fixed guided segments must be identical, initially straight and parallel to each other. By this way, we obtain a compliant parallel-guiding mechanism [2] where rigid segment 4 performs curvilinear translation. In the case of an extreme downward loading, fixed guided segments may buckle which makes rigid segment 4 nonparallel to its initial position.

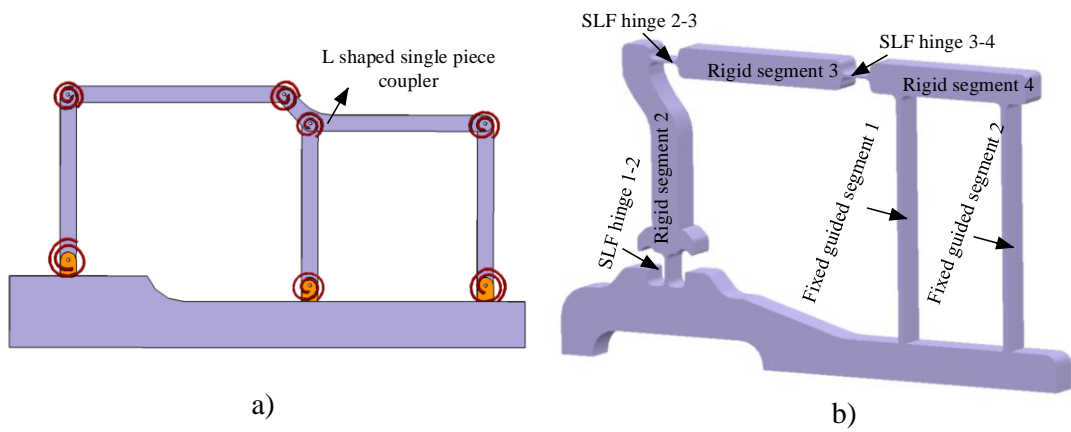


Figure 3.2. a) PRBM b) isometric view of the mechanism whose slider is composed of fixed guided compliant segments



## CHAPTER 4

### KINEMATIC ANALYSIS OF THE CASCADE PARALLELOGRAM FOUR-BAR MECHANISM

#### 4.1. Kinematic Analysis

Initially, kinematic analysis of the PRBM, which is essentially a rigid cascade parallelogram four-bar mechanisms is performed. The PRBM in Figure 4.1 is formed as follows: input (link 2) and connecting rod (link 3) of the mechanism are combined with a parallelogram four-bar mechanism whose coupler link (link 4) acts as a slider of the fully compliant slider-crank mechanism in Figure 3.2.b.

Kutzbach criterion [21] for DOF of a planar mechanism is  $N = 3(l - 1) - 2j_1 - j_2$  where  $j_1$  refers to the number of single DOF joints and  $j_2$  refers to the number of two DOF joints. The PRBM has six links and seven revolute joints. Thus, according to Kutzbach criterion, DOF of the mechanism is calculated as  $N = 1$ .

The PRBM is formed by links  $r_2, r_3, r_4, r_5, r_6, r_8$ , and  $r_{10}$  and their related springs are given in Figure 4.1. Referring to Figure 4.1, the revolute joints at  $A_0, C_0$ , and  $D_0$  are pivoted to the ground. Length of  $r_1$  is  $A_0C_0$ , length of link 2 is  $r_2 = A_0A$ , length of link 3 is  $r_3 = AB$ . Link 4 that is formed by  $BCD$  is single piece and  $r_8 = BC$ ,  $r_4 = CD$ , length of links 5 and 6 are  $r_5 = C_0C = r_6 = D_0D$ . The horizontal distance between the revolute joints of the parallelogram four-bar is  $r_{10} = C_0D_0 = r_4$ .  $\theta_{ij}$  are position variables measured counter-clockwise (in the right handed sense) from the horizontal axis.  $\alpha$  is constant angle between the horizontal axis and  $A_0C_0$ .  $\gamma_{54}$  is a variable angle between links 4 and 5 measured counter-clockwise from the vertical axis. Note that,  $\gamma_{54} + \theta_{14}$  is a constant angle.

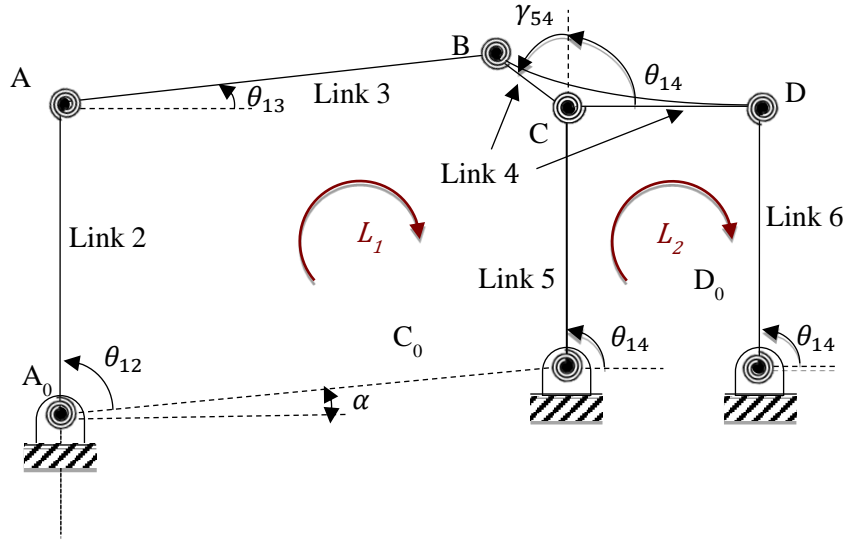


Figure 4.1. Structure parameters and variables for the kinematic analysis

The main objective of the position analysis is to derive closed form equations according to the position variables as a function of input angle  $\theta_{12}$  and the structure parameters. There are two independent loops  $L_1$  and  $L_2$  as shown in Figure 4.1. The relationship between the position variables, the structure parameters, and the input angle is obtained by substituting trigonometric identities into the loop closure equations. The loop closure equation in complex numbers is:

$$r_3 e^{i\theta_{13}} = r_1 e^{i\alpha} - r_2 e^{i\theta_{12}} + r_5 e^{i\theta_{14}} + r_8 e^{i(\theta_{14} + \gamma_{54})} \quad (4-1)$$

And its complex conjugate is:

$$r_3 e^{-i\theta_{13}} = r_1 e^{-i\alpha} - r_2 e^{-i\theta_{12}} + r_5 e^{-i\theta_{14}} + r_8 e^{-i(\theta_{14} + \gamma_{54})} \quad (4-2)$$

Multiplying Equations (4-1) and (4-2) side by side:

$$\begin{aligned}
r_3^2 = r_1^2 - r_2 r_1 e^{i(\alpha - \theta_{12})} + r_5 r_1 e^{i(\alpha - \theta_{14})} + r_8 r_1 e^{i(\alpha - \theta_{14} - \gamma_{54})} & \quad (4-3) \\
- r_2 r_1 e^{i(\theta_{12} - \alpha)} + r_2^2 - r_2 r_5 e^{i(\theta_{12} - \theta_{14})} \\
- r_2 r_8 e^{i(\theta_{12} - \theta_{14} - \gamma_{54})} + r_5 r_1 e^{i(\theta_{14} - \alpha)} - r_2 r_5 e^{i(\theta_{14} - \theta_{12})} \\
+ r_5^2 + r_5 r_8 e^{i(\theta_{14} - \theta_{14} - \gamma_{54})} + r_8 r_1 e^{i(\theta_{14} + \gamma_{54} - \alpha)} \\
- r_2 r_8 e^{i(\theta_{14} + \gamma_{54} - \theta_{12})} + r_5 r_8 e^{i(\theta_{14} - \theta_{14} + \gamma_{54})} + r_8^2
\end{aligned}$$

Rearranging the Equation (4-3) reduces it to (4-4):

$$\begin{aligned}
r_3^2 = r_1^2 - r_2 r_1 e^{i(\alpha - \theta_{12})} + r_5 r_1 e^{i(\alpha - \theta_{14})} + r_8 r_1 e^{i(\alpha - \theta_{14} - \gamma_{54})} & \quad (4-4) \\
- r_2 r_1 e^{i(\theta_{12} - \alpha)} + r_2^2 - r_2 r_5 e^{i(\theta_{12} - \theta_{14})} \\
- r_2 r_8 e^{i(\theta_{12} - \theta_{14} - \gamma_{54})} + r_5 r_1 e^{i(\theta_{14} - \alpha)} - r_2 r_5 e^{i(\theta_{14} - \theta_{12})} \\
+ r_5^2 + r_5 r_8 e^{-i\gamma_{54}} + r_8 r_1 e^{i(\theta_{14} + \gamma_{54} - \alpha)} \\
- r_2 r_8 e^{i(\theta_{14} + \gamma_{54} - \theta_{12})} + r_5 r_8 e^{i\gamma_{54}} + r_8^2
\end{aligned}$$

Equation (4-4) is further simplified to:

$$\begin{aligned}
r_3^2 = r_1^2 + r_2^2 + r_5^2 + r_8^2 - 2r_2 r_1 \cos(\theta_{12} - \alpha) + 2r_5 r_1 \cos(\theta_{14} - \alpha) & \quad (4-5) \\
+ 2r_1 r_8 \cos(\theta_{14} + \gamma_{54} - \alpha) + 2r_2 r_5 \cos(\theta_{14} - \theta_{12}) \\
- 2r_2 r_5 \cos(\theta_{14} + \gamma_{54} - \theta_{12}) + 2r_5 r_8
\end{aligned}$$

However, obtaining a closed form relationship between  $\theta_{12}$  and  $\theta_{14}$  is very hard if not impossible. In the next section, we propose an alternative method to obtain a closed form solution.

## 4.2. A Novel Kinematic Analysis Approach for the PRBM

It is clear that link 4 performs curvilinear translation motion due to the parallelogram structure of the four-bar mechanism. Thus, any point on the coupler link moves on congruent curves. Points  $C$  and  $D$  performs fixed axis rotation about  $C_0$  and  $D_0$  respectively with a radius of curvature of  $r_5$ . This brings us a very useful property for the analysis of the mechanism described as follows:

Let an imaginary link 7 is drawn parallel to link 5 between points  $BE$  ( $E$  is pivoted to the ground with a revolute joint) as shown in Figure 4.2. The length of link 7;  $r_7$  is equal to  $r_5$  that is also equal to the radius of curvature. Furthermore, another imaginary link 9 is formed between points  $A_0E$  with length of  $r_9$ . Finally, an imaginary link 8 is drawn between points  $C_0E$  with length of  $r_8$ . Thus, now an additional imaginary parallelogram four-bar mechanism is formed composing links 4, 5, 7, and 8. Link 8 is parallel to  $CB$  and  $CB = C_0E = r_8$ . Referring to Figure 4.3,  $\delta$  and  $\chi$  are constant angles between the horizontal axis and  $A_0E$ ,  $C_0E$  respectively.  $\mu_{73}$  can be called as the transmission angle between links 3 and 7. By this way, the new PRBM transforms to the mechanism in Figure 4.2. This mechanism can be analyzed as two cascade four-bar mechanisms.

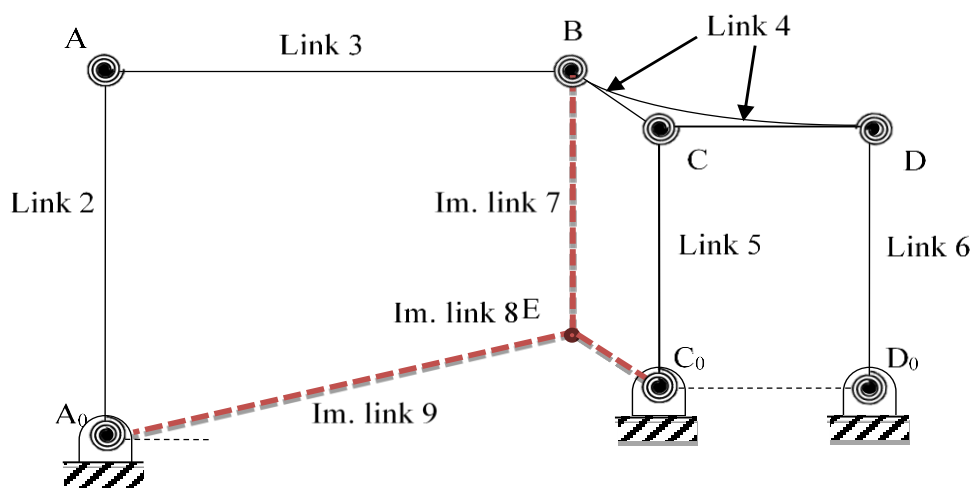


Figure 4.2. PRBM with an imaginary parallelogram four-bar mechanism

Initially, kinematic analysis of the first four-bar mechanism in Figure 4.2, composed of links 9, 2, 3, and 7 is performed.  $\theta_{14}$  is determined as a function of  $\theta_{12}$ . Note that  $\theta_{14}$  is the input of the second four-bar mechanism. Next, kinematic analysis of the second mechanism (links 4, 5, 7, and 8) is performed. By this way, all of the necessary position variables of the complete mechanism are determined by a novel way. Because, once the angle of link 7 w.r.t ground is obtained, the angles of the links 5-6 will be the same due to two coherent parallelograms;  $BEC_0C$  and  $C_0CDD_0$ .

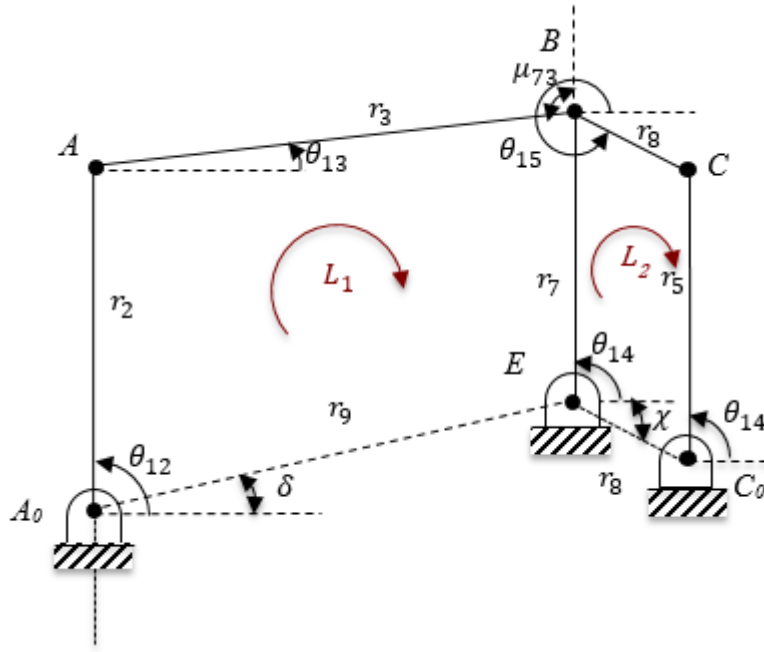


Figure 4.3. Structure parameters and variables for the cascade four-bar mechanism

In order to obtain relationship between input  $\theta_{12}$  and position variable  $\theta_{14}$ , the loop closure equation of the first four-bar mechanism can be written as:

$$r_2 e^{i\theta_{12}} + r_3 e^{i\theta_{13}} = r_9 e^{i\delta} + r_7 e^{i\theta_{14}} \quad (4-6)$$

Equation (4-6) and its complex conjugate can be written as:

$$r_3 e^{i\theta_{13}} = r_9 e^{i\delta} - r_2 e^{i\theta_{12}} + r_7 e^{i\theta_{14}} \quad (4-7)$$

$$r_3 e^{-i\theta_{13}} = r_9 e^{-i\delta} - r_2 e^{-i\theta_{12}} + r_7 e^{-i\theta_{14}} \quad (4-8)$$

Multiplying equations (4-7) and (4-8):

$$\begin{aligned} r_3^2 e^{i(\theta_{13}-\theta_{13})} &= r_9^2 e^{i(\delta-\delta)} - r_2 r_9 e^{i(\delta-\theta_{12})} + r_7 r_9 e^{i(\delta-\theta_{14})} \\ &\quad - r_2 r_9 e^{i(\theta_{12}-\delta)} + r_2^2 e^{i(\theta_{12}-\theta_{12})} - r_2 r_7 e^{i(\theta_{12}-\theta_{14})} \\ &\quad + r_7 r_9 e^{i(\theta_{14}-\delta)} - r_2 r_7 e^{i(\theta_{14}-\theta_{12})} + r_7^2 e^{i(\theta_{14}-\theta_{14})} \end{aligned} \quad (4-9)$$

Equation (4-9) reduces to:

$$\begin{aligned} r_2^2 - r_3^2 + r_7^2 + r_9^2 + 2r_7r_9 \cos(\theta_{14} - \delta) - 2r_2r_9 \cos(\theta_{12} - \delta) \\ = 2r_2r_7 \cos(\theta_{14} - \theta_{12}) \end{aligned} \quad (4-10)$$

Dividing the equation (4-10) by  $2r_2r_7$ ;

$$\begin{aligned} \frac{r_9}{r_2} \cos(\theta_{14} - \delta) - \frac{r_9}{r_2} \cos(\theta_{12} - \delta) + \frac{r_2^2 - r_3^2 + r_7^2 + r_9^2}{2r_2r_7} \\ = \cos(\theta_{14} - \theta_{12}) \end{aligned} \quad (4-11)$$

$$K_1 \cos(\theta_{14} - \delta) - K_2 \cos(\theta_{12} - \delta) + K_3 = \cos(\theta_{14} - \theta_{12}) \quad (4-12)$$

Where the constants are:

$$K_1 = \frac{r_9}{r_2}, K_2 = \frac{r_9}{r_2}, K_3 = \frac{r_2^2 - r_3^2 + r_7^2 + r_9^2}{2r_2r_7} \quad (4-13)$$

Substituting the half tangent formulas, the quadratic Equation (4-16) can be determined:

$$\sin\theta_{14} = \frac{2\tan\left(\frac{1}{2}\theta_{14}\right)}{\left[1 + \tan^2\left(\frac{1}{2}\theta_{14}\right)\right]} \quad (4-14)$$

$$\cos\theta_{14} = \frac{\left[1 - \tan^2\left(\frac{1}{2}\theta_{14}\right)\right]}{\left[1 + \tan^2\left(\frac{1}{2}\theta_{14}\right)\right]} \quad (4-15)$$

$$A\tan^2\left(\frac{\theta_{14}}{2}\right) + B\tan\left(\frac{\theta_{14}}{2}\right) + C = 0 \quad (4-16)$$

Where:

$$A = \cos\theta_{12}(1 - K_2) + K_3 - K_1 \quad (4-17)$$

$$B = -2\sin\theta_{12}$$

$$C = \cos\theta_{12}(1 + K_2) + K_3 + K_1$$

The quadratic equation (4-16) can be solved as:

$$\tan\left(\frac{\theta_{14}}{2}\right) = \frac{-B \pm \sqrt{(B^2 - 4AC)}}{2A} \quad (4-18)$$

$$\theta_{14} = 2\tan^{-1}\left[\frac{-B \pm \sqrt{(B^2 - 4AC)}}{2A}\right] \quad (4-19)$$

Then the angle of the coupler link of the first 4-bar mechanism can be obtained as:

$$\theta_{13} = \arg[r_7 e^{i(\theta_{14} + \delta)} + r_9 - r_2 e^{i(\theta_{12} + \delta)}] - \delta \quad (4-20)$$

Considering the parallelogram four-bar mechanism displayed in Figure 4.3,

$$\theta_{15} = 2\pi - \chi \quad (4-21)$$

Referring Figure 4.3, input, output, and coupler link angles of the parallelogram mechanism are equal to each other ( $\theta_{14}$ ). Therefore, after the kinematic analysis of the cascade four-bar mechanism, slider equivalent part of the mechanism can be readily analyzed.

### 4.3. Transmission Angle

During rigid body replacement synthesis, if the undeflected position of the compliant segment between rigid segments 3 and 4 is set to  $180^\circ$  in Figure 3.2.b, the deflection of this compliant segment will be the same in both directions. In addition,  $\mu$  is the transmission angle of the PRBM. Since the mechanism is equivalent to a slider-crank mechanism; transmission angle is between the coupler and the slider. If we define  $\mu_{73} = 90^\circ$  where the transmission angle is optimum, the motion quality of the synthesized mechanism will be better. It should be noted that for a compliant mechanism, compliance of flexural hinges of may cause differences in transmission characteristics when compared to its rigid body counterpart [16]. However, it is verified that transmission characteristics of a compliant mechanism will be similar to those of its rigid body counterpart, if the output loading is large enough relative to the stiffness of compliant links [16].

## CHAPTER 5

### DESIGN APPROACH FOR THE RIGID BODY EQUIVALENT OF THE COMPLIANT SLIDER-CRANK MECHANISM

#### 5.1. Objectives of the Design Approach

In this section, the design approach targets three main objectives. First objective is the minimization of the relative link rotations while maximizing the translational motion of coupler of the second four-bar mechanism. Note that, relative rotations of the links determine the deflection amount of the flexible hinges of the compliant slider-crank mechanism. The second objective is to equate the relative rotation of links from a reference position. Because, it is well known that equality of deflection in both directions minimizes deflection peaks in a compliant mechanism design. The third objective is to equate all relative rotations of the links to a specific value, if possible. By this way, all flexible hinges of compliant slider-crank mechanism can be designed with same dimensions to yields a robust design. It should be noted that in a compliant mechanism design, generally, the dominant loading is generally due to bending [2]. Bending stress will be similar for all hinges with same dimensions and deflections. The design of the rigid body equivalent is performed considering these three objectives.

#### 5.2. Function Generation with Complex Number Modelling

Figure 5.1 shows a four-bar mechanism in two positions. The  $j$ th position may be expressed as [26]:

$$\vec{Z}_2 e^{i\phi_j} + \vec{Z}_3 e^{i\gamma_j} - \vec{Z}_5 e^{i\gamma_j} - \vec{Z}_4 e^{i\psi_j} - \vec{Z}_1 = 0 \quad (5-1)$$

where  $\phi_j$ ,  $\gamma_j$ , and  $\psi_j$  are the changes in the angles of links 2, 3, and 4, respectively, from position 1 to position  $j$ .

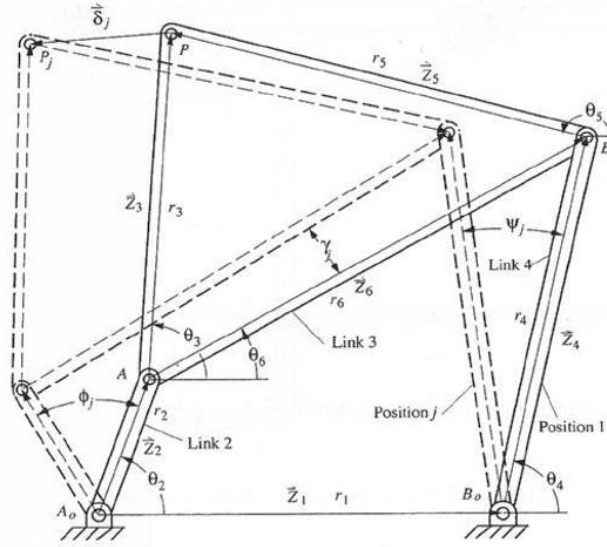


Figure 5.1. Vector loop for a four-bar mechanism with coupler point P [26]

In function generation, the positions of the output link are prescribed corresponding to given values of the input link position. Only one vector is required to represent link 3 [26].

$$\vec{Z}_2 + \vec{Z}_6 - \vec{Z}_4 - \vec{Z}_1 = 0 \quad (5-2)$$

$$\vec{Z}_2 e^{i\phi_j} + \vec{Z}_6 e^{i\gamma_j} - \vec{Z}_4 e^{i\psi_j} - \vec{Z}_1 = 0 \quad (5-3)$$

where,

$$\vec{Z}_6 = \vec{Z}_3 - \vec{Z}_5 \quad (5-4)$$

Vector  $\vec{Z}_1$  may be eliminated by subtracting equation (5-2) from equation (5-4), resulting in [26]:

$$\vec{Z}_2(e^{i\phi_j} - 1) + \vec{Z}_6(e^{i\gamma_j} - 1) - \vec{Z}_4(e^{i\psi_j} - 1) = 0 \quad (5-5)$$

Values of  $\phi_j$  and  $\psi_j$  are prescribed according to the desired function,  $\psi_j = (\phi_j)$ . The magnitude and direction of  $\vec{Z}_2$ ,  $\vec{Z}_6$ , and  $\vec{Z}_5$  are undefined, as is the angle  $\gamma_j$ . Therefore, the total number of unknowns is  $6 + (n - 1)$ , where  $n$  is the total number of precision points.

Since each vector equation results in two scalar equations, the total number of available scalar equations is  $2(n - 1)$ . The number of free choices is the difference between the number of unknowns and the number of equations. Or the four-bar function generator, the number of free choices is given by  $6 + (n - 1) - 2(n - 1) = 7 - n$ .

### 5.3. Function Generation for Three Precision Points

Initially, the first four-bar mechanism ( $A_0ABE$ ) is designed. This mechanism with the same input and output oscillations of  $\Delta\beta$  (to obtain the same deflections) is synthesized by function generation for three precision points. The forward and fully withdrawn positions of the mechanism are shown in Figure 5.2. Subscript  $f$  is used for the fully withdrawn position that is represented with black lines, whereas subscript  $e$  is used for the forward positions that is represented by green lines in Figure 5.2. Let the vertical position of links 2 and 7 correspond to the undeflected positions of the related flexural hinges. Here, the forward and fully withdrawn positions are achieved when links 2 and 7 move at an angle of  $\Delta\beta/2$  from the vertical position.

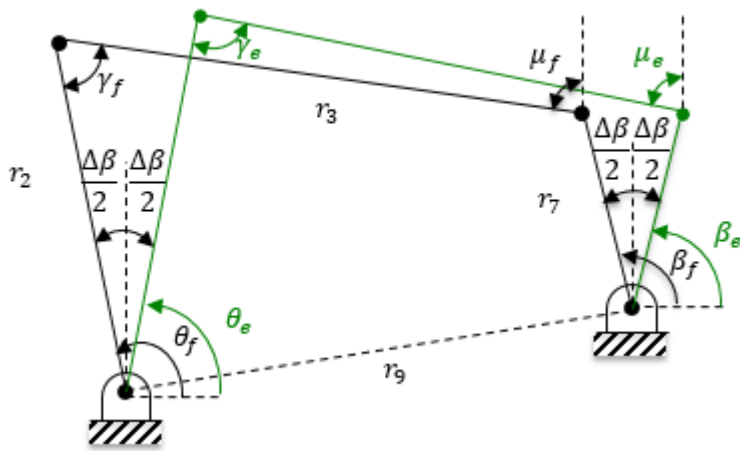


Figure 5.2. Four-bar mechanism in forward and fully withdrawn positions

A parallelogram four bar mechanism as presented in Figure 5.3 is a neat solution according to the requirements. Green, black, and red lines represent the fully withdrawn, undeflected, and forward positions of the mechanism, respectively. With this approach, the angle between the extreme positions of links 2 and 7 is  $\Delta\beta$ , and the undeflected position is exactly in the middle of these two positions. In other words, the extreme positions are symmetric with respect to the undeflected (vertical) position.

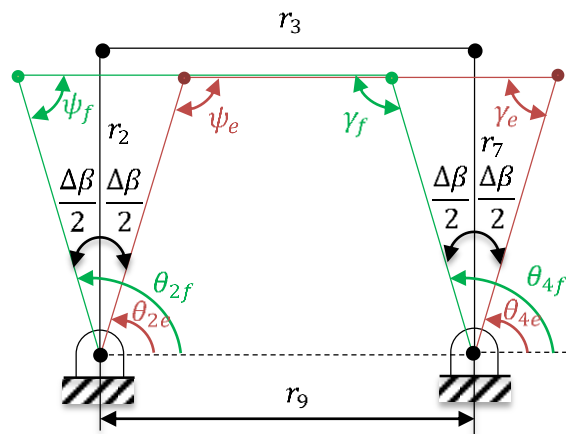


Figure 5.3. Four-bar mechanism in three positions

Considering the free design parameters, there is an infinite set of solution. However, in every solution it is determined that  $r_2$  and  $r_7$  are equal to each other that yield a parallelogram four-bar mechanism. After function generation synthesis for three precision points, we obtained a solution where the complete mechanism is formed from two cascade parallelogram four-bar mechanisms. In Figure 5.4, this mechanism is sketched in three positions that are undeflected, forward, and fully withdrawn positions. Remember that,  $r_7$  is equal to  $r_5$  that is obtained from the imaginary parallelogram four-bar mechanism.  $L$  can be chosen as a free design parameter as in Equation (5-6).

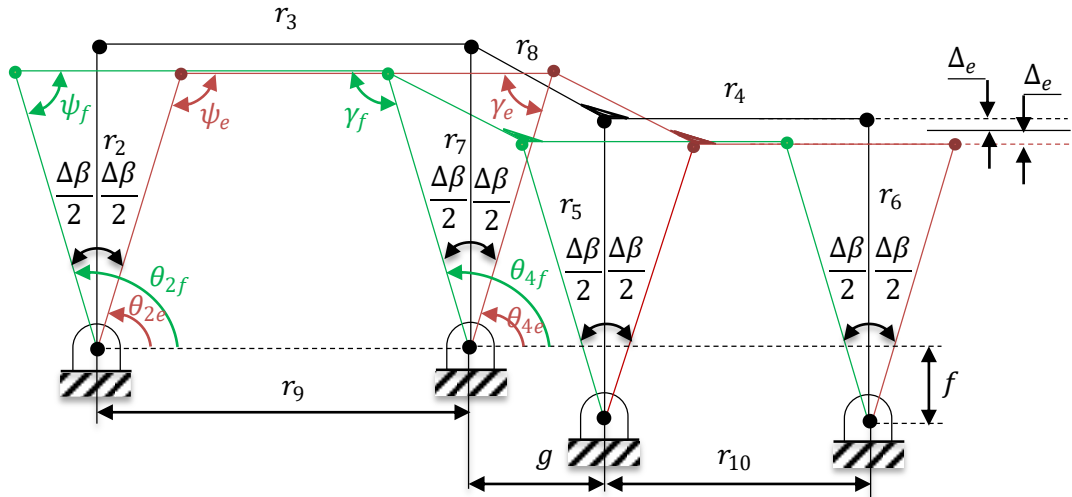


Figure 5.4. Four-bar mechanism in three positions (forward-undeflected-fully withdrawn) with design parameters

$$r_2 = r_5 = r_7 = L \quad (5-6)$$

$r_2, r_3, r_7,$  and  $r_9$  links form a parallelogram four-bar, therefore all of the compliant segments have the same angular displacements between the forward and fully withdrawn positions of the mechanism as presented in Equation (5-7).

$$(\psi_e - \psi_f) = (\gamma_f - \gamma_e) = (\theta_{2f} - \theta_{2e}) = (\theta_{4f} - \theta_{4e}) \quad (5-7)$$

Then, from parallelogram four-bar mechanism, the equality of  $r_3$  and  $r_9$  can be written as:

$$r_3 = r_9 \quad (5-8)$$

Kinematic analysis of the mechanism is straightforward due to the symmetrical link proportions: The stroke of the mechanism, which is the horizontal motion of  $r_4$ , is:

$$\begin{aligned} \Delta S_{total} &= 2L\sin(\Delta\beta/2) \\ \Delta S_{left} &= \Delta S_{right} = L\sin(\Delta\beta/2) \end{aligned} \quad (5-9)$$

The axis drift of  $r_4$  can be defined as:

$$\Delta e = \frac{L}{2}(1 - \cos(\Delta\beta/2)) \quad (5-10)$$

Here, note that the axis drift is measured from the midpoint of the maximum and minimum vertical position of link  $r_4$ ; i.e. slider of the compliant slider-crank.

## CHAPTER 6

### DESIGN OF THE FULLY COMPLIANT SLIDER-CRANK MECHANISM

Design of compliant mechanisms is more complicated than the rigid ones. High amount of deflection can cause have fractures on flexural pivots so an iterative design approach should be used.

The introduced design approach is presented as a flowchart in Figure 6.7. In the following section, a fully compliant slider-crank mechanism is designed regarding this flow chart.

#### 6.1. Dimension Synthesis of the Fully Compliant Cascade Parallelogram Four-Bar Mechanism

A mechanism is designed for  $40^\circ$  input swing angle of the crank. The output stroke is kept as large as possible. Also the parameters of the design are optimized and the link lengths of the PRBM are determined according to the design considerations listed as follows:

- If deflections of the flexural hinges are high, then stresses at the flexural hinges will also be high. Thus, deflection values should be kept as low as possible.
- On the other hand, to obtain a useful mechanism in practice the output stroke should not be low.
- For the ease of production, a mechanism which is on the horizontal plane while at rest (undeflected) is designed. At the undeflected position, crank angle is equal to  $\pi / 2$ .

Geometry of the hinges is optimized as follows. The width and the thickness of small length flexural hinge (rectangular cross-section) is chosen as  $w = 15 \text{ mm}$  and  $t_{SLF} = 1.5 \text{ mm}$ , respectively according to the stress calculations. Note that the material of the mechanism is selected as polypropylene and polypropylene with a plate thickness of 15 mm is readily available in the market. The length of the flexural hinge is chosen as  $l = 12 \text{ mm}$ . To have an acceptable error when the real model is compared with its PRBM, the ratio of the rigid segment's length to flexible section's length is taken about ten [2].

From the imaginary parallelogram four-bar mechanism it is obtained that  $r_7$  is equal to  $r_5$  and  $r_2$ .  $L$  can be chosen as a free design parameter as mentioned in Equation (5-6).

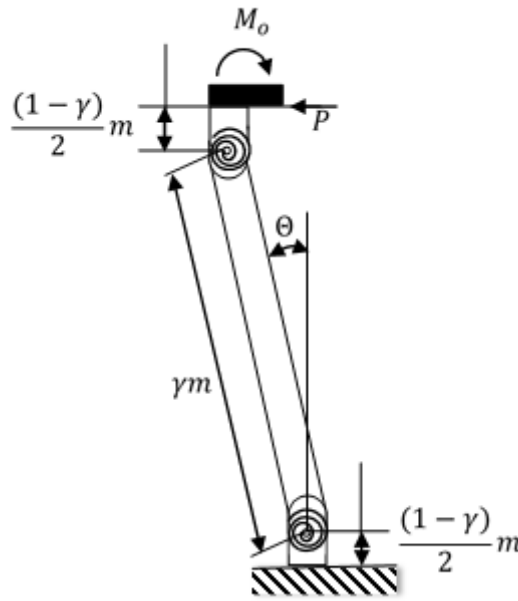


Figure 6.1. Pseudo-rigid-body model of fixed guided beam [2]

From the PRBM displayed in Figure 6.2, links 4, 5, and 6 form a parallelogram four-bar mechanism where link 5 and 6 correspond to fixed guided beams. PRBM of the fixed guided beam can be seen in Figure 6.1. In this model, the length of the top and bottom parts of the fixed guided beams are equal to  $\frac{(1-\gamma)m}{2}$  and length of the middle

part is equal to  $\gamma m$  which is also equal to  $r_6$  of the PRBM. In our design fixed guided segment 1 and 2 are dimensioned as: thickness;  $t_{FG} = 2.85$  mm, width;  $w = 15$  mm with respect to the stress calculations. The lengths of  $r_2, r_5, r_7$  links are chosen as 100 mm that is also equals to  $L = 100$  mm. Then length of the fixed guided beam is calculated as  $m = 117.4$  mm, since  $\gamma = 0.8517$ . Here,  $\gamma$  is characteristic radius factor and it can be determined from [2] as :  $\gamma = 0.8517$  for  $(\Delta\beta/2)_{\max} = 65^\circ$ .

Generally, if deflections of flexural hinges are large, then stresses of flexural hinges will also be high. These stresses can also be decreased by using thinner and/or longer flexible hinges, however that yields a non-useful mechanism. Thus, in practice, deflection values should be kept in a feasible range to obtain a robust mechanism where the output stroke is as high as possible when compared with crank length. By using the rigid body replacement method, the fully compliant slider-crank mechanism can be dimensioned as shown in Figure 6.2.

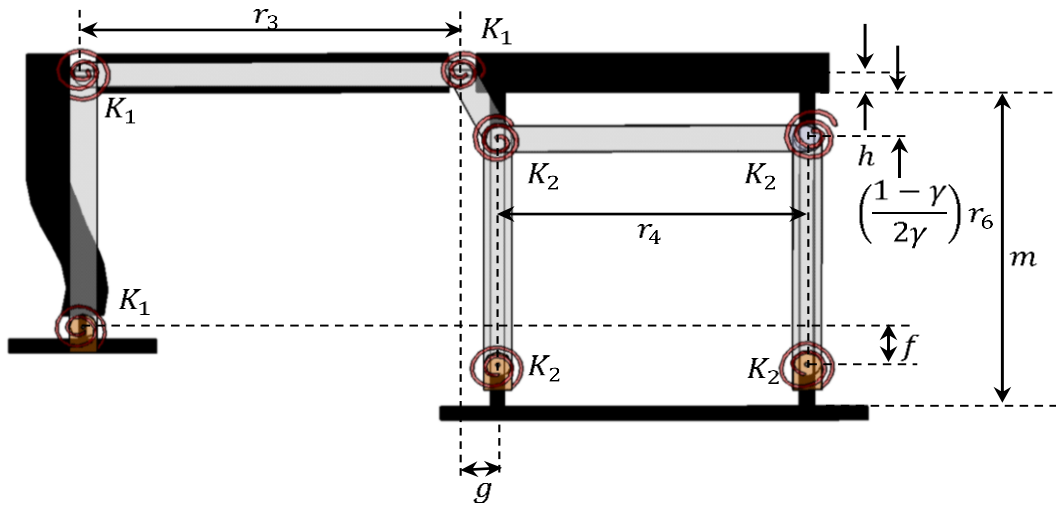


Figure 6.2. Fully compliant slider-crank mechanism overlapped with its PRBM

Rigid segments 3 and 4 are aligned. Thus, Equations (6-1) and (6-2) can be determined referring to Figure 6.2 as:

$$h + \frac{(1-\gamma)r_6}{2\gamma} + r_6 - f = r_6 \quad (6-1)$$

where  $h$  is half thickness of upper the rigid segment.

$$f = h + \left(\frac{1 - \gamma}{2\gamma}\right)r_6 \quad (6-2)$$

Note that,  $g, r_3,$  and  $r_4$  are the free structure parameters.

The isometric view and dimensions of the mechanism are displayed in Figure 6.3 and Figure 6.4.

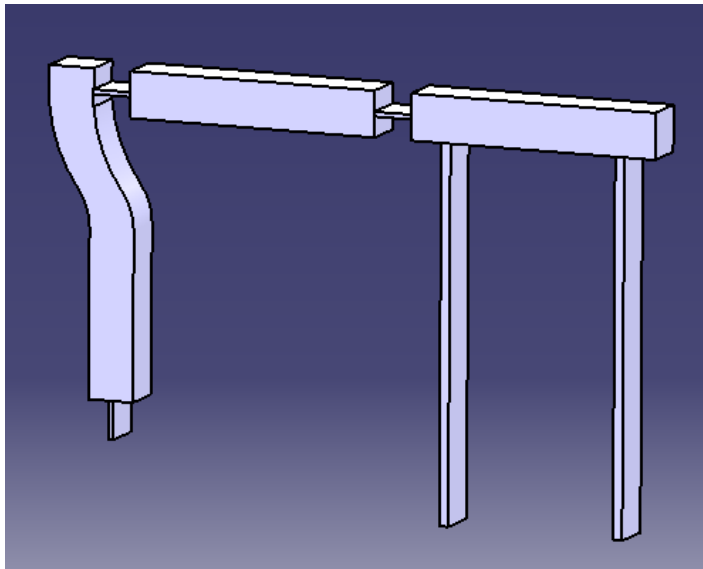


Figure 6.3. Isometric view of the mechanism without fillets

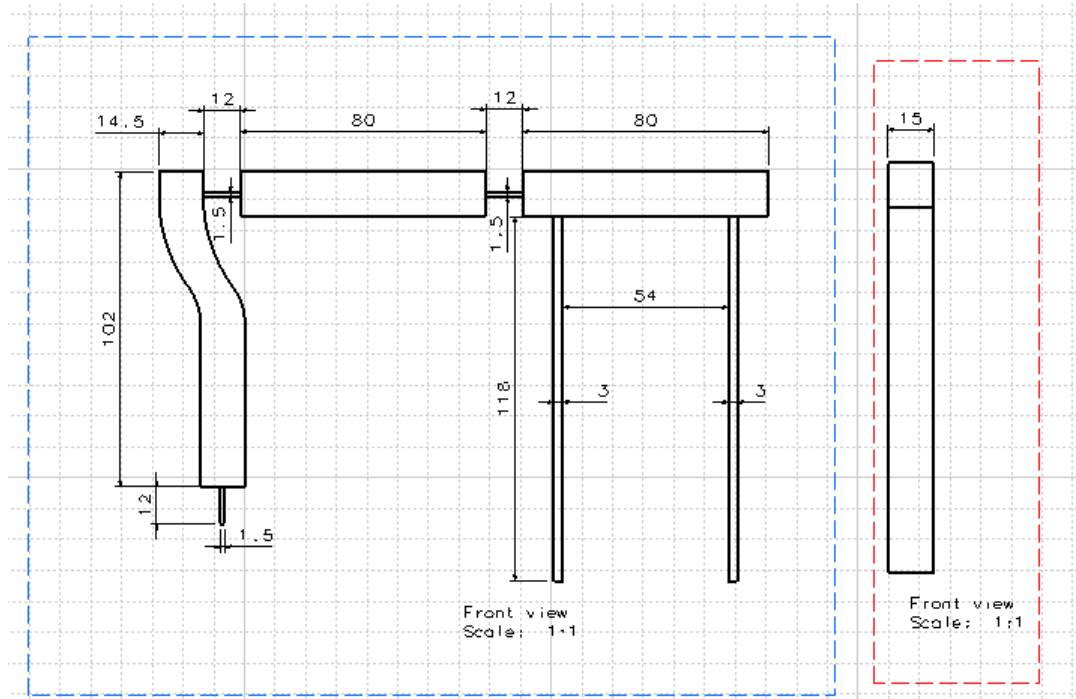


Figure 6.4. Dimensions of the mechanism without fillets

To reduce the stress intensity factor, sharp corners must be eliminated. Therefore, fillets are used in the design. According to the radius of the cutting tool that is used in manufacturing process, radius of fillet is taken as 3 mm. In Figure 6.5, the mechanism with fillets is presented.

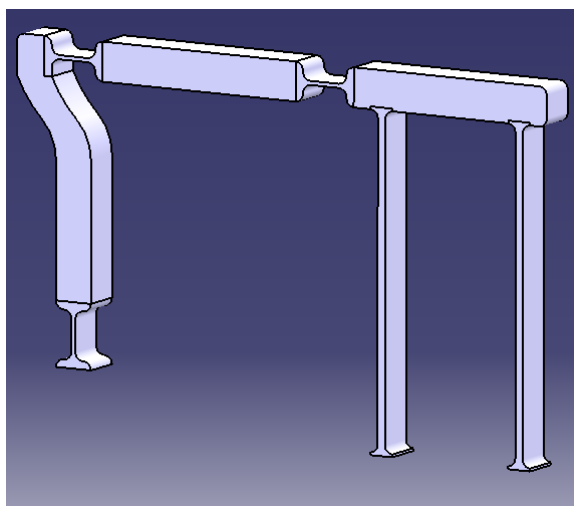


Figure 6.5. Isometric view of the mechanism with fillets

## 6.2. Stroke of the System

Stroke of the fully compliant cascade parallelogram 4-bar mechanism can be determined as:

$$\Delta S_{total} = 2L\sin(\beta/2) \quad (6-3)$$

$$\Delta S_{left} = \Delta S_{right} = L\sin(\beta/2) \quad (6-4)$$

where  $L = 100$  mm and  $\beta/2 = 20^\circ$ .

$$\Delta S_{left} = \Delta S_{right} = 100\sin(20^\circ) = 34.2 \text{ mm} \quad (6-5)$$

## 6.3. Axis Drift of the System

Axis drift of the fully compliant cascade parallelogram 4-bar mechanism can be obtained as:

$$\Delta e = \frac{L}{2}(1 - \cos(\beta/2)) \quad (6-6)$$

where  $L = 100$  mm and  $\beta/2 = 20^\circ$ .

$$\Delta e = \frac{100}{2}(1 - \cos(20^\circ)) = 3.02 \text{ mm} \quad (6-7)$$

## 6.4. Stress Analysis for Small Length Flexural Hinges

Stress can be written in terms of moment as:

$$\sigma = \frac{Mc}{I} \quad (6-8)$$

where,

$$M = \frac{\theta EI}{L} \quad (6-9)$$

Recalling Equations (6-8) and (6-9), and rearranging them:

$$\sigma = \frac{\theta Ec}{L} \quad (6-10)$$

In our case  $c$  is half thickness of the small length flexural hinge,  $c = t_h/2$ ; length of the hinge is  $l$ , and maximum deflection  $\theta$  is  $\Delta\beta/2$ . Therefore, Equation (6-10) becomes,

$$\sigma_{max} = \frac{\beta Et}{4l} \quad (6-11)$$

Material of the mechanism is selected as polypropylene which has modulus of elasticity  $E = 1.5$  GPa and a yield strength of 40 MPa. The small length flexural hinges are dimensioned as: thickness;  $t_{SLF} = 1.5$  mm, and length  $l = 12$  mm. The maximum stress of the small length flexural hinges is calculated analytically for  $\Delta\beta = 40^\circ$  from (6-11).

$$\sigma_{max} = \frac{0.7 \text{ rad} \times 1500 \text{ MPa} \times 1.5 \text{ mm}}{4 \times 12 \text{ mm}} = 32.81 \text{ MPa} \quad (6-12)$$

### 6.5. Stress Analysis for Fixed Guided Flexible Segment

For fixed guided compliant segments, the maximum stress equation in terms of  $P$ ,  $a$ ,  $c$ , and  $I$  is available in Equation (6-18). In our case, a relationship between stress and deflection is required.

There is no moment at the midpoint, therefore the free-body diagram for one-half of the flexible member is as shown in Figure 6.6. The half-beam only has a force at the end, so it is similar to the flexible segment with a force at the free end. The pseudo-

rigid-body model of the half is then the same as discussed previously in section 2.2.7, only half of the beam length is used. Previously, the length of  $r_5$  rigid link equals to  $L$ , hence length of the half-beam is determined as  $\frac{L}{2\gamma}$ .

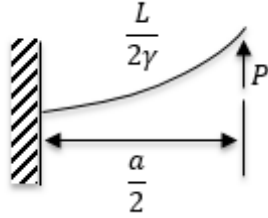


Figure 6.6. Free body diagram of one-half of the beam

A nondimensionalized torsional spring constant  $K_{\theta}$  (stiffness coefficient) is used to model resistance of the beam to deflection. The stiffness coefficient is plotted as a function of  $n$ , and a polynomial curve is fitted. The relationship between  $K_{\theta}$  and  $n$  is described in Equation (6-13) as :

$$K_{\theta} = \{3.024112 + 0.121290n + 0.003169n^2\} \quad (6-13)$$

$$\text{for } (-5 < n \leq -2.5)$$

$$K_{\theta} = \{1.967647 - 2.616021n - 3.738166n^2 - 2.649437n^3 \\ - 0.891906n^4 - 0.113063n^5\}$$

$$\text{for } (-2.5 < n \leq -1)$$

$$K_{\theta} = \{2.654855 - 0.509896 \times 10^{-1}n + 0.126749 \times 10^{-1}n^2 \\ - 0.142039 \times 10^{-2}n^3 + 0.584525 \times 10^{-4}n^4\}$$

$$\text{for } (-1 < n \leq 10)$$

.Consider the flexible beam seen in Figure 6.6 with constant cross section and linear material properties

$$n = 0 \text{ (for vertical force)} \quad (6-14)$$

$$\eta = \sqrt{1 + n^2} = 1 \text{ and } K_{\theta} = 2.6549 \text{ (for } n = 0)$$

in cantilever beam with a force at the free end, the transverse (or tangential) component of the load is:

$$F_t = F \sin(\phi - \theta) = \eta P \sin(\phi - \theta) \quad (6-15)$$

Or:

$$F_t = \frac{K\theta}{\gamma l} \quad (6-16)$$

The force,  $P$ , is found by combining the Equations (6-15) and (6-16) and rearranging them to form:

$$P = \frac{K\theta}{\gamma l \eta \sin(\phi - \theta)} \quad (6-17)$$

The maximum stress occurs at the beam ends where the maximum moment occurs and has a value of:

$$\sigma_{max} = \frac{Pac}{2I} \quad (6-18)$$

where:  $a = l[1 - \gamma(1 - \cos \theta)]$  (6-19)

Substituting Equations (1.30), (6-17) and (6-19) in (6-18) and rearranging to form:

$$\sigma_{max} = \frac{K_\theta E \theta [1 - \gamma(1 - \cos \theta)] (t_{FG}/2)}{l \eta \sin(\phi - \theta)} \quad (6-20)$$

Write  $L/2\gamma$  for each  $l$ , because half beam is considered and pseudo rigid link length had been taken as  $L$  previously.

$$\sigma_{max} = \frac{K_\theta E \theta t_{FG} \gamma [1 - \gamma(1 - \cos \theta)]}{L \sin(\phi - \theta)} \quad (6-21)$$

The fixed guided beams are dimensioned as: thickness;  $t_{FG} = 2.85$  mm, width;  $w = 15$  mm and length  $m = 117.4$  mm, since  $L = 100$  mm and  $\gamma = 0.8517$ . Stresses at the fixed guided beam are determined analytically from Equation (6-21).

$$\begin{aligned}
& \sigma_{max} && (6-22) \\
& = \frac{2.68 \times 1500 \text{ MPa} \times 0.35 \text{ rad} \times 2.85 \text{ mm} \times 0.85 \times [1 - 0.85(1 - \cos 20^\circ)]}{100 \text{ mm} \times \sin(90^\circ - 20^\circ)} \\
& = 34.4 \text{ MPa}
\end{aligned}$$

### 6.6. Determination of the Torque Value for the Cascade Four-Bar Mechanism with Fixed Guided Flexible Segment

The small length flexural hinges are dimensioned as: thickness;  $t_{SLF} = 1.5 \text{ mm}$ , and length  $l = 15 \text{ mm}$ . The area moment of inertia of the small length flexural,  $I_1$ , is determined analytically as,

$$I_1 = \frac{wt_{h_1}^3}{12} = \frac{(15 \text{ mm})(1.5 \text{ mm})^3}{12} = 4.219 \text{ mm}^4 \quad (6-23)$$

$$K_1 = \frac{EI}{l} \quad (6-24)$$

$$K_1 = \frac{1500 \text{ MPa} \times 4.219 \text{ mm}^4}{12 \text{ mm}} = 527.38 \text{ N. mm/rad} \quad (6-25)$$

The fixed guided beams are dimensioned as: thickness;  $t_{FG} = 2.85 \text{ mm}$ , width;  $w = 15 \text{ mm}$ . The area moment of inertia of the fixed guided beams,  $I_2$ , is determined analytically as,

$$I_2 = \frac{wt_{h_2}^3}{12} = \frac{(15 \text{ mm})(2.85 \text{ mm})^3}{12} = 28.94 \text{ mm}^4 \quad (6-26)$$

for each  $K$  in fixed guided flexible segment,

$$K_2 = 2\pi\gamma^2 \frac{EI}{L} \quad (6-27)$$

$$K_2 = \frac{2\pi(0.85)^2 \times 1500 \text{ MPa} \times 28.94 \text{ mm}^4}{118 \text{ mm}} = 1670 \text{ N.mm/rad} \quad (6-28)$$

$$\begin{aligned} K_{total} &= 2K_1 + 4K_2 \quad (6-29) \\ &= \left(2 \times 527.38 \text{ N} \cdot \frac{\text{mm}}{\text{rad}}\right) + \left(4 \times 1670 \text{ N} \cdot \frac{\text{mm}}{\text{rad}}\right) \\ &= 7734.76 \text{ N.mm/rad} \end{aligned}$$

$$\begin{aligned} T &= K_{total}\theta = 7734.76 \text{ N} \cdot \frac{\text{mm}}{\text{rad}} \times 0.35 \text{ rad} = 2707.17 \text{ N.mm} \quad (6-30) \\ &\cong 2.7 \text{ N.m} \end{aligned}$$

The summary of the design procedure of the fully compliant slider-crank mechanism is displayed in Table 6.1. Firstly, stroke of the mechanism is presented in terms of size and deflection. And then axis drift of the slider is determined in terms of deflection and size. Finally, the maximum stress in fixed-guided beam is shown. The design steps are presented as a flowchart in Figure 6.7.

Table 6.1. Design table for fully compliant slider-crank mechanisms

<b>Stroke;</b>	$\Delta S = 2L \sin\left(\frac{\Delta\beta}{2}\right)$	Unit length
<b>Stroke in terms of size (compactness);</b>	$\frac{\Delta S}{L} = 2 \sin\left(\frac{\Delta\beta}{2}\right)$	Unitless
<b>Stroke in terms of deflection;</b>	$\frac{\Delta S}{L\beta} = 2 \sin\left(\frac{\Delta\beta}{2}\right)$	Unitless
<b>Axis drift in terms of deflection;</b>	$\Delta e = \frac{L}{2} \left(1 - \cos\left(\frac{\Delta\beta}{2}\right)\right)$	Unit length
<b>Axis drift in terms of size;</b>	$\frac{\Delta e}{L} = \frac{1}{2} \left(1 - \cos\left(\frac{\Delta\beta}{2}\right)\right)$	Unitless
<b>Maximum stress in Fixed Guided Beam;</b>	$\sigma_{max} = \frac{K_\theta E \theta t_{FG} \gamma [1 - \gamma (1 - \cos \theta)]}{L \sin(\phi - \theta)}$	

By using Table 6.1, numerous fully compliant slider crank mechanisms can be designed for different dimensions. This generalized design table will be beneficial during preliminary design stages satisfying very large slider strokes with acceptable stresses.

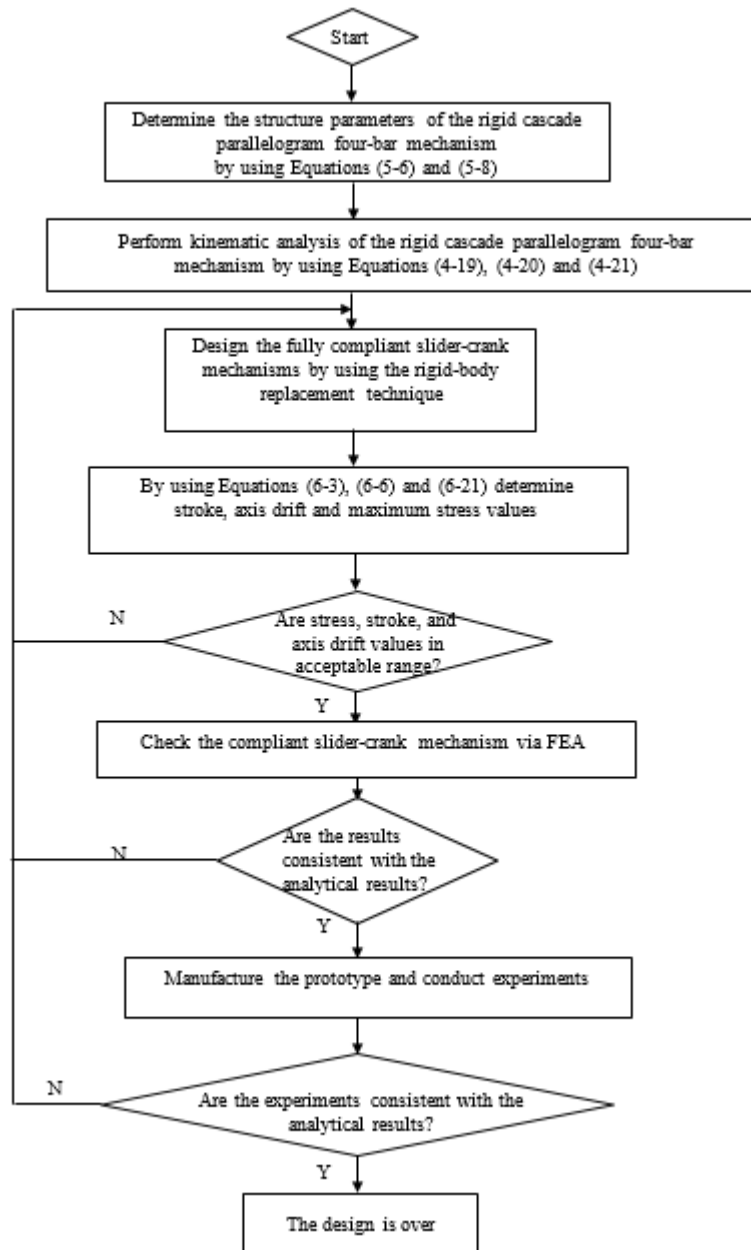


Figure 6.7. Flow chart of the design procedure



## CHAPTER 7

### FINITE ELEMENT ANALYSIS

#### 7.1. Proposed Design

A fully compliant slider-crank mechanism is designed by using the method given in Chapter 5 and the Equations in Table 6.1 as follows: Let the lengths of the rigid segments 2, 4, and 6 be  $L = 100$  mm and the input rotation be  $\Delta\beta = 40^\circ$ . Material of the mechanism is selected as polypropylene which has a modulus of elasticity  $E = 1.5$  GPa and a yield strength of 40 MPa. The fixed guided beams are dimensioned as: thickness;  $t_{FG} = 2.85$  mm, width;  $w = 15$  mm and length  $m = 117.4$  mm, since  $L = 100$  mm and  $\gamma = 0.8517$ . The stroke and axis drift of the slider are calculated analytically for  $\Delta\beta/2$  in Equations (6-5) and (6-7). Stresses at the fixed guided beam are determined analytically from Equation (6-22). Recalling these equations as follows:

$$\Delta S = 100 \sin(20^\circ) = 34.2 \text{ mm} \quad (7-1)$$

$$\Delta e = \frac{100}{2} (1 - \cos(20^\circ)) = 3.02 \text{ mm} \quad (7-2)$$

$$\begin{aligned} \sigma_{max} &= \frac{2.68 \times 1500 \text{ MPa} \times 0.35 \text{ rad} \times 2.85 \text{ mm} \times 0.85 \times [1 - 0.85(1 - \cos 20^\circ)]}{100 \text{ mm} \times \sin(90^\circ - 20^\circ)} \\ &= 34.4 \text{ MPa} \end{aligned} \quad (7-3)$$

#### 7.2. Effective Length Analysis

Sudden changes in cross-section leads to an increase in local stress level. Therefore, fillets are commonly used in mechanical parts to provide smooth transition in these

regions. Fillets are usually the critical regions in mechanical parts especially under fatigue loading. An increase in the maximum stress level considerably shortens the fatigue life of a part. A measure of this increase is expressed by the stress concentration factor  $K_t$  shown in Equation (7-4), which is the ratio of the maximum stress developed in this region,  $\sigma_{max}$ , to nominal stress  $\sigma_o$ :

$$K_t = \frac{\sigma_{max}}{\sigma_o} \quad (7-4)$$

In our design fillets with 3 mm radius is used to decrease stress concentration factor ( $K_t$ ) in the shoulders between the compliant and rigid segments. Considering two compliant segments with the same length, the design with fillets is stiffer than the design without fillets. Therefore the concept of effective length is revealed. There is no analytical approach in the literature for the compliant segments goes under large deflection. The effective length of the compliant segment is obtained via FEA accordingly. Solid models of the small length flexural hinge with and without fillets are constructed as seen in Figure 7.1.

Moment value to bend the flexural hinge  $20^\circ$  is found as 0.185 N.m analytically in Equation (7-7) for  $\theta = 20^\circ$ ,  $I = 4.219 \text{ mm}^4$ ,  $E = 1500 \text{ MPa}$ , and  $l = 12 \text{ mm}$ . Using the PRBM stroke of the small length flexural is calculated as 2.05 mm in Equation (7-8).

$$M = \frac{EI\theta}{l} \quad (7-5)$$

$$K = \frac{EI}{l} = 527.4 \text{ N.mm/rad} \quad (7-6)$$

$$M = K\theta = 527.4 \text{ N.mm/rad} \times 0.35 \text{ rad} = 0.185 \text{ N.m} \quad (7-7)$$

$$\Delta S = \frac{l}{2} \sin(20^\circ) = 6 \times \sin(20^\circ) = 2.05 \text{ mm} \quad (7-8)$$

In FEA, calculated moment value 0.185 N.m is applied to the hinges with different dimensions and the corresponding stroke values are obtained. After simulations the analytical stroke value 2.05 mm is achieved with the flexural hinge with a length of 9.96 mm. Therefore, effective length is found as  $0.83l = 9.96$  mm.

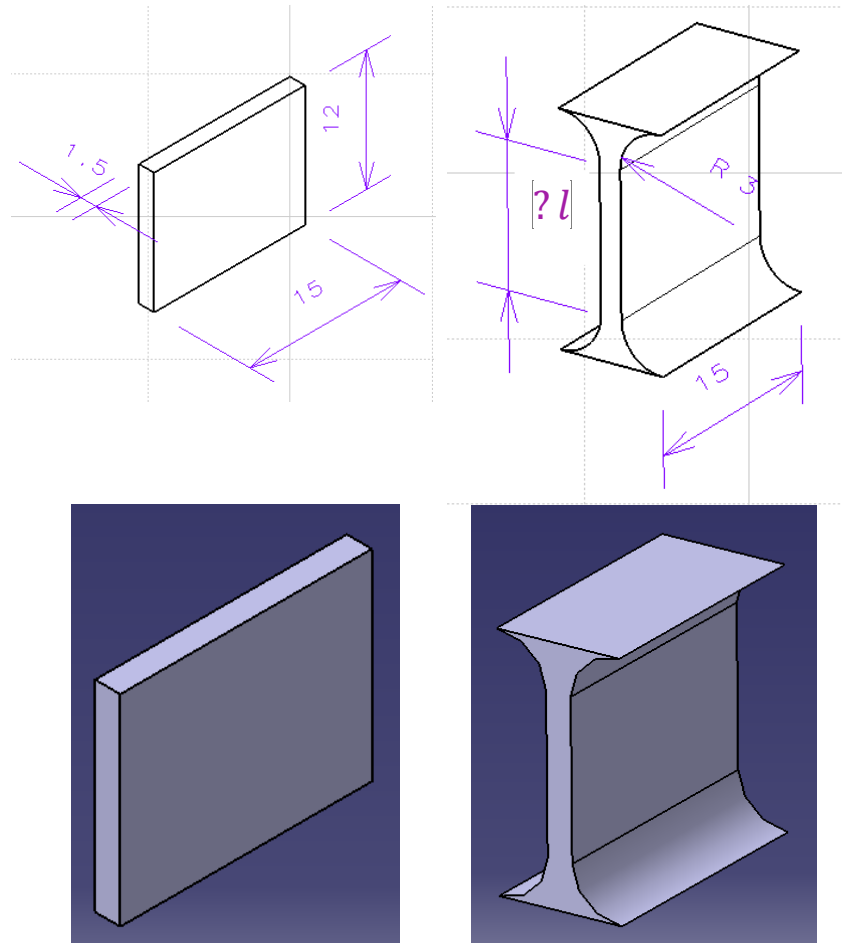


Figure 7.1. Small length flexural hinge dimensions with and without fillets

### 7.3. Finite Element Analysis with Effective Length

After effective length analyses, a new geometry is designed whose hinge lengths are 9.96 mm. Then FEA method is employed by using ANSYS® to compare output stroke, axis drift of the slider, and resultant stresses at the flexural hinges. The fully

compliant slider-crank mechanism is analyzed for different sets of input rotations (5°, 10°, 15°, 20°). For large rotations nonlinear analysis is selected. The flow chart of the analysis can be seen in Figure 7.2. Details of the analysis will be explained in the following sections.

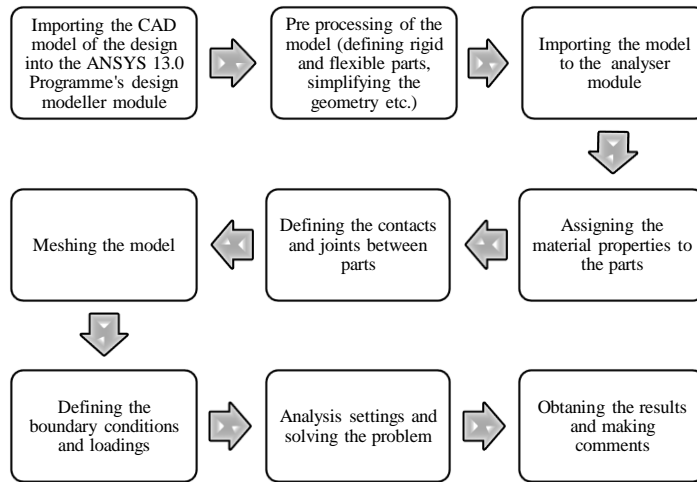


Figure 7.2. Flow chart of the analysis

### 7.3.1. Boundary Conditions and Meshing

The fully compliant slider-crank mechanism is divided into subgroups whose characteristics will be different in the analysis. Small length and fixed guided flexural hinges are the most critical parts of the design. Therefore these hinges are finely meshed so that the number of elements per unit area is the highest value for these hinges compared to the other parts. Other relatively more rigid parts are coarsely meshed. As a result, the analysis takes less time with sufficiently accurate results.

In Figure 7.3 the model is divided into three main parts with different element sizes. Small length flexural and fixed guided flexural hinges are meshed with of 0.75 mm

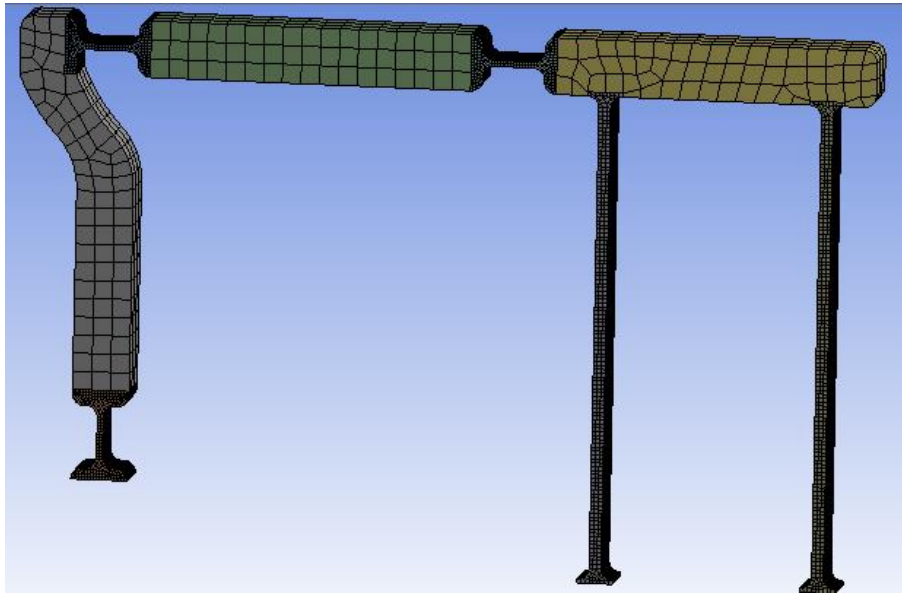


Figure 7.3. Meshing of the model

For the numerical solution, the model with effective length displayed in Figure 7.4 is used. Three ends of the SLF hinge 1-2 and the fixed guided segments 1 and 2 are fixed and the rigid segment 2 is bent from analysis settings by inserting supports (fixed support) and remote displacement. Remote displacement command is used by rotating the rigid segment 2 in the desired direction and for the desired input angle.

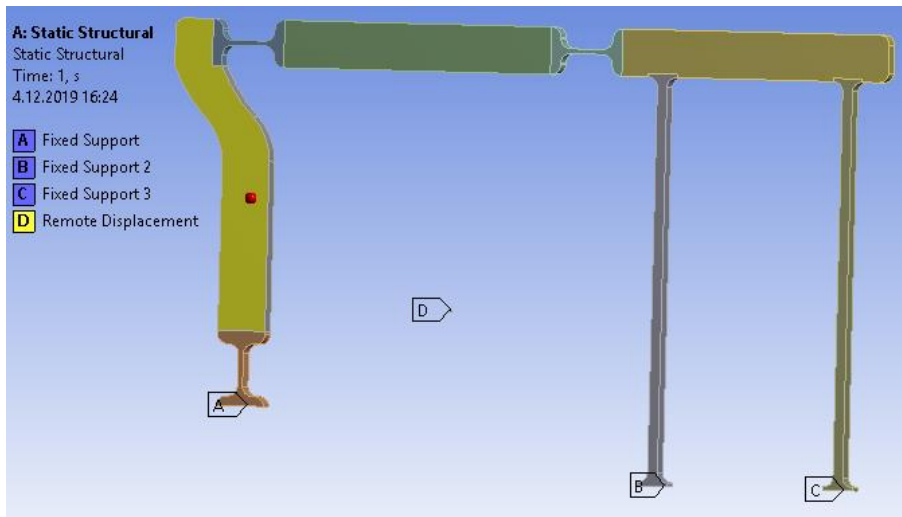


Figure 7.4. Representation of the boundary conditions

### 7.3.2. Stroke Analysis for Fully Compliant Slider-Crank Mechanism

The fully compliant slider-crank mechanism is analyzed for different sets of input rotations ( $5^\circ$ ,  $10^\circ$ ,  $15^\circ$ ,  $20^\circ$ ) in clockwise (CW) and counterclockwise (CCW) directions. Thus, results are displayed in both directions; left and right in Table 7.1.

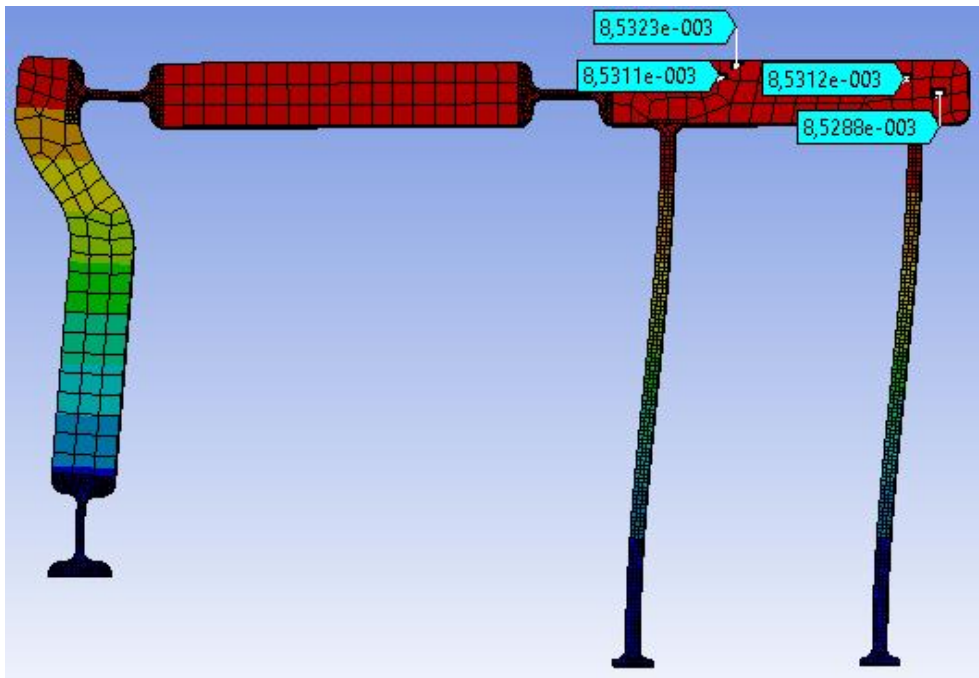


Figure 7.5. Stroke analyses for fully compliant slider-crank mechanism ( $5^\circ$  right)

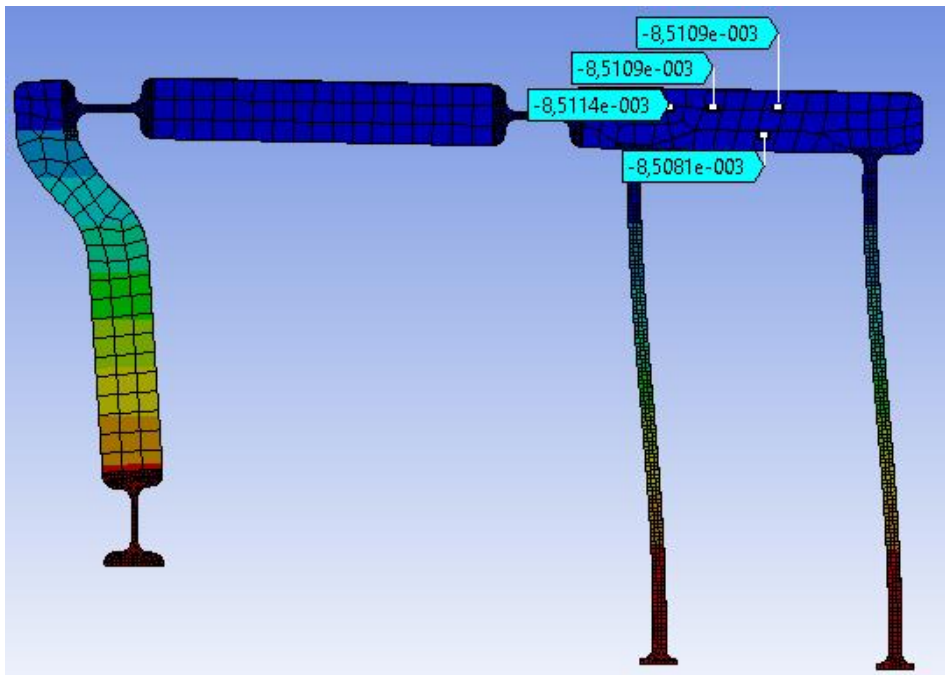


Figure 7.6. Stroke analyses for fully compliant slider-crank mechanism (5° left)

The fully compliant slider-crank mechanism is analyzed for 5° CW (Figure 7.5) and CCW (Figure 7.6) input rotation, average output stroke value of the slider is 8.53 mm and 8.51 mm respectively.

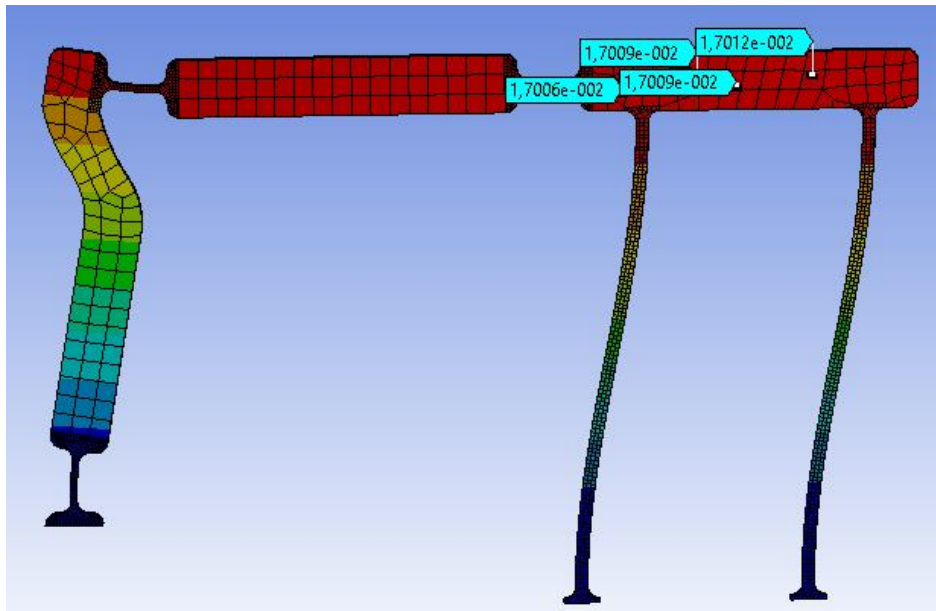


Figure 7.7. Stroke analyses for fully compliant slider-crank mechanism (10° right)

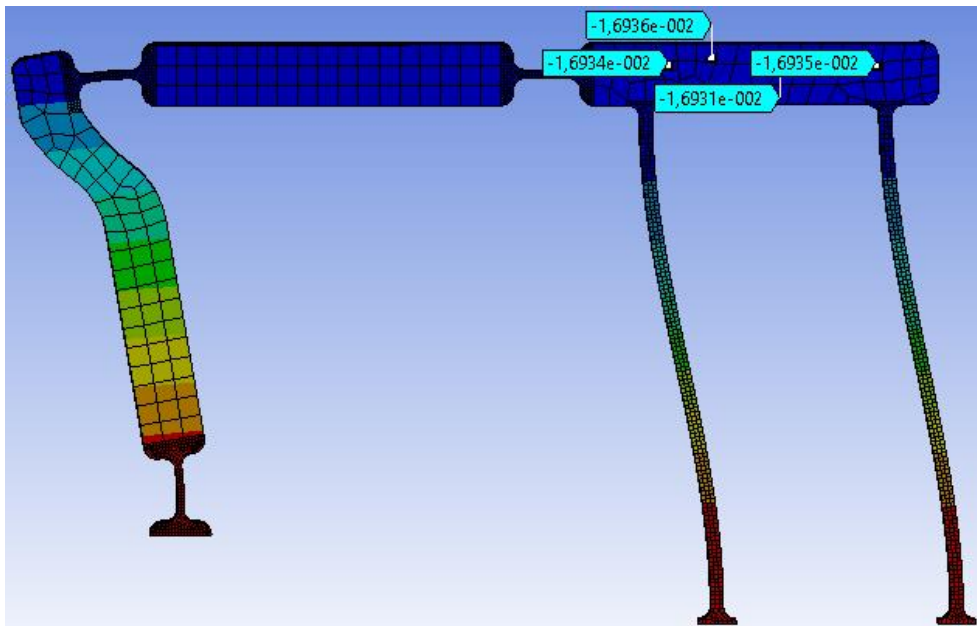


Figure 7.8. Stroke analyses for fully compliant slider-crank mechanism (10° left)

The fully compliant slider-crank mechanism is analyzed for 10° CW (Figure 7.7) and CCW (Figure 7.8) input rotation, average output stroke value of the slider is 17.01 mm and 16.94 mm respectively. It should be noted that for large rotations nonlinear analysis is selected.

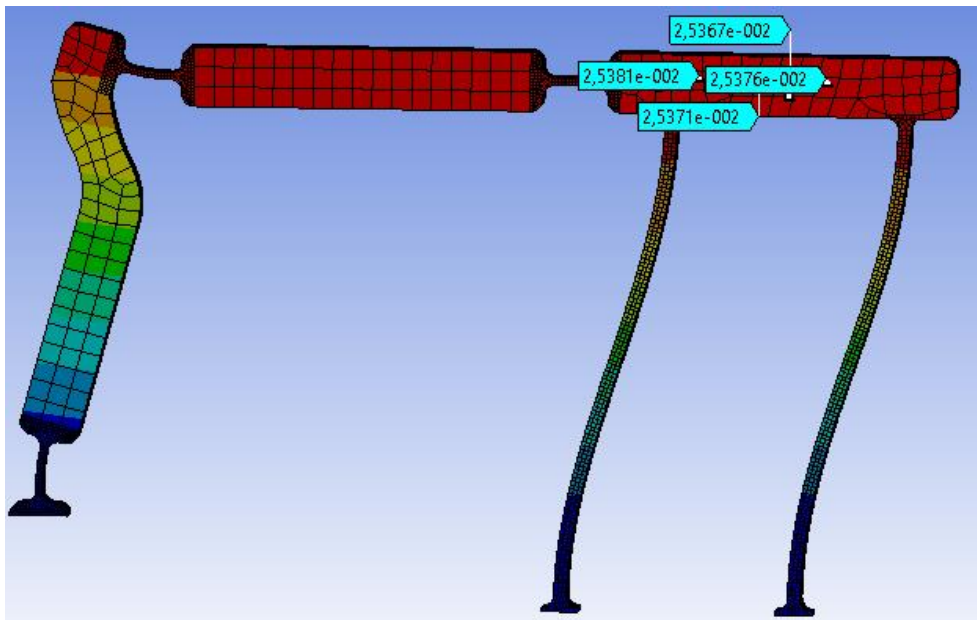


Figure 7.9. Stroke analyses for fully compliant slider-crank mechanism (15° right)

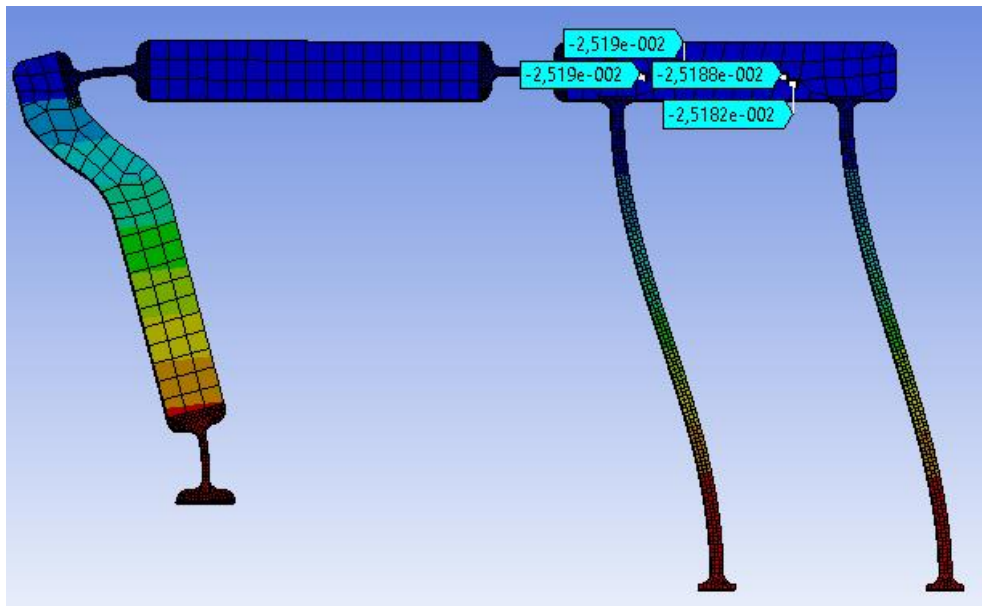


Figure 7.10. Stroke analyses for fully compliant slider-crank mechanism (15° left)

The fully compliant slider-crank mechanism is analyzed for 15° CW (Figure 7.9) and CCW (Figure 7.10) input rotation, average output stroke value of the slider is 25.37 mm and 25.19 mm respectively.

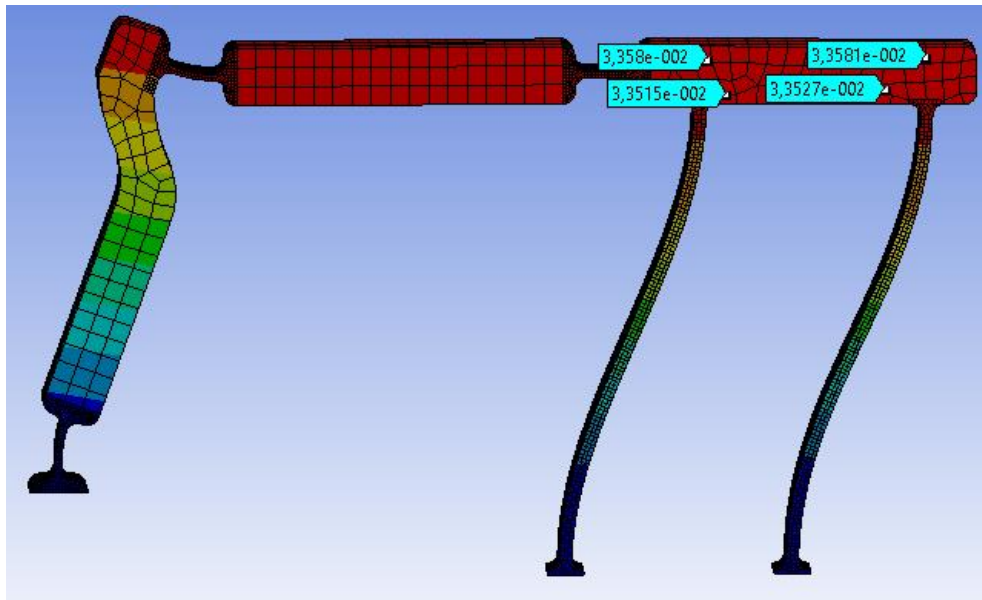


Figure 7.11. Stroke analyses for fully compliant slider-crank mechanism (20° right)

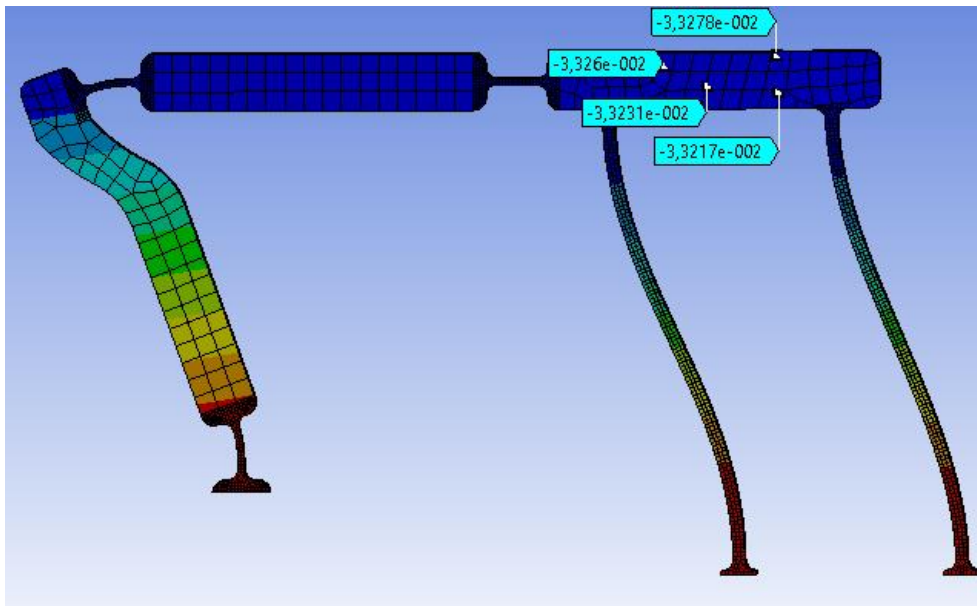


Figure 7.12. Stroke analyses for fully compliant slider-crank mechanism (20° left)

The fully compliant slider-crank mechanism is analyzed for 20° CW (Figure 7.11) and CCW (Figure 7.12) input rotation, average output stroke value of the slider is 33.55 mm and 33.23 mm respectively.

Table 7.1. Theoretical and FEA stroke data of the fully compliant slider-crank mechanism

Angle(deg)	THEOR. <i>Right-Left</i>	STROKE (mm)			
		ANSYS			
		<i>Right</i>	% err	<i>Left</i>	% err
0	0	0		0	
5	8.7	8.53	2.13	8.51	2.36
10	17.4	17.01	2.04	16.94	2.45
15	25.9	25.37	1.98	25.19	2.67
20	34.2	33.55	1.91	33.23	2.84
		Mean	2.01		2.58

It is validated that, averages of the output stroke values of the slider are in close agreement with the analytical results.

### 7.3.3. Stress Analysis for Fully Compliant Slider-Crank Mechanism

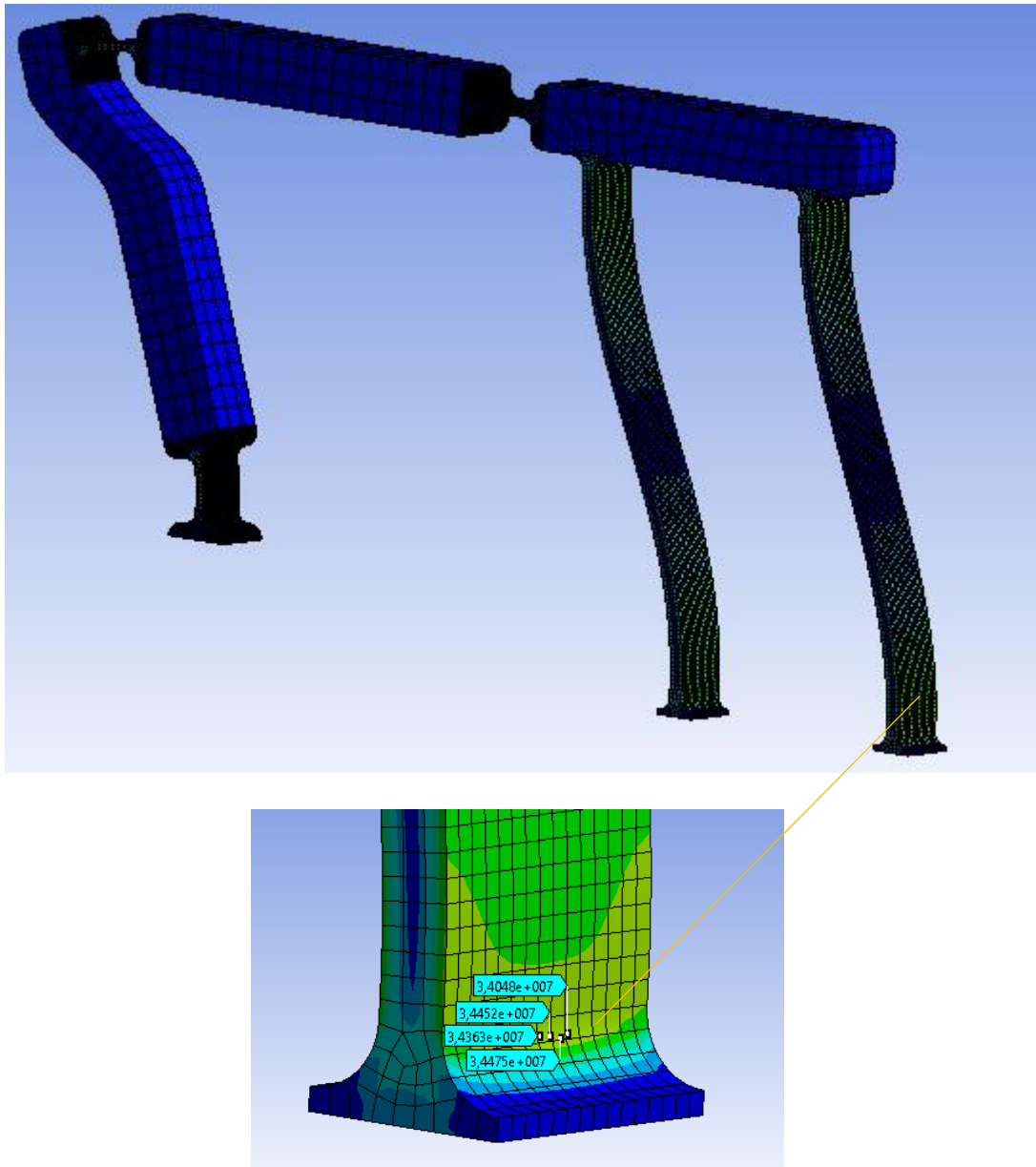


Figure 7.13. Maximum stress values at compliant segments for fully compliant slider-crank mechanism ( $20^\circ$  left)

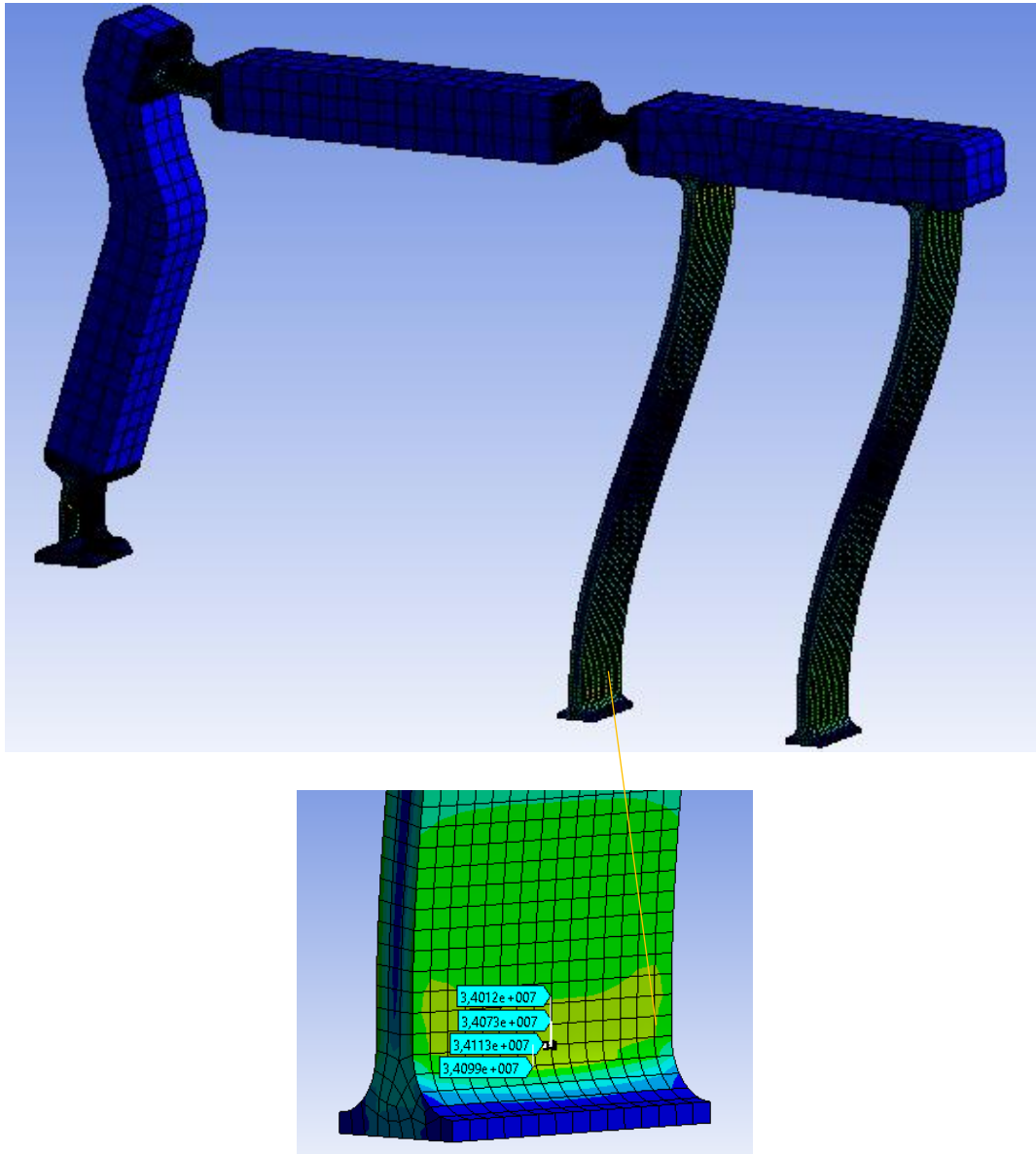


Figure 7.14. Maximum stress values at compliant segments for fully compliant slider-crank mechanism ( $20^\circ$  right)

FEA method is again employed to determine and check the resultant stresses at the flexural hinges. The resultant stress at the flexural hinges obtained by ANSYS<sup>®</sup> is the equivalent (von Mises) stress. The analysis results are presented in Figure 7.13 and Figure 7.14 when the input crank rotation is  $20^\circ$  for both CW and CCW

directions. For the fixed-guided flexible segments, analytical maximum stress value at compliant segments is determined as 34.4 MPa from Equation (6-22), 34.2 MPa from ANSYS. For the selected material polypropylene, yield strength is equal to 35-40 MPa. The maximum stress value for the 20° crank input is smaller than the yield strength. Therefore, the design is in safe elastic region.

#### **7.3.4. Study of Mesh Refinement for Fully Compliant Slider-Crank Mechanism**

Mesh refinement is an important tool for editing finite element meshes to increase the accuracy of the solution. However, finer meshes increases the computation time. The density of mesh must satisfactorily balance accuracy and computing resources. Refinement is performed in an iterative manner in which a solution is found, error estimates are calculated, and elements in regions of high error are refined. This process is repeated until the desired accuracy is obtained.

For the model with the thickness of 2.85 mm finite element analyses are done for different mesh densities with input crank angle of 20°. The most critical part of the mechanism is one set of the fixed-guided flexural hinges are meshed with three different mesh densities. During the refinement study one, two and three elements are used through the thickness and the results are shown in Table 7.2.

At least three convergence runs are required to plot a curve which can then be used to indicate when convergence is achieved or, how far away the most refined mesh is from full convergence. Therefore, convergence curve is plotted and shown in Table 7.2. Three runs of different mesh density give the nearly same result, therefore convergence is already achieved and no more refinement is necessary. After this study of refinement 3 elements through the thickness are used.

Table 7.2. Number of elements through the thickness vs. maximum von-Mises stress for fixed-guided flexural hinge

Number of Elements through the Thickness	Maximum von-Mises Stress (MPa)
0	0
1	34.19
2	34.22
3	34.23

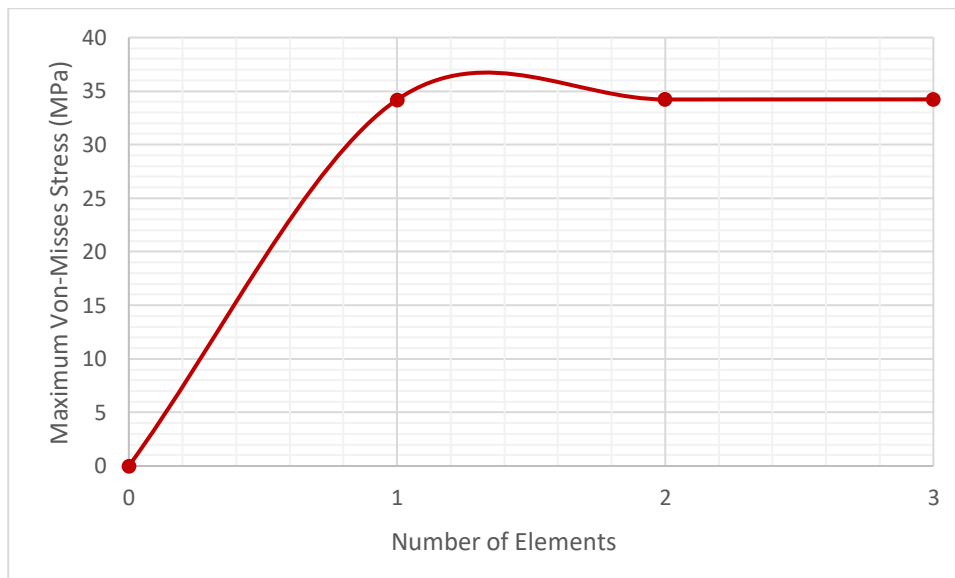


Figure 7.15. Number of elements through the thickness vs. maximum von-Mises stress for fixed-guided flexural hinge

## CHAPTER 8

### EXPERIMENTAL ANALYSIS OF THE FULLY COMPLIANT SLIDER-CRANK MECHANISM

#### 8.1. Manufacturing of the Prototype

After theoretical calculations are performed, a prototype of the mechanism is built for collecting experimental data. The mechanism seen in Figure 8.1 is manufactured in one piece from polypropylene with a plate thickness of 15 mm which is available in the market. The properties of the polypropylene are given Appendix A.

During the manufacturing process seen in Figure 8.2, three axis CNC router is used with 7.5 mm/s cutting rate, 1.5 mm depth of cut and 4500 rpm spindle speed. An experiment setup is prepared in order to measure the stroke and axis drift of the slider precisely for the provided input rotation.

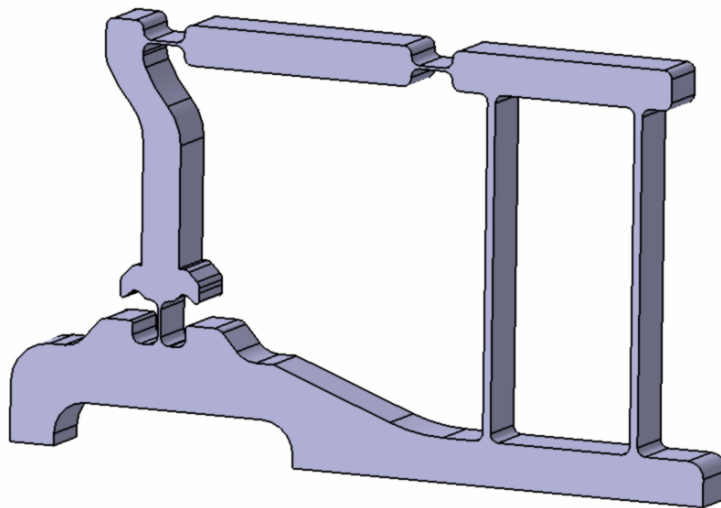


Figure 8.1. CAD design of the prototype

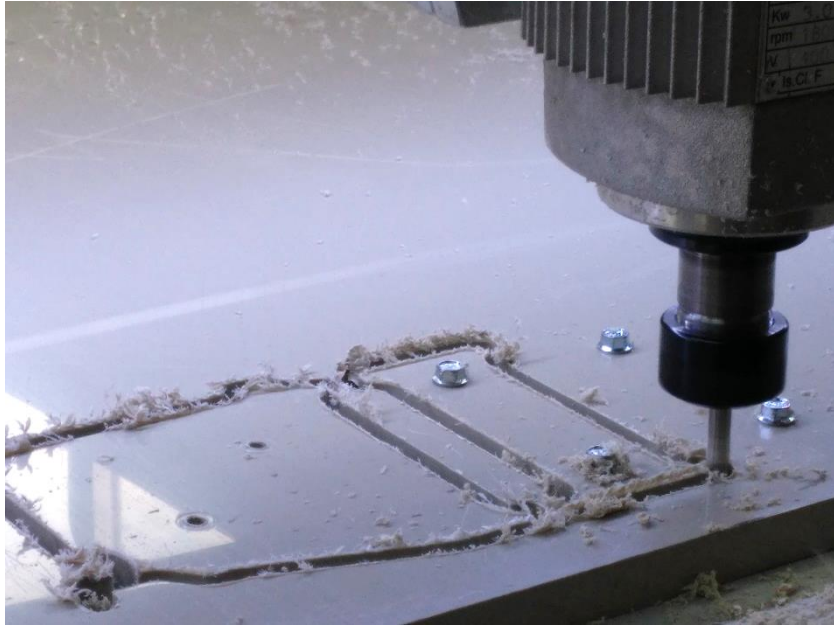


Figure 8.2. Manufacturing process of the prototype

The mechanism is fixed to a wooden platform. A screw mechanism is attached to the crank of the mechanism to prescribe the required input rotation. To measure the stroke and axis drift of the mechanism dial indicators are assembled as seen in Figure 8.3.

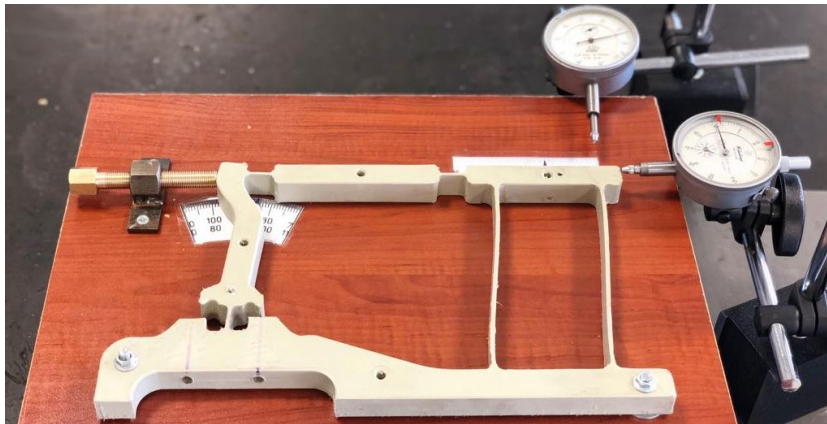


Figure 8.3. Experimental setup

## 8.2. Experimental Validation

Experimental setup presented in Figure 8.3 is established in order to measure stroke and axis drift of the slider precisely under the required rotation. Therefore, we can compare the theoretical and experimental values. Initially the position of the crank at  $5^\circ$  is set by power screw. Each revolution of the screw corresponds to 1.75 mm translation and thus  $1^\circ$  rotation of the crank is measured. Corresponding output stroke and axis drift values are measured by dial indicators. The same procedure is repeated for different crank positions and the output data are collected. The experimental values are very close to the analytical results as displayed in Table 8.1 and Table 8.2.

Table 8.1. Theoretical and experimental stroke data of the fully compliant slider-crank mechanism

		STROKE (mm)			
THEOR.		EXPERIMENTAL			
Angle(deg)	Right-Left	Right	% err	Left	% err
0	0	0		0	
5	8.7	8.82	1.20	8.86	1.66
10	17.4	17.2	0.95	17.32	0.26
15	25.9	25.8	0.32	25.82	0.24
20	34.2	34.18	0.06	34.45	0.73
			<b>0.63</b>	<b>0.72</b>	

It is calculated that the mean absolute error of all data points for the stroke measurements is 0.675 mm. If this value is compared with the reference dimension  $L = 100$  mm, the percent error is 0.68. If this value is compared with the stroke of the slider  $\Delta S = 68.4$  mm, the percent error is 0.98.

The datum point (zero axis drift position) is selected as follows: The datum axis is the mid-point of highest and lowest positions of the output Figure 5.4; when the input is at  $0^\circ$  and  $\pm 20^\circ$ . Note that, there are differences in error values for the left and right

axis drifts. Because, fine manufacturing of the long compliant segments with classical machining process is rather difficult.

Table 8.2. Theoretical and experimental axis drift data of the fully compliant slider-crank mechanism

		AXIS DRIFT (mm)			
		THEOR.	EXPERIMENTAL		
<i>Angle(deg)</i>	<i>Right-Left</i>	<i>Right</i>	<i>error</i>	<i>Left</i>	<i>error</i>
0	3.015	3.11	0.095	3.11	0.095
5	2.635	2.71	0.075	2.87	0.235
10	1.496	1.51	0.014	1.66	0.164
15	-0.392	-0.41	0.018	-0.4	0.008
20	-3.015	-3.11	0.095	-3.11	0.095
		Average	<b>0.06</b>		<b>0.12</b>

For the axis drift the mean absolute error of all data points is 0.09 mm. If this value is compared with the reference dimension  $L = 100$  mm, the percent error is 0.09. If this value is compared with the stroke  $\Delta S = 68.4$  mm, the percent error is 0.13.

Finally, we compared the theoretical and experimental values as shown in Figure 8.4.

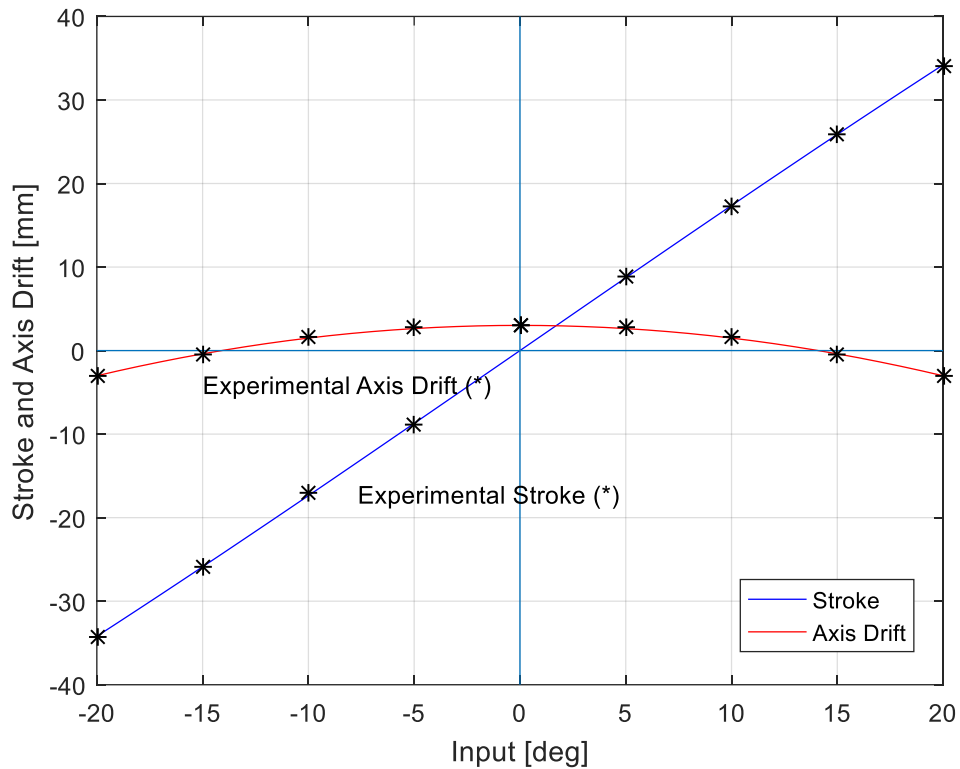


Figure 8.4. Theoretical and experimental stroke and axis drift data of the fully compliant slider-crank mechanism

In the design of compliant mechanisms, there are always some errors due to roughness of PRBM approach. The design approach in this study is no exception. However, it should be noted that PRBM is not used for final dimensioning of a compliant mechanism. It is a tool which is used during the preliminary design stage. Precise dimensioning of compliant mechanism is generally finalized with finite element analysis tool.



## CHAPTER 9

### CONCLUSIONS

#### 9.1. Summary

Slider-crank mechanism is one of the most commonly used mechanism in the industry and has numerous applications. In this thesis, a novel design procedure for a fully compliant slider-crank mechanism is proposed. In this design, the prismatic joint is replaced with a compliant parallel guiding mechanism. The compliant parallel-guiding mechanism is the output of the system that performs curvilinear translation provided that the output is not loaded with large forces.

A design approach for optimum link proportions of the rigid body equivalent of the fully compliant slider-crank mechanism is proposed. The optimization objective is to maximize the translational motion of the slider equivalent of the fully compliant slider-crank mechanism while minimizing stresses in compliant segments. Input-output motion relationship of the mechanism and analytical stress values at flexural hinges are determined. A design table is prepared for generalization of the dimensions that will be beneficial for other researchers. As an example, a mechanism is synthesized using the design table. This mechanism is analyzed with FEA method to verify analytical results. It is shown that the results of the proposed theoretical model and FEA model are consistent.

Finally, a real prototype is manufactured from polypropylene in single piece. Thus, it shows the advantage of ease of manufacturing when compared with the partially compliant cases. Experimental setup is employed for stroke and axis drift measurements. It is observed that the output displacement and the axis drift in the mathematical models and the real model are almost the same. Hence, it is verified that the proposed methods are consistent.

We believe this fully compliant slider-crank mechanism design procedure will be beneficial for many designers and may find many applications especially where backlash free design is required.

## **9.2. Key Findings and Outcomes**

Compliant slider-crank mechanisms in the literature possess a rigid prismatic joint (slider) in their structure. Prismatic joints inherently have disadvantages due to backlash and friction problems. In our design, the prismatic joint is replaced with a compliant parallel guiding mechanism.

In our study, a fully compliant slider-crank mechanism is proposed. Also, to the best of our knowledge, this is the first complete study on any of type of fully compliant slider crank mechanism with a presented design table.

In the literature, there are several studies available on the “paired double parallelogram” type compliant mechanism. The advantage of paired double parallelogram type is approximate straight line motion generation characteristics. However, there is a big major disadvantage; if PRBM of this type of mechanism is constructed, it can be calculated that  $DOF < 0$ , that yields a locking mechanism. Compliant version of this mechanism works with axial deformation of compliant segments as well as bending. This property increases the stresses and therefore is a major constraint on the stroke of the mechanism.

In our study we targeted applications where slider stays always parallel to its previous positions.

In our study, link 2 does not fully rotate and should not be called as crank. However, if we used slider-rocker mechanism in the title, when the study is published, only very few of the researchers could realize that the mechanism is actually the slider-crank mechanism that they know.

The manufacturing error that deteriorates initial parallelism of the long compliant

segments causes difference between theoretical and experimental results. If the prototype were produced by plastic injection molding with a metal mold such as in mass production, we would be able to achieve smaller errors.

### **9.3. Future Work**

Evaluating the key findings and outcomes, some suggestions can be presented as future work.

The magnitudes of the inertia forces are small relative to the external load therefore this study does not focus on dynamic force analysis. As a future work dynamic analysis of the mechanism can be done that will give an opportunity to study the dynamic characteristics of the mechanism being investigated.

During this study the fully compliant slider-crank mechanism is investigated whose slider part is composed of fixed-guided flexible beams. In future studies different types of compliant segments can be used as a slider.

The fully compliant slider-crank mechanism can be designed and optimized as a constant force mechanism.

Roberts or Watt four bar mechanisms can be implemented as a linear guide as another study. Specific points of coupler link of these mechanisms trace approximate straight line. However, their coupler link performs rotation as well as well translation. In our case the coupler link performs no rotation but only curvilinear translation. Thus, this choice is a tradeoff.



## REFERENCES

- [1] A. Midha, T. W. Norton, and L. L. Howell, "On the nomenclature, classification, and abstractions of compliant mechanisms," *J. Mech. Des. Trans. ASME*, 1994.
- [2] L. L. Howell, *Compliant Mechanisms*. Wiley-Interscience Publications, 2001.
- [3] L. L. Howell and A. Midha, "A loop-closure theory for the analysis and synthesis of compliant mechanisms," *J. Mech. Des. Trans. ASME*, 1996.
- [4] Y.-Q. Yu, S.-K. Zhu, Q.-P. Xu, and P. Zhou, "A novel model of large deflection beams with combined end loads in compliant mechanisms," *Precis. Eng.*, vol. 43, pp. 395–405, 2016.
- [5] P. Liu and P. Yan, "A modified pseudo-rigid-body modeling approach for compliant mechanisms with fixed-guided beam flexures," *Mech. Sci.*, 2017.
- [6] G. Hao, H. Li, A. Nayak, and S. Caro, "Design of a compliant gripper with multimode jaws," *J. Mech. Robot.*, 2018.
- [7] A. Alqasimi, C. Lusk, and J. Chimento, "Design of a linear bistable compliant crank-slider mechanism," *J. Mech. Robot.*, 2016.
- [8] S. Pardeshi, S. Kandharkar, and B. Deshmukh, "Monolithic compliant slider crank mechanism for motion amplification," in *Materials Today: Proceedings*, 2017.
- [9] T. Dao and S. Huang, "Design and Analysis of Flexible Slider Crank Mechanism," *World Acad. Sci. Eng. Technol. Int. J. Aerosp. Mech. Eng.*, 2014.

- [10] N. T. Pavlović and N. D. Pavlović, “Compliant mechanism design for realizing of axial link translation,” *Mech. Mach. Theory*, 2009.
- [11] H. Zhao, S. Bi, and J. Yu, “A novel compliant linear-motion mechanism based on parasitic motion compensation,” *Mechanism and Machine Theory*, 2012.
- [12] H. Zhao, D. Han, L. Zhang, and S. Bi, “Design of a stiffness-adjustable compliant linear-motion mechanism,” *Precis. Eng.*, 2017.
- [13] E. Tanik and V. Parlaktaş, “A new type of compliant spatial four-bar (RSSR) mechanism,” *Mech. Mach. Theory*, 2011.
- [14] V. Parlaktas and E. Tanik, “Partially compliant spatial slider-crank (RSSP) mechanism,” *Mech. Mach. Theory*, vol. 46, no. 11, pp. 1707–1718, 2011.
- [15] V. Parlaktaş and E. Tanik, “Single piece compliant spatial slider-crank mechanism,” *Mech. Mach. Theory*, vol. 81, pp. 1–10, 2014.
- [16] E. Tanik, “Transmission angle in compliant slider-crank mechanism,” *Mech. Mach. Theory*, vol. 46, no. 11, pp. 1623–1632, 2011.
- [17] S. Erkaya, S. Doğan, and Ş. Ulus, “Effects of joint clearance on the dynamics of a partly compliant mechanism: Numerical and experimental studies,” *Mech. Mach. Theory*, vol. 88, pp. 125–140, 2015.
- [18] S. Erkaya, S. Doğan, and E. Şefkathoğlu, “Analysis of the joint clearance effects on a compliant spatial mechanism,” *Mech. Mach. Theory*, vol. 104, pp. 255–273, 2016.
- [19] B. P. Trease, Y. M. Moon, and S. Kota, “Design of large-displacement compliant joints,” *J. Mech. Des. Trans. ASME*, 2005.
- [20] T.-S. Yang, P.-J. Shih, and J.-J. Lee, “Design of a spatial compliant translational joint,” *Mech. Mach. Theory*, 2016.
- [21] J. E. Shigley and J. J. Uicker, *Theory of Machines and Mechanisms*. 1980.

- [22] B. A. Salamon, "Mechanical Advantage Aspects in Compliant Mechanisms Design," Purdue University, 1989.
- [23] L. L. Howell and A. Midha, "A method for the design of compliant mechanisms with small-length flexural pivots," *J. Mech. Des. Trans. ASME*, 1994.
- [24] L. L. Howell and A. Midha, "Parametric deflection approximations for end-loaded, large-deflection beams in compliant mechanisms," *J. Mech. Des. Trans. ASME*, 1995.
- [25] X. C. Li, Y. Li, Ding B. X., and H. Y. Xu, "An investigation on kinematics and dynamics performance of a novel 3-PRC-compliant parallel micromanipulator," *Adv. Mech. Eng.* , vol. 10, 2018.
- [26] A. G. Erdman, G. N. Sandor, and S. Kota, *Mechanism Design: Analysis and Synthesis (4th Edition)*, vol. 1. 2001.



## APPENDICES

### A. Properties of Polypropylene



TYPICAL PROPERTIES OF POLYPROPYLENE (PP)					
ASTM or UL Test	Property	HPP*	HPP-filled	CPP**	CPP-filled
D792	Specific gravity	0.90-0.91	0.97-1.27	0.89-0.91	0.98-1.24
D570	Water absorption (%)	0.01-0.03	0.01-0.09	0.03	0.01-0.02
D638	Tensile strength (psi)	4,500-6,000	3,500-16,000	4,000-5,500	2,500-10,000
D638	Elongation at break (%)	100-600	1.5-80	200-500	2.2-50
D638	Tensile modulus (psi)	16,500-22,500	37,500-100,000	13,000-18,000	5,000-35,000
D790	Flexural modulus (psi)	17,000-25,000	21,000-100,000	13,000-20,000	21,000-96,000
D256	Impact strength, Izod (ft-lb/in of notch)	0.4-1.4	0.6-12	1.1-14	0.6-4.0
D785	Hardness, Rockwell R	80-102	75-117	65-96	81-105
C177	Thermal conductivity (10 <sup>-4</sup> cal-cm/sec-cm <sup>2</sup> -°C)	2.8	2.4-9	3.5-4.0	3-9
D696	Coefficient of thermal expansion (10 <sup>-5</sup> in/in-°C)	8-10	1.5-5	6-10	2-6
D648	Deflection temperature (°F)				
	At 264 psi	120-140	130-330	120-140	116-280
	At 66 psi	225-250	220-300	185-220	170-305
UL 94	UL flammability rating***	HB	HB	HB	HB

\*Homopolymer polypropylene. \*\*Copolymer polypropylene. \*\*\*V-2, V-1, V-0, V-5 grades available.

TYPICAL PROPERTIES OF POLYPROPYLENE (PP)					
ISO or UL Test	Property	HPP*	HPP-filled	CPP**	CPP-filled
ISO1183	Specific gravity	0.90-0.91	0.97-1.27	0.89-0.91	0.98-1.24
ISO62	Water absorption (%)	0.01-0.03	0.01-0.09	0.03	0.01-0.02
ISO527	Tensile strength (MPa)	31.03-41.37	24.13-110.32	27.58-37.92	17.24-68.95
ISO527	Elongation at break (%)	100-600	1.5-80	200-500	2.2-50
ISO527	Tensile modulus (MPa)	113.7-155.1	258.5-689.5	89.6-124.1	34.4-241.3
ISO178	Flexural modulus (MPa)	117.2-172.3	144.8-689.5	89.6-137.9	144.8-661.9
ISO180	Notched Izod impact strength (J/m)	21-75	32-641	59-747	32-214
ASTM D785	Hardness, Rockwell R	80-102	75-117	65-96	81-105
ISO8302	Thermal conductivity (W/(mK))	0.22	0.25-0.51	0.22	0.25-0.51
ISO11359	Coefficient of thermal expansion (10 <sup>-4</sup> m/m-°C)	1.4-1.8	0.27-0.90	1.08-1.80	0.36-1.08
ISO75	Deflection temperature (°C)				
	At 1.80 MPa	49-60	54-166	49-60	47-138
	At 0.45 MPa	107-121	104-149	85-104	77-152
UL 94	UL flammability rating***	HB	HB	HB	HB

\*Homopolymer polypropylene. \*\*Copolymer polypropylene. \*\*\*V-2, V-1, V-0, V-5 grades available.

## B. MathCad and MatLab Codes for the Calculations

### Function Generation for Two Precision Points

#### Kinematic Synthesis

##### Required parameters (2 Scalar)

$$\beta := 20\text{deg} \quad \beta = 0.349$$

$$\text{Input oscillation} \quad \theta_{ef} := \beta \quad \text{Output oscillation} \quad \beta_{ef} := \beta$$

##### Free choices (5 Scalar)      $i := \sqrt{-1}$

$$\text{Initial crank length and position} \quad a_2 := 1 \quad \text{and} \quad \text{angle} \quad \theta_{21} := 50\text{-deg}$$

$$Z_2 := a_2 \cdot \cos(\theta_{21}) + i \cdot a_2 \cdot \sin(\theta_{21}) \quad Z_2 = 0.643 + 0.766i$$

$$\text{Initial rocker length and position} \quad a_4 := 1 \quad \text{and} \quad \text{angle} \quad \theta_{41} := \left(\frac{\pi}{2} - \frac{\beta}{2}\right) = 1.3$$

$$Z_4 := a_4 \cdot \cos(\theta_{41}) + i \cdot a_4 \cdot \sin(\theta_{41}) \quad Z_4 = 0.174 + 0.985i$$

Coupler link rotation

$$\gamma_{ef} := -\beta$$

##### The equations that must be satisfied are: (2 Scalar)

$$Z_3 := \frac{Z_4 \cdot (e^{i \cdot \beta_{ef}} - 1) - Z_2 \cdot (e^{i \cdot \theta_{ef}} - 1)}{e^{i \cdot \gamma_{ef}} - 1} \quad Z_1 := Z_2 + Z_3 - Z_4$$

$$Z_3 = 0.516 - 0.045i$$

$$Z_1 = 0.985 - 0.264i$$

$$a_2 := |Z_2| \quad a_3 := |Z_3| \quad a_4 := |Z_4| \quad a_1 := |Z_1|$$

Link proportions can be determined as:

$$a_2 = 1 \quad a_3 = 0.518 \quad a_4 = 1 \quad a_1 = 1.02$$

Maximum to minimum link length ratio ( $< 10$ )

$$\frac{\max(a_1, a_2, a_3, a_4)}{\min(a_1, a_2, a_3, a_4)} = 1.97$$

## Function Generation for Three Precision Points

### Kinematic Synthesis

Required parameters ( Scalar)

$$\beta := 20.\text{deg}$$

$$\alpha := 4.\text{deg}$$

+

Input\_oscillation

$$\theta_{2.2} := \frac{\beta}{2}$$

$$\theta_{2.3} := \beta$$

Output\_oscillation

$$\theta_{4.2} := \frac{\beta}{2}$$

$$\theta_{4.3} := \beta$$

Coupler-link-rotation

$$\gamma_{12} := \frac{\beta - \alpha}{2}$$

$$\gamma_{13} := \beta - \alpha$$

Free choices ( Scalar)

$$i := \sqrt{-1}$$

Initial rocker length and position  $a_4 := 100$  and angle  $\theta_{41} := \left( \frac{\pi}{2} - \frac{\beta}{2} \right) = 1.39$

$$Z_4 := a_4 \cdot \cos(\theta_{41}) + i \cdot a_4 \cdot \sin(\theta_{41}) = 17.365 + 98.481i$$

**The equations that must be satisfied are: (4 Scalar)**

$$AA := \begin{pmatrix} e^{i\gamma_2} - 1 & e^{i\theta_{2,2}} - 1 \\ e^{i\gamma_3} - 1 & e^{i\theta_{2,3}} - 1 \end{pmatrix} = \begin{pmatrix} -9.732 \times 10^{-3} + 0.139i & -0.015 + 0.174i \\ -0.039 + 0.276i & -0.06 + 0.342i \end{pmatrix}$$

$$BB := \begin{bmatrix} Z_4(e^{i\theta_{4,2}} - 1) \\ Z_4(e^{i\theta_{4,3}} - 1) \end{bmatrix} = \begin{pmatrix} -17.365 + 1.519i \\ -34.73 \end{pmatrix}$$

$$\begin{pmatrix} Z_3 \\ Z_2 \end{pmatrix} := AA^{-1} \cdot BB = \begin{pmatrix} -5.116 \times 10^{-13} - 1.137i \times 10^{-13} \\ 17.365 + 98.481i \end{pmatrix}$$

$$Z_1 := Z_2 + Z_3 - Z_4$$

$$Z_1 = -2.593 \times 10^{-13} - 1.421i \times 10^{-13}$$

$$Z_2 = 17.365 + 98.481i$$

$$Z_3 = -5.116 \times 10^{-13} - 1.137i \times 10^{-13}$$

$$Z_4 = 17.365 + 98.481i$$

$$a_2 := |Z_2| \quad a_3 := |Z_3| \quad a_4 := |Z_4| \quad a_1 := |Z_1|$$

**Link proportions can be determined as:**

$$a_2 = 100$$

$$a_3 = 5.241 \times 10^{-13}$$

$$a_4 = 100$$

$$a_1 = 2.957 \times 10^{-13}$$

**Maximum to minimum link length ratio (< 10)**

$$\frac{\max(a_1, a_2, a_3, a_4)}{\min(a_1, a_2, a_3, a_4)} = 3.381 \times 10^{14}$$

## Cascade 4bar Kinematic Analysis

### First Part

$$r_1 := 300 \quad r_2 := 150 \quad r_3 := 300 \quad r_4 := 180$$

**Maximum to minimum link length ratio (< 10)**

$$\frac{\max(r_1, r_2, r_3, r_4)}{\min(r_1, r_2, r_3, r_4)} = 2$$

$$\text{Tilt angle } \delta \text{ (CW)} \quad \delta := -0.4 \quad \frac{\delta}{\text{deg}} = -22.918 \quad i := \sqrt{-1}$$

$$j := 80..110 \quad \theta_{2j} := j \cdot \text{deg}$$

$$K_{11} := \frac{r_1}{r_2} \quad K_{21} := \frac{r_1}{r_4} \quad K_{31} := \frac{r_1^2 + r_2^2 - r_3^2 + r_4^2}{2 \cdot r_2 \cdot r_4}$$

$$A1_j := K_{31} - K_{11} + (1 - K_{21}) \cdot \cos(\theta_{2j} + \delta) \quad B1_j := -2 \cdot \sin(\theta_{2j} + \delta)$$

$$C1_j := K_{11} + K_{31} - (1 + K_{21}) \cdot \cos(\theta_{2j} + \delta)$$

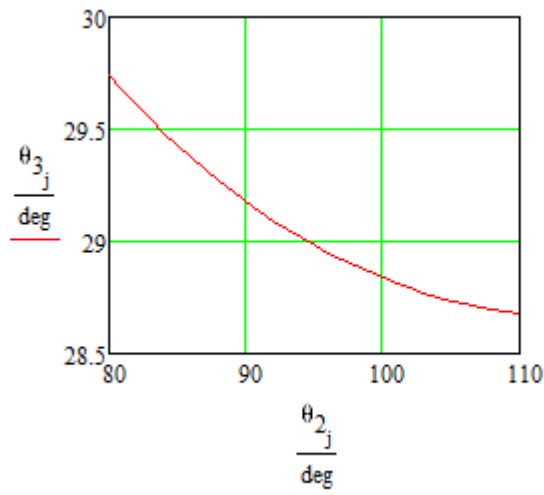
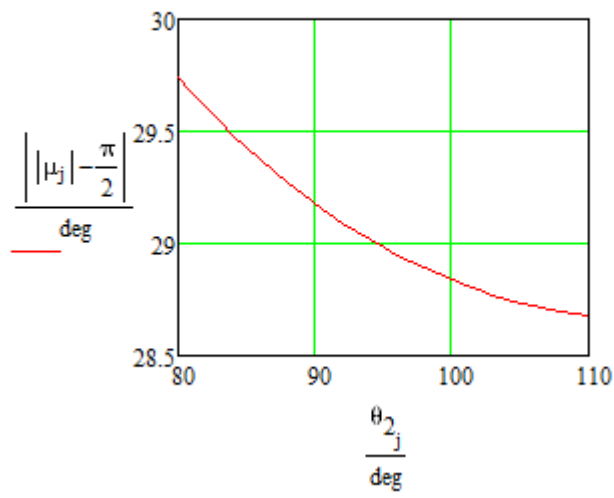
$$\theta_{4j} := 2\pi + 2 \cdot \text{atan2}\left[2 \cdot A1_j, -B1_j - \sqrt{(B1_j)^2 - 4 \cdot A1_j \cdot C1_j}\right] - \delta$$

$$\theta_{3j} := \arg\left[r_4 \cdot e^{i(\theta_{4j} + \delta)} + r_1 - r_2 \cdot e^{i(\theta_{2j} + \delta)}\right] - \delta$$

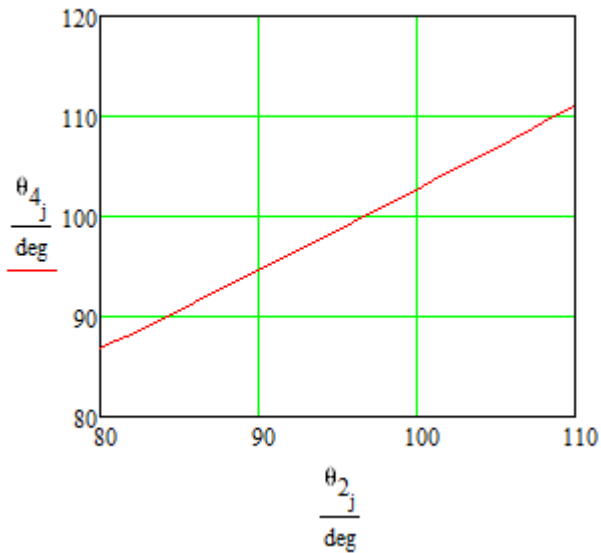
Transmission angle

$$\mu_j := \frac{\pi}{2} + \theta_{3j}$$

The deviation of the transmission angle from 90°



### Input and output angle correlation of the synthesized mechanism



Stroke

$$\max(\theta_4) - \min(\theta_4) = 111 \cdot \text{deg}$$

### Animation (Movability Check)

$$a := \frac{\pi}{2} + \frac{\text{FRAME}}{15}$$

$$\theta_2 := a = 1.571$$

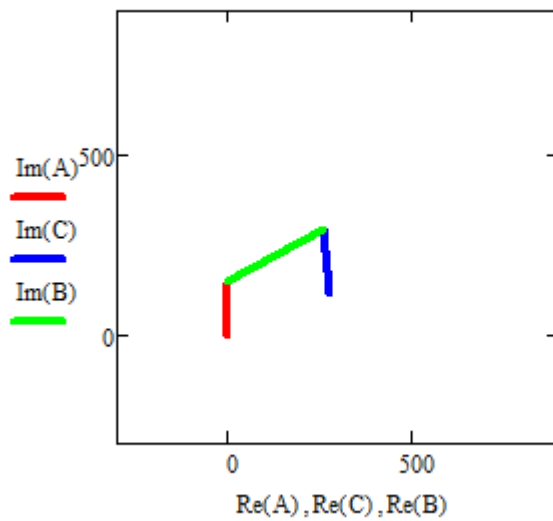
$$\underline{A} := K_{31} - K_{11} + (1 - K_{21}) \cdot \cos(\theta_2 + \delta) = -1.243 \quad B := -2 \cdot \sin(\theta_2 + \delta) = -1.842$$

$$\underline{C} := K_{11} + K_{31} - (1 + K_{21}) \cdot \cos(\theta_2 + \delta) = 1.978$$

$$\theta_4 := 2 \cdot \text{atan2}[2 \cdot A, -B - \sqrt{(B)^2 - 4 \cdot A \cdot C}] - \delta \quad \theta_3 := \arg[r_4 \cdot e^{i(\theta_4 + \delta)} + r_1 - r_2 \cdot e^{i(\theta_2 + \delta)}] - \delta$$

$$\underline{A}_0 := 0 + 0 \cdot i \quad A_1 := A_0 + r_2 \cdot e^{i \cdot \theta_2} \quad \underline{B}_0 := A_1 \quad B_1 := B_0 + r_3 \cdot e^{i \cdot \theta_3}$$

$$\underline{C}_0 := r_1 \cdot \cos(-\delta) + r_1 \cdot \sin(-\delta) \cdot i \quad C_1 := C_0 + r_4 \cdot e^{i(\theta_4)}$$



### Second Part

$r_6 := r_4$     $r_5 := 200$     $r_7 := 200$    Because of the parallelogram  $r_4=r_6$  and  $r_5=r_7$

### Maximum to minimum link length ratio (< 10)

$$\frac{\max(r_4, r_5, r_6, r_7)}{\min(r_4, r_5, r_6, r_7)} = 1.111$$

Tilt angle  $\chi$  (CW)    $\chi := 0.4$     $\frac{\chi}{\text{deg}} = 22.918$     $i := \sqrt{-1}$

$$\theta_{4j} := 2\pi + 2 \cdot \text{atan2}\left[2 \cdot A1_j, -B1_j - \sqrt{(B1_j)^2 - 4 \cdot A1_j \cdot C1_j}\right] - \delta$$

$$K_{12} := \frac{r_7}{r_4} \quad K_{22} := \frac{r_7}{r_6} \quad K_{32} := \frac{r_7^2 + r_4^2 - r_5^2 + r_6^2}{2 \cdot r_4 \cdot r_6}$$

$$A2_j := K_{32} - K_{12} + (1 - K_{22}) \cdot \cos(\theta_{4j} + \chi) \quad B2_j := -2 \cdot \sin(\theta_{4j} + \chi)$$

$$C2_j := K_{12} + K_{32} - (1 + K_{22}) \cdot \cos(\theta_{4j} + \chi)$$

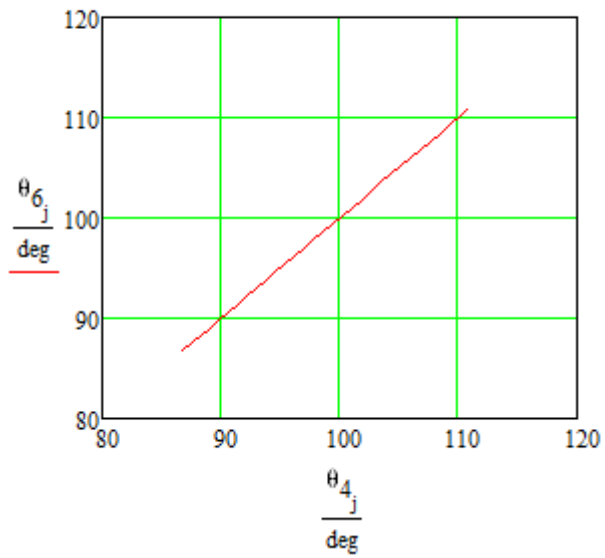
$$\theta_{6j} := 2\pi + 2 \cdot \text{atan2}\left[2 \cdot A2_j, -B2_j - \sqrt{(B2_j)^2 - 4 \cdot A2_j \cdot C2_j}\right] - \chi$$

$$\theta_{5j} := 2 \cdot \pi + \arg\left[r_6 \cdot e^{i(\theta_{6j} + \chi)} + r_7 - r_4 \cdot e^{i(\theta_{6j} + \chi)}\right] - \chi$$

Transmission angle

$$\mu_{2j} := \theta_{5j} - \pi$$

**Input and output angle correlation of the synthesized mechanism**



Stroke

$$\max(\theta_6) - \min(\theta_6) = 111 \cdot \text{deg}$$

### Animation (Movability Check)

$$\theta_4 := \theta_{4_{90}} = 1.651$$

$$b := \theta_4 + \frac{\text{FRAME}}{15} = 1.651$$

$$\theta_4 := b$$

$$D := K_{32} - K_{12} + (1 - K_{22}) \cdot \cos(\theta_4 + \chi) = -0.06 \quad E := -2 \cdot \sin(\theta_4 + \chi) = -1.774$$

$$F := K_{12} + K_{32} - (1 + K_{22}) \cdot \cos(\theta_4 + \chi) = 3.086$$

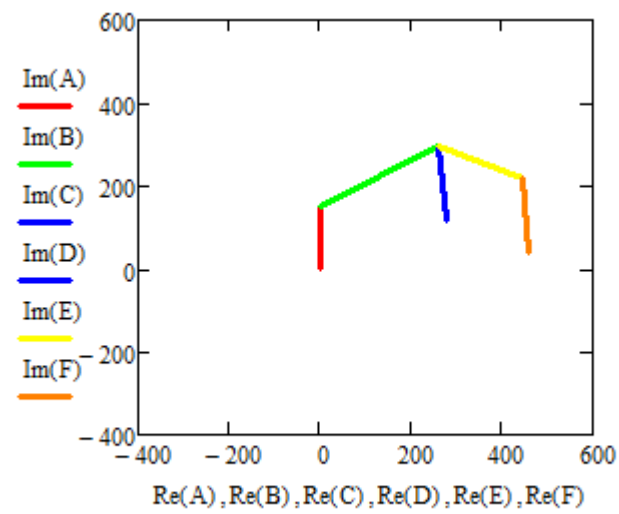
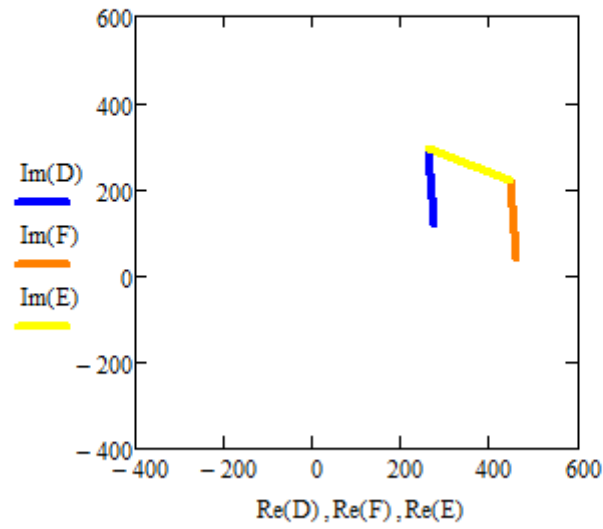
$$\theta_6 := 2 \cdot \text{atan2}\left[2 \cdot D, -E - \sqrt{(E)^2 - 4 \cdot D \cdot F}\right] - \chi \quad \theta_5 := \arg\left[r_6 \cdot e^{i(\theta_6 + \chi)} + r_7 - r_4 \cdot e^{i(\theta_4 + \chi)}\right] - \chi$$

$$D_0 := r_1 \cdot e^{-i \cdot \delta} \quad D_1 := D_0 + r_4 \cdot e^{i \cdot \theta_4}$$

$$E_0 := D_1 \quad E_1 := E_0 + r_5 \cdot e^{i \cdot \theta_5}$$

$$\vec{F}_{\lambda 0} := D_0 + (r_7 \cdot \cos(\chi) - r_7 \cdot \sin(\chi) \cdot i)$$

$$F_1 := F_0 + r_6 \cdot e^{i \cdot (\theta_6)}$$



```

%Theoretical and experimental stroke and axis drift data of the
fully compliant slider-crank mechanism

x = -20: 1 : 20;
l=100;
y1 = l*sin((x*pi)/180);
y2 = (l/2)*(1-cos((20*pi)/180))-l*(1-cos((x*pi)/180));
plot(x, y1, 'blue', x, y2, 'red')

hold on
ylabel('Stroke and Axis Drift [mm]')
xlabel('Input [deg]')
xL = xlim;
yL = ylim;
line([0 0], yL); %x-axis
line(xL, [0 0]); %y-axis

hold on

% Experimental Stroke Data Left
% 5 deg
sle1 = -5;
sle1r = -8.91;
plot(sle1,sle1r,'k--*')
% 10 deg
sle2 = -10;
sle2r = -17.12;
plot(sle2,sle2r,'k--*')
txt2 = '          Experimental Stroke (*)';
text(sle2,sle2r,txt2)
% 15 deg
sle3 = -15;
sle3r = -25.94;
plot(sle3,sle3r,'k--*')
% 20 deg

```

```

sle4 = -20;
sle4r = -34.26;
plot(sle4,sle4r,'k--*')
grid on

% Experimental Stroke Data Right
% 5 deg
se1 = 5;
se1r = 8.82;
plot(se1,se1r,'k--*')

% 10 deg
se2 = 10;
se2r = 17.21;
plot(se2,se2r,'k--*')
% 15 deg
se3 = 15;
se3r = 25.82;
plot(se3,se3r,'k--*')
% 20 deg
se4 = 20;
se4r = 34.16;
plot(se4,se4r,'k--*')
grid on

% Experimental Axis Drift Data Left
% 0 deg
ale0 = 0;
ale0r = 3.11;
plot(ale0,ale0r,'k--*')
% 5 deg
ale1 = -5;
ale1r = 2.87;
plot(ale1,ale1r,'k--*')
% 10 deg
ale2 = -10;

```

```

ale2r = 1.66;
plot(ale2,ale2r,'k--*')
% 15 deg
ale3 = -15;
ale3r = -0.4;
plot(ale3,ale3r,'k--*')
txt3 = 'Experimental Axis Drift (*)';
text(ale3,-4,txt3)
origin = [0,0]
% 20 deg
ale4 = -20;
ale4r = -3.11;
plot(ale4,ale4r,'k--*')
grid on
% Experimental Axis Drift Data Right
% 0 deg
ae0 = 0;
ae0r = 3.11;
plot(ae0,ae0r,'k--*')
% 5 deg
ae1 = 5;
ae1r = 2.71;
plot(ae1,ae1r,'k--*')
% 10 deg
ae2 = 10;
ae2r = 1.52;
plot(ae2,ae2r,'k--*')
txt1= 'Experimental Axis Drift (*)';

% 15 deg
ae3 = 15;
ae3r = -0.4;
plot(ae3,ae3r,'k--*')

% 20 deg
ae4 = 20;

```

```
ae4r = -3.11;  
plot(ae4,ae4r,'k--*')  
grid on  
  
legend('Stroke','Axis Drift')
```



## CURRICULUM VITAE

### PERSONAL INFORMATION

### PERSONAL INFORMATION

Surname, Name : Tanık, Çağıl Merve  
Nationality : Turkish (TC)  
Date and Place of Birth : 29 October 1988, Bolu  
Phone : +90 535 729 86 74  
E-mail : cmervecan@gmail.com

### EDUCATION

Degree	Institution	Year of Graduation
MS	METU Mechanical Engineering	2014
BS	Hacettepe University Mechanical Engineering	2011
High School	Atatürk Anadolu High School, Ankara	2006

### WORK EXPERIENCE

Year	Place	Enrollment
2011-2020	METU Mechanical Engineering	Teaching Assistant
2010 August	AUDI AG	Intern Engineering Student
2009 July	Oyak-Renault	Intern Engineering Student
2008 June	Mercedes-Benz Türkiye	Intern Engineering Student

### FOREIGN LANGUAGES

Advanced English, Fluent German, Basic Japanese

## **PUBLICATIONS**

**Tanık, Ç.M.**, Parlaktaş, V., Tanık, E., Kadioğlu, S., Steel Compliant Cardan Universal Joint, *Mechanism and Machine Theory*, 92 (2015) 171-183

Parlaktaş, V., Tanık, E., **Tanık, Ç.M.**, "On the design of a novel fully compliant spherical four-bar mechanism", *Advances in Mechanical Engineering*, (2019) 11(9) 1–12

**Tanık, Ç.M.**, Tanık, E., Parlaktaş, V., Yazıcıoğlu, Y., "On the analysis and design of a fully compliant large stroke slider-crank (rocker) mechanism", *Mechanical Sciences*, 11, (2020) 29–38